# Life and extinction of megafauna in the ice-age Arctic

Daniel H. Mann[a,1], Pamela Groves[b], Richard E. Reanier[c], Benjamin V. Gaglioti[d], Michael L. Kunz[e], and Beth Shapiro[f,1]

[a]Geosciences Department, University of Alaska, Fairbanks, AK 99775; [b]Institute of Arctic Biology, University of Alaska, Fairbanks, AK 99775; [c]Reanier & Associates, Inc., Seattle, WA 98166; [d]Water and Environmental Research Center, University of Alaska, Fairbanks, AK 99775; [e]Cooperative Extension and Resources, University of Alaska, Fairbanks, AK 99775; and [f]Department of Ecology and Evolutionary Biology and University of California, Santa Cruz Genomics Institute, University of California, Santa Cruz, CA 95064

Edited by Richard G. Klein, Stanford University, Stanford, CA, and approved September 23, 2015 (received for review June 29, 2015)

**Understanding the population dynamics of megafauna that inhabited the mammoth steppe provides insights into the causes of extinctions during both the terminal Pleistocene and today. Our study area is Alaska's North Slope, a place where humans were rare when these extinctions occurred. After developing a statistical approach to remove the age artifacts caused by radiocarbon calibration from a large series of dated megafaunal bones, we compare the temporal patterns of bone abundance with climate records. Megafaunal abundance tracked ice age climate, peaking during transitions from cold to warm periods. These results suggest that a defining characteristic of the mammoth steppe was its temporal instability and imply that regional extinctions followed by population reestablishment from distant refugia were characteristic features of ice-age biogeography at high latitudes. It follows that long-distance dispersal was crucial for the long-term persistence of megafaunal species living in the Arctic. Such dispersal was only possible when their rapidly shifting range lands were geographically interconnected. The end of the last ice age was fatally unique because the geographic ranges of arctic megafauna became permanently fragmented after stable, interglacial climate engendered the spread of peatlands at the same time that rising sea level severed former dispersal routes.**

ice age | megafauna | extinction | paleoecology | mammoth steppe

One of the most intriguing examples of mass extinction and the most accessible in terms of its geological record occurred around the end of the Wisconsin ice age ca. 10–45 calendar ka B.P. (10,000–45,000 calendar y ago) when some 65% of terrestrial megafauna genera (animals weighing >45 kg) became globally extinct (1). Based on what we know about recent species extinctions, the causes of extinction are usually synergistic, often species-specific, and therefore, complex, which implies that there is no universal explanation for end-Pleistocene extinctions (2, 3). Globally and specifically in the Arctic (3–10), megafaunal extinctions have been variously blamed on overhunting, rapid climate change, habitat loss, and introduced diseases (3–10). Further complicating a clear understanding of the causes of ice-age extinctions is that the magnitude and tempo of environmental change during the last 100,000 y of the Pleistocene were fundamentally different than during the Holocene (11), and these differences had far-reaching implications for community structure, evolution, and extinction causes (12).

A recent survey comparing the extinction dates of circumboreal megafauna with ice-age climate suggests that extinctions and genetic turnover were most frequent during warm, interstadial events (13). However, the mechanisms for these extinctions remain unclear, partly because this previous study considered multiple taxa living in many different ecosystems. Here, we focus on five megafaunal species that coinhabited a region of the Arctic with an ecological setting that is relatively well-understood. To avoid the methodological problems involved in pinpointing extinction dates (13), we infer population dynamics from changes in the relative abundance of megafauna over time. Using a uniquely large dataset of dated megafaunal bones from one particular area, we test a specific paleoecological hypothesis relating rapid climate change to population dynamics—namely, that transitions from cold to warm intervals were briefly optimal for grazing megafauna.

The study area is Alaska's North Slope, the tundra region bordered to the south by the Brooks Range and to the north by the Arctic Ocean (Fig. 1). The North Slope is a particularly interesting place to study end-Pleistocene extinctions for several reasons. First, its ice-age megafauna included iconic species like woolly mammoth (*Mammuthus primigenius*), steppe bison (*Bison priscus*), and cave lion (*Panthera spelaea*) (14). Second, the local extinctions of megafauna on Alaska's North Slope occurred at a time when archaeological remains are rare, suggesting that people seldom ventured there (15, 16). Third, bone preservation in arctic environments tends to be excellent because of the presence of permafrost (perennially frozen ground), which makes it possible to $^{14}$C date large numbers of bones from many different species (*SI Appendix*, Table S1). Our record of dated bones provides key insights into the temporal dynamics and biogeographical characteristics of the mammoth steppe, a biome that was unique to the ice ages and the exact nature of which has been long debated (17).

## Background

**Mammoth Steppe.** Episodically during the late Pleistocene, the mammoth steppe extended from Europe to northwestern Canada (18). Its soils were relatively dry, warm, and fertile compared with those of the present day (19, 20) (*SI Appendix*, *SI Text*), and its vegetation supported large herds of grazing mammals in species-rich communities (14, 17, 18). The biomasses and diversities of these ice-age communities contrast starkly with the impoverished megafaunal communities living in the same regions today (10, 21). The climate supporting the mammoth steppe was more continental than today (18) and, as detailed below, it was much more changeable at millennial and centennial timescales.

The nature and, for some authors, even the veracity of the mammoth steppe remain controversial (14, 17). Some paleobotanists

### Significance

**Understanding species extinction is a major concern today, and past extinctions provide valuable lessons. Numerous mammal species became extinct in the Arctic at the end of the ice age, but it is unclear why. By comparing numbers of dated bones with climate records, we find that megafaunal species, like mammoth, horse, and bison, experienced boom and bust cycles during the ice age as they tracked rapid climate changes. For these species to persist, long-distance dispersal was necessary. Their extinction on the North Slope occurred as the ice age ended, because rising sea level severed dispersal routes and spreading peat simultaneously degraded range quality. This finding suggests that arctic mammals can be resilient to environmental changes but only if their habitats remain widely interconnected.**

Author contributions: D.H.M., M.L.K., and B.S. designed research; D.H.M., P.G., B.V.G., M.L.K., and B.S. performed research; D.H.M., P.G., and R.E.R. contributed new analytic tools; P.G. and R.E.R. analyzed data; and D.H.M., P.G., R.E.R., B.V.G., and B.S. wrote the paper.

The authors declare no conflict of interest.

This article is a PNAS Direct Submission.

Freely available online through the PNAS open access option.

[1]To whom correspondence may be addressed. Email: bashapir@ucsc.edu or dhmann@alaska.edu.

This article contains supporting information online at www.pnas.org/lookup/suppl/doi:10.1073/pnas.1516573112/-/DCSupplemental.

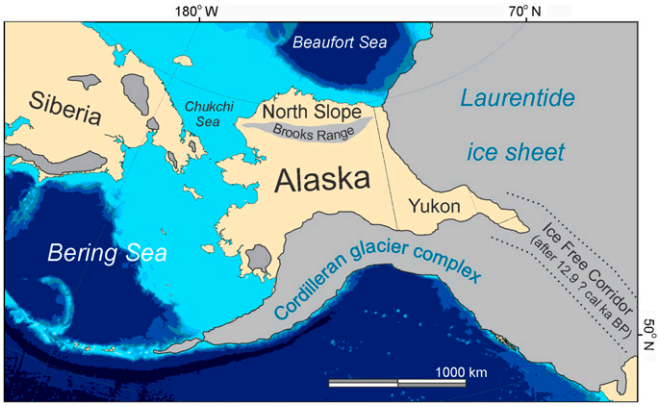


**Fig. 1.** The North Slope is the tundra region between the Brooks Range and the Arctic Ocean. The light blue area shows the extent of the Bering Land Bridge during the last glacial maximum (LGM) ca. 19,000 calendar y B.P. Glacier extent (gray) during the LGM is based on the works by Dyke (64) and Brigham-Grette et al. (71). The timing of the opening of the ice-free corridor is still uncertain.

argue that the palynological evidence is inconsistent with the productive grasslands that paleozoologists infer based on the nature of the megafauna (22). Compromise solutions to this debate have suggested a spatial mosaic of habitats: some polar desert-like in character and others more steppe-like (23–27).

**Timing of Regional Extinctions on Alaska's North Slope.** Based on current evidence, the regional extinction of the ice-age megafauna was complete in arctic Alaska before 12 calendar ka B.P. (10), leaving caribou (*Rangifer tarandus*), tundra muskox (*Ovibos moschatus*), and brown bear (*Ursus arctos*) as the only surviving megafaunal species. Of the Pleistocene species, horse (*Equus* cf. *ferus*) and steppe bison survived the longest. The most recent horse lived between 12.4 and 12.7 calendar ka B.P. (Beta-339279) (*SI Appendix*, Table S1), and the most recent bison lived between 12.2 and 12.6 calendar ka B.P. (CAMS-53767). The most recent lion lived between 13.0 and 13.3 calendar ka B.P. (CAMS-53909), and the most recent mammoth lived between 13.5 and 14.1 calendar ka B.P. (AA-26006). Moose (*Alces alces*) is a postglacial newcomer, arriving north of the Brooks Range ca. 14 calendar ka B.P. (CAMS-91810). There is no direct paleontological evidence in the form of dated bones in mainland Alaska supporting claims based on ancient DNA (aDNA) that mammoth and horse survived as late as 7,500 calendar y B.P. (28). The DNA in question was extracted from wind-blown sediment that may have incorporated biological material previously stored in permafrost.

**Climate Change, Paludification, and the Demise of the Mammoth Steppe.** Guthrie (14, 18) cited climate change, specifically the loss of climatic continentality, as the ultimate cause of the disappearance of the mammoth steppe at the end of the Pleistocene. As sea level rose across Alaska's continental shelves and storm tracks shifted poleward, maritime air masses invaded more frequently, transforming the North Slope's summer climate from sunny, dry, and relatively warm to its present state of cloudy, damp, and relatively cool (29, 30). Guthrie (14, 18) identified paludification, the spread of peat and organic soil horizons across previously well-drained landscapes, as the proximate cause of the demise of the mammoth steppe (31).

Peat flourishes during cool, moist summers, and its presence has transformative effects on ecosystems. Peat stabilizes hillslopes and dune fields and restricts loess deposition, which allows soil acidification to proceed unhindered by inputs of unweathered mineral material (20). As organic matter accumulates and soils acidify, nutrient cations, including Ca, K, $NH_4$, and Na, are leached away, whereas other nutrients, like phosphorous compounds, are increasingly bound to organic matter and made unavailable to plants (32, 33). In response, vegetation shifts toward plant taxa that are heavily defended with antiherbivory compounds (*SI Appendix*, *SI Text*).

Peat also cools the underlying ground (34), which allows permafrost to rise nearer the surface and it perches the water table there. The resulting combination of increased moisture and colder temperature retards decomposition, reduces nutrient availability, and encourages more peat to form (35). Many regions in northern Eurasia and northwestern North America that supported mammoth steppe during the ice age are today blanketed by peat-rich plant communities (36) incapable of supporting large biomasses of grazing mammals.

**Warm Transitions Were Briefly Optimal Hypothesis.** Guthrie (37) identified the Pleistocene–Holocene transition (12–16 calendar ka B.P.) as a highly favorable time for megafauna (Fig. 2). Guthrie (37) speculated that this was the case because the Pleistocene–Holocene transition was a period of ecological disequilibrium, during which the climate had become warmer and wetter but the vegetation cover had not yet had time to equilibrate with these changes. During this lag period, the edible graminoids and forbs that had dominated the mammoth steppe became more productive and could support more animals. Today, grasses and forbs flourish at tundra sites where soils and vegetation have been disturbed (38, 39) but only until paludification recurs. On the North Slope, 500–700 y are required for peat to accumulate to a steady-state thickness on a previously bare surface of a mineral soil (35). During the ice age, short-lived pulses of high-quality range occurring before either paludification became widespread or full glacial climate resumed may have created transitory bonanzas for megafaunal grazers, which resulted in short-lived peaks in the relative abundance of these animals on the landscape.

## Approach

**Predictions from the Warm Transitions Were Briefly Optimal Hypothesis.** The hypothesis by Guthrie (37) makes a number of predictions that can be addressed using our data and analyses.

*i*) Megafaunal abundance peaked during warm interstadial periods, particularly during their initial stages.
*ii*) In the course of the most recent of these interstadials, the Bølling–Allerød [Greenland Interstadial-1 (GI-1)], megafaunal abundance declined as paludification progressed.

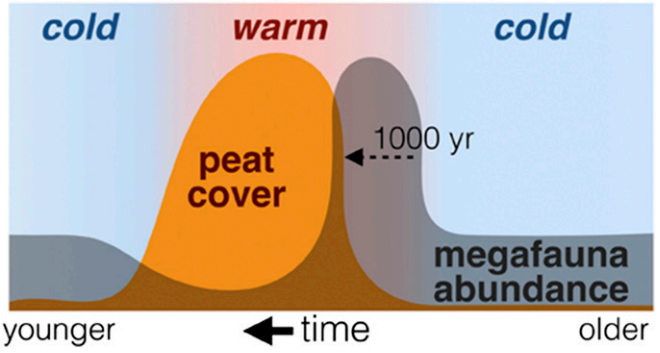


**Fig. 2.** Death by peat? The warm transitions were briefly optimal hypothesis asserts that highest range quality and hence, the largest numbers of megafauna occurred during the initial stages of interstadial (warm) periods before widespread paludification could occur and before climate reverted to full glacial conditions. A short-lived bloom of ruderal plant species provided a grazing bonanza during this transition period, when both soils and climate were relatively warm and moist. Megafauna populations crashed after widespread paludification occurred and moist acidic tundra vegetation became widespread, a process requiring ~1,000 y after an interstadial began (35). Mammoth steppe consisting of sparse grass and forb vegetation was widespread during the colder, drier stadials, when megafauna existed at some intermediate level of abundance. Between 11,700 and 50,000 calendar y B.P., the duration of interstadials varied between 100 and 2,600 y, whereas the intervening cold stadials lasted 500–8,000 y (47).

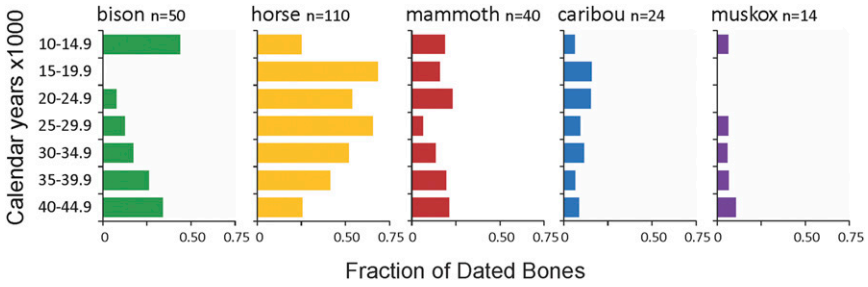


**Fig. 3.** Changes in the relative abundances of megafaunal herbivore taxa on the North Slope of Alaska between 10,000 and 45,000 calendar y B.P. Details of these $^{14}$C dates are given in *SI Appendix*, Table S1.

*iii*) Widespread paludification took place during lengthy interstadials.
*iv*) Megafaunal diets shifted in response to widespread paludification during these long-lasting interstadials.
*v*) Population declines caused by the spread of organic soils during lengthy interstadials caused population bottlenecks among arctic megafauna that are recorded by changes in gene frequencies.

**Distinguishing Calibration Noise in Cumulative Probability Distributions of $^{14}$C Dates.** To test the warm transitions were briefly optimal hypothesis, we need to compare temporal trends in megafaunal abundance with climate records. Cumulative probability distributions (CPDs) of $^{14}$C dates can be informative proxies for changes in abundance through time, and they have been widely used in paleontology, archaeology, and geomorphology (6, 40–42). Unfortunately, the interpretation of CPDs is complicated by artifacts introduced during the calibration of $^{14}$C dates to calendar ages by variations in slope of the curve relating $^{14}$C age to calendar age (42–44) (*SI Appendix*, *SI Text*). Here, we use a Monte Carlo-based approach to separate data-derived peaks in CPDs from calibration-induced noise. This method compares the CPD of a set of real calibrated dates with the CPDs of multiple simulated sets of calibrated dates to identify peaks in bone abundance that are unlikely to result from calibration artifacts. If the warm transitions were briefly optimal hypothesis is correct, peaks in megafaunal abundance should coincide with the warm interstadials, specifically the initial stages of interstadial warming.

## Results

The relative abundances of herbivorous megafaunal species living on the North Slope of Alaska shifted markedly through time (Fig. 3). Horses increased in relative abundance after 40 calendar ka B.P., whereas muskoxen were apparently absent between 15 and 25 calendar ka B.P. along with steppe bison between 15 and 20 calendar ka B.P. The combined CPD of 263 megafaunal bones dating to between 10 and 45 calendar ka B.P. has numerous peaks (Fig. 4). The curve loses some of this spiky character before 30 calendar ka B.P., because the range of possible calibrated ages increases as error terms of individual dates increase.

The Monte Carlo procedure allows us to identify peaks in the bone–abundance curve that are not caused by calibration effects. Eight of the peaks in the CPD rise above the calibration noise at the $P \leq 0.05$ level, suggesting that these eight peaks were times of unusually abundant megafauna (Fig. 4). In general, peaks in megafaunal abundance coincide with warm, mid-Wisconsin interstadials between 30 and 50 calendar ka B.P. The most recent peak in abundance occurred during GI-1e, which in northwest Europe, was manifested as the Bølling–Allerød warm period.

The $\delta^{15}$N values of horse bone collagen reflect dietary changes over time (45). On the North Slope, starting ca. 47 calendar ka B.P. and ending at 10 calendar ka B.P., *Equus* bone collagen $\delta^{15}$N values became increasingly less positive, with values changing from +8‰ to +10‰ between 30 and 47 calendar ka B.P. to from +1‰ to +2‰ at the time of extirpation ca. 12.6 calendar ka B.P. (Fig. 5).

## Discussion

**Comparing Bone Abundance to Climate.** Although peaks in bone abundance generally coincide with warm interstadials, correlations differ slightly according to which proxy record is compared (Fig. 6). Some of these differences are caused by the dating uncertainties present in all of the records, and others probably reflect real differences in how global climate trends were expressed in different regions. Of the three proxy records, methane ($CH_4$) is the most globally applicable because of its rapid mixing in the atmosphere. Compared with the $CH_4$ record, megafauna populations peaked on the North Slope during GI-12, -11, -8, -6–7, -5, -4, and -1. Another bone peak occurred at the outset of GI-2 at ca. 24 calendar ka B.P. (Fig. 6).

Comparison of bone abundances with $\delta^{18}$O records from speleothems in southeast China suggests similar correlations (Fig. 6, *Middle*), with peaks in megafaunal abundance early in GI-1 and -2.

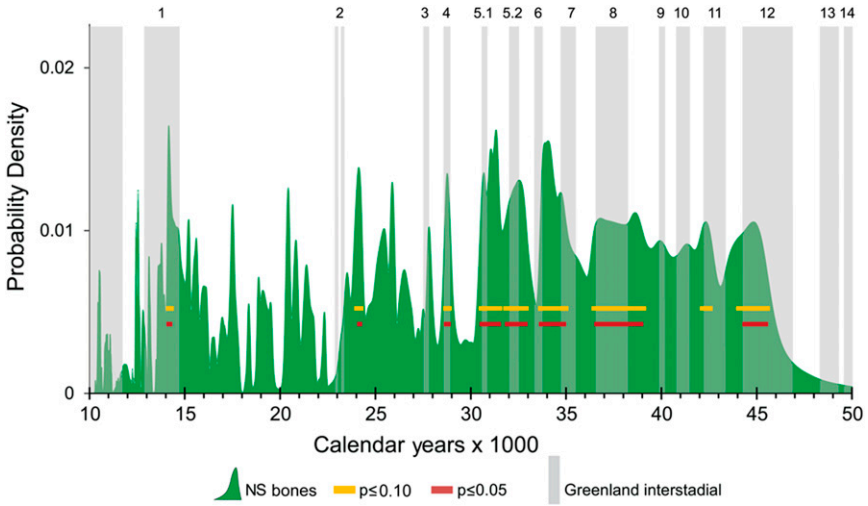


**Fig. 4.** The CPD of 263 calibrated ages of North Slope (NS) megafaunal bones (solid green). Yellow bars mark times when there is a $P \leq 0.10$ of the peaks in bone abundance being explicable as artifacts of the $^{14}$C calibration process. Red bars mark peaks where $P \leq 0.05$. Vertical gray bars depict the Greenland Interstadials (GIs) after Rasmussen et al. (47).

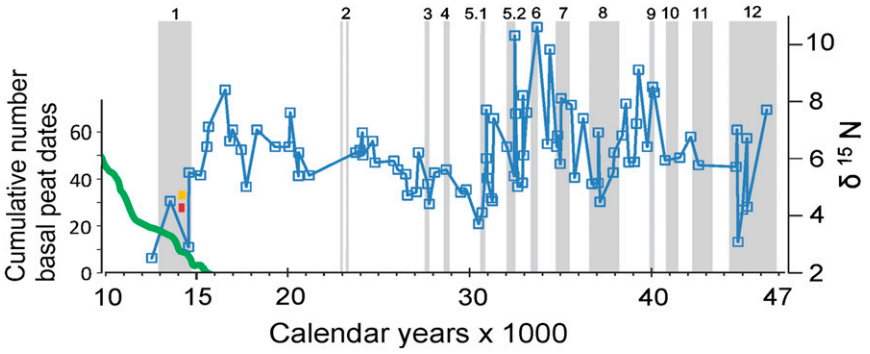


**Fig. 5.** The $\delta^{15}N$ of 90 bones of caballine horses of differing ages from Alaska's North Slope. The numbered columns show the GIs. The green line shows the cumulative number of basal peat dates from Alaska (72). Red and yellow bars show the timing of the bone abundance peak in the early stages of GI-1. Horse diet changed radically as peat spread during GI-1. Similar shifts in diet occurred during some of the earlier interstadials. Bone ages are plotted by their median calibrated ages.

A bone peak ca. 28.5–29 calendar ka B.P. may correlate to the beginning of GI-3, although this particular interstadial is not recorded clearly in the Chinese record. There are suggestions that bone peaks also occurred during the initial stages of GI-11, -8, and -6. Comparisons to the Greenland Ice Core Project (GRIP) $\delta^{18}O$ record suggest that bone peaks occurred during GI-1, -4, -5.1, -5.2, -8, and -12 (Fig. 6, *Bottom*). A bone peak occurred at the onset of GI-2.2, and a similar timing is suggested for GI-5.1 and possibly, GI-10.

**Testing the Warm Transitions Were Briefly Optimal Hypothesis.**

***Prediction 1: Megafaunal abundance peaked during warm interstadial periods, particularly during their initial stages.*** The youngest interstadials, GI-2.2 and -1, are of particular interest because the precision of age control in both the ice-core records and the $^{14}C$ dating technique decline with age (46, 47) (*SI Appendix, SI Text*). The warming trend culminating in GI-2.2 began ca. 24 calendar ka B.P.(Fig. 6). The peak in bone abundance at 23.9–24.3 calendar ka B.P. occurred, therefore, during its earliest stages. In the $CH_4$ and Chinese $\delta^{18}O$ records, peak megafaunal abundance occurred in the initial stages of GI-1. In the GRIP $\delta^{18}O$ record, this same bone peak falls during the warmest part of GI-1 but is still within the first millennium of this lengthy interstadial. These correlations tend to confirm predictions made by the hypothesis by Guthrie (37).

***Prediction 2: In the course of the most recent interstadial, the Bølling–Allerød (GI-1), megafaunal abundance declined as paludification progressed.*** Consistent with this prediction, the bone peak occurring ca. 14 calendar ka B.P. ended ∼1,100 y before GI-1 terminated (Fig. 6). Furthermore, it coincided with the initial rapid spread of peat across the North Slope and preceded the widespread paludification occurring later (Fig. 5) (31).

***Prediction 3: Widespread paludification took place during lengthy interstadials.*** Peat layers dating to mid-Wisconsin interstadials are widespread in both Siberia and Alaska (48). In northwest Alaska, peat layers and elevated percentages of spruce pollen suggest that paludification accompanied the intermittent presence of forests there between 40 and 60 calendar ka B.P. (49). On Siberia's Lena River Delta, buried peat layers date to 32–52 calendar ka B.P. (45). Along the Kolyma River, peat-rich buried soils date to 44–46, 40–43, 36, and 32 calendar ka B.P. (50), and on the New Siberian Islands, buried soils suggest that paludification occurred at 73° N during some mid-Wisconsin interstadials (51). These reports confirm that paludification was widespread in the Arctic during at least some interstadials, suggesting that a short-lived grazing bonanza followed by the spread of peat may have occurred during lengthy (>1,000 y) interstadials.

***Prediction 4: Megafaunal diets shifted in response to widespread paludifcation during lengthy interstadials.*** At the outset of GI-1, the shift from mammoth steppe to the moist tundra vegetation accompanying widespread paludification coincided with a striking change in the diet of horses (Fig. 5). Similar shifts in $\delta^{15}N$ occurred earlier during several of the longest interstadials, including GI-8, which lasted 1,640 y, and GI-12, which lasted 2,580 y (47). Declining $\delta^{15}N$ during interstadials is consistent with paludification's impact on vegetation composition, soil temperature, soil moisture, and rooting depths of plants (10, 52).

***Prediction 5: Population declines caused by the spread of organic soils during lengthy interstadials caused population bottlenecks among arctic megafauna that are recorded by changes in gene frequencies.*** Consistent with this prediction, paleontological records and aDNA indicate that population bottlenecks affected a number of megafaunal species at high latitudes between 36 and 48 calendar ka B.P., the interval that saw some of the longest interstadials. Noncaballine

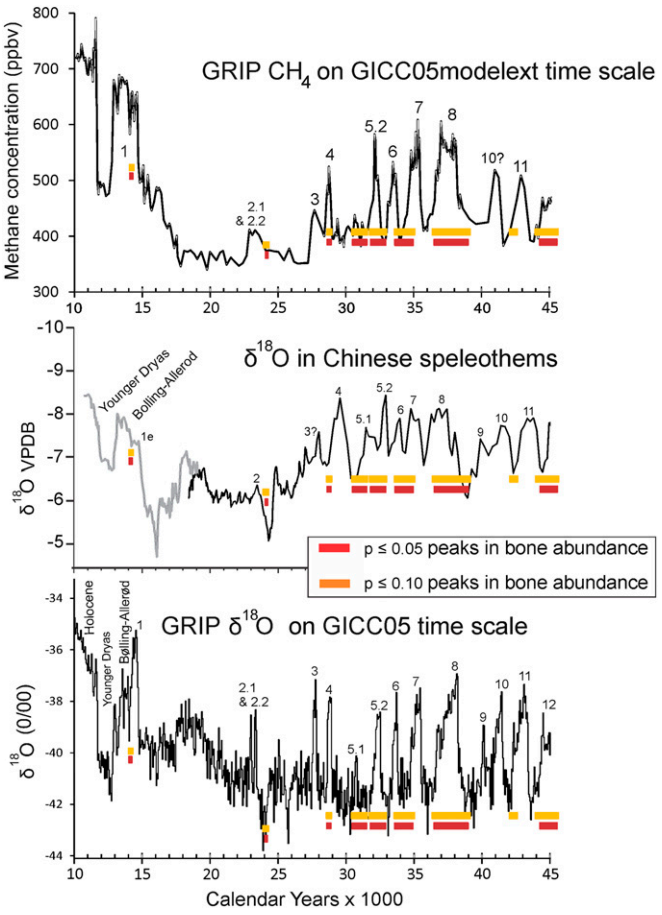


**Fig. 6.** Comparisons between peaks in megafaunal bone abundance and climate proxy records. The terminology and timing of the GIs are from Rasmussen et al. (47). (*Top*) Methane concentrations in the GRIP core (47). (*Middle*) The $\delta^{18}O$ record from Chinese speleothems (73). The dynamics of $\delta^{18}$ in southeast China are dominated by changing evaporative source areas and transport distances of precipitation. (*Bottom*) $\delta^{18}O$ in the GRIP core (47). The close correlation between the $CH_4$ record and the $\delta^{18}O$ record attests to the global extent of the climatic events recorded in Greenland. ppvb, Parts per billion by volume; VPDV, Vienna Pee Dee Belemnite.

horses became extinct in Alaska ca. 36 calendar ka B.P. (53). Based on aDNA, Alaskan brown bears experienced a significant population decline around that same time (54). Ancient DNA further suggests the numbers of steppe bison, horses, and mammoths living at high latitudes decreased markedly 35–45 calendar ka B.P. (3, 55, 56). Also based on aDNA, population bottlenecks affected cave lions sometime after 50 calendar ka B.P. (57) and muskoxen after 48 calendar ka B.P. (3, 58). Although the precise timing of these population bottlenecks remain obscure (13), their occurrence during the mid-Wisconsin interstadials is consistent with the hypothesis by Guthrie (37). We interpret these bottlenecks as side effects of widespread paludification during lengthy interstadials, such as GI-14, -12, and -8.

## Synthesis

Accepting the warm transitions were briefly optimal hypothesis (Fig. 2) leads to new inferences concerning the nature of the mammoth steppe, the biogeography of its megafaunal inhabitants, and the probable causes of their end-Pleistocene extinctions.

**Mammoth Steppe: A Biome Defined by Its Instability.** Concurrence between peaks in numbers of bones and periods of climatic transitions implies the occurrence of boom and bust cycles in ice-age megafaunal populations in arctic Alaska (Fig. 6). Changes in the abundance of taxa through time—for instance, the absence of bison between 15 and 20 calendar ka B.P. (Fig. 3)—suggest the occurrence of regional-scale extinctions followed by recolonization. Megafaunal populations were fluctuating because the ecosystems supporting them were changing. Together with the global climate records (Fig. 6), our data suggest that short-term ($10^1$–$10^3$ y) ecological instability was a characteristic feature of the mammoth steppe in arctic Alaska during the last ice age.

Like an azonal soil that never equilibrates with regional climate and has properties that are, instead, determined by the nature and timing of the last geomorphic or ecological disturbance, the mammoth steppe may have been an azonal biome that never fully equilibrated to any single climate state. If true, this implies that, in addition to being a spatial mosaic of ecosystems (26), the mammoth steppe was also a temporal mosaic with soils, vegetation, and fauna that were chronically engaged in ecological successions triggered by repeated, short-lived, and radical shifts in climate. One reason that no clear analogs of the mammoth steppe exist today may be simply that the degree of climatic instability experienced at high latitudes during the late Pleistocene is absent today.

**Ice-Age Dispersability Imperative.** Survival in an azonal biome requires coping with incessant environmental change, and arctic megafauna may have been forced to play a game of musical chairs across continental distances. Survival would have been especially challenging for populations dependent on either long-distance migration, like some caribou herds are today in northern Alaska, or episodic long-distance dispersal between shifting locations of suitable habitat. In Africa today, the regional persistence of elephant populations depends on episodic dispersals of subpopulations between patches of favorable habitat, often across hundreds of kilometers (59). During some Pleistocene stadials (14), mammoth steppe covered a region three times that of sub-Saharan Africa, and the very un-Holocene tempo of ice-age climate change meant that patches of suitable forage were flickering in and out of existence every few centuries. The imperative may have been to disperse or be extirpated.

**Fatal Intersection of Events.** With this dispersability imperative in mind, the intersection of two events made GI-1 (the Bølling–Allerød) uniquely fatal for megafauna in arctic Alaska. First, paludification had ample time to transform soils and vegetation over this interstadial's 1,800-y span (Fig. 5). Second, relative sea level was rising rapidly, reducing the land area of northern Alaska, weakening the continentality of the climate, and blocking dispersal routes to Siberia.

The degree of isolation between Alaska and Siberia established after 14 calendar ka B.P. was extreme compared with most of the late Pleistocene. The Bering Land Bridge was finally submerged between 12 and 13 calendar ka B.P. (60, 61) when sea level surpassed the −50-m level, a height not reached for the previous 40,000 y. By the early Holocene, relative sea level stood higher along the coast of northern Alaska than it had at any time in the previous 100,000 y (62, 63).

As the Bering Land Bridge was closing, the ice-free corridor between the Cordilleran and Laurentide Ice Sheets was slowly opening. The corridor may have first appeared 13.5–14 calendar ka B.P. (64), but it probably remained ecologically impassable to megafauna until after GI-1 ended ca. 12.9 calendar ka B.P. (55, 65, 66). The end of the last ice age was probably uniquely fatal for arctic megafauna because of the unusual intersection of two events: widespread paludification that drastically reduced range quality for megafaunal grazers and simultaneously hindered their ability to disperse across the resulting soggy landscape and flooding of dispersal routes to Asia before the ice-free corridor leading to lower-latitude North America fully opened.

## Materials and Methods

**$^{14}$C Dating of Bones and Analysis of Bone $\delta^{15}$N.** We dated 496 bones from disarticulated skeletons on Alaska's North Slope (10) (*SI Appendix, SI Text* and Table S1). These bones were in good condition and were identified by their definitive morphological characteristics. In certain instances, temporal and ecological assumptions were used in our identifications (*SI Appendix*, Table S1). Bone collagen was dated by accelerator MS techniques without ultrafiltration (*SI Appendix, SI Text*). We excluded bones with nonfinite ages, bones of extant taxa that were <10 calendar ka B.P. in age, and bones with finite ages >43,500 $^{14}$C y B.P., and included 41 previously published bone dates from the North Slope that met these criteria (10). We therefore use 263 megafaunal bones to make CPDs for comparison with proxy records of climate change. The species composition of these 263 bones is 113 caballine horses, 52 steppe bison, 40 woolly mammoths, 26 caribou, 16 tundra muskoxen, 7 cave lions, 3 moose, 2 wolves (*Canis lupus*), 2 saiga antelope (*Saiga tatarica*), 1 short-faced bear (*Arctodus simus*), and 1 brown bear. We described the changing species composition of the megafauna through time by calculating the percentage of the total number of bones of each taxon where median-calibrated ages fall within 5,000-y age bins between 10 and 45 calendar ka B.P. Smaller bin sizes tended to distort abundance trends because of the spikey nature of the dated bone record. We measured $\delta^{15}$N in bone collagen of $^{14}$C -dated horse bones using an Elemental Analyzer Isotope Mass Spectrometer.

**Distinguishing Calibration Noise in CPDs of $^{14}$C Dates.** Some peaks and valleys in the CPDs of calibrated $^{14}$C dates are artifacts resulting from the calibration process (*SI Appendix, SI Text*). We use a Monte Carlo approach to distinguish which peaks in a CPD of $^{14}$C dates are not caused by calibration noise. We calibrated the $^{14}$C dates using the OxCal program [version 4.2.4 (67)] and the IntCal13 calibration curve (68) to produce a summed CPD. For the simulated datasets, we cannot simply produce sets of randomly chosen $^{14}$C dates; unlike randomly chosen calendar ages, every $^{14}$C age is not equally likely, because randomly chosen $^{14}$C ages are not uniformly distributed in calendar time (*SI Appendix, SI Text*). Instead, we generate 999 sets of 263 random calendar ages using OxCal from the time interval corresponding to 9,310–43,100 $^{14}$C y B.P. Error estimates for each of these simulated dates come from a regression equation relating SD to calendar age in the real bone dataset. We next use the R_Simulate procedure in OxCal to assign a $^{14}$C date and an error term to each of the randomly chosen calendar ages. These simulated $^{14}$C dates are calibrated using R_Simulate to create 999 CPDs containing 263 calibrated dates each in 5-y bins, which then become the Monte Carlo trials against which the CPD of the real $n$ = 263 calendar ages is compared. Finally, we estimate how extreme the upper-tail probability of the actual bone CPD is with respect to the CPDs of the randomly generated dates. We calculate empirical $P$ values by tallying the number of times 999 simulated probability values in each bin equaled or exceeded the bone data values using the relation $P = (r + 1)/(n + 1)$, where $r$ is the number of random values greater than or equal to the observed bone value, and $n$ is the number of randomly generated datasets (69, 70). The timespans where $P \leq 0.05$, for example, define time periods when the bone CPD peaks are different from what would be expected by chance at the $\alpha = 0.05$ level. This procedure allows us to identify peaks in the CPD that warrant comparison with climate proxy data.

**ACKNOWLEDGMENTS.** We thank D. Meltzer and D. Guthrie for useful discussion. Comments by two anonymous reviewers improved an earlier version of this manuscript. This research was supported by grants from the Bureau of Land Management and the National Science Foundation Grants PLR-1417036 and PLR-1417611.

1. Barnosky AD, Koch PL, Feranec RS, Wing SL, Shabel AB (2004) Assessing the causes of late Pleistocene extinctions on the continents. *Science* 306(5693):70–75.
2. Meltzer DJ (2015) Pleistocene overkill and North American mammalian extinctions. *Annu Rev Anthropol*, in press.
3. Lorenzen ED, et al. (2011) Species-specific responses of Late Quaternary megafauna to climate and humans. *Nature* 479(7373):359–364.
4. MacPhee RD, Marx PA (1997) The 40,000-year plague. Humans, hyperdisease, and first-contact extinctions. *Natural Change and Human Impact in Madagascar*, eds Goodman S, Patterson B (Smithsonian Institution, Washington, DC), pp 169–217.
5. Nogués-Bravo D, Rodríguez J, Hortal J, Batra P, Araújo MB (2008) Climate change, humans, and the extinction of the woolly mammoth. *PLoS Biol* 6(4):e79.
6. Nikolskiy PA, Sulerzhitsky LD, Pitulko VV (2011) Last straw versus Blitzkrieg overkill: Climate-driven changes in the Arctic Siberian mammoth population and the Late Pleistocene extinction problem. *Quat Sci Rev* 30(17-18):2309–2328.
7. Stuart AJ, Lister AM (2011) Extinction chronology of the cave lion *Panthera spelaea*. *Quat Sci Rev* 30(17-18):2329–2340.
8. Stuart AJ, Lister AM (2012) Extinction chronology of the woolly rhinoceros *Coelodonta antiquitatis* in the context of late Quaternary megafaunal extinctions in northern Eurasia. *Quat Sci Rev* 51:1–17.
9. MacDonald GM, et al. (2012) Pattern of extinction of the woolly mammoth in Beringia. *Nat Commun* 3:893.
10. Mann DH, Groves P, Kunz ML, Reanier RE, Gaglioti BV (2013) Ice-age megafauna in Arctic Alaska: Extinction, invasion, survival. *Quat Sci Rev* 70:91–108.
11. Roy K, Valentine JW, Jablonski D, Kidwell SM (1996) Scales of climatic variability and time averaging in Pleistocene biotas: Implications for ecology and evolution. *Trends Ecol Evol* 11(11):458–463.
12. Hewitt GM (2004) Genetic consequences of climatic oscillations in the Quaternary. *Philos Trans R Soc Lond B Biol Sci* 359(1442):183–195.
13. Cooper A, et al. (2015) Paleoecology. Abrupt warming events drove Late Pleistocene Holarctic megafaunal turnover. *Science* 349(6248):602–606.
14. Guthrie RD (1990) *Frozen Fauna of the Mammoth Steppe: The Story of Blue Babe* (University of Chicago Press, Chicago).
15. Kunz ML, Reanier RE (1994) Paleoindians in Beringia Evidence from arctic Alaska. *Science* 263(5147):660–662.
16. Goebel T, Waters MR, O'Rourke DH (2008) The late Pleistocene dispersal of modern humans in the Americas. *Science* 319(5869):1497–1502.
17. Hopkins DM, Matthews JV, Schweger CE (1982) *Paleoecology of Beringia* (Academic, New York).
18. Guthrie RD (2001) Origin and causes of the mammoth steppe: A story of cloud cover, woolly mammal tooth pits, buckles, and inside-out Beringia. *Quat Sci Rev* 20(1-3):549–574.
19. Young SB (1982) The vegetation of land-bridge Beringia. *Paleoecology of Beringia*, eds Hopkins DM, Matthews JV, Schweger CE, Young SB (Acedemic, New York), pp 179–194.
20. Walker DA, et al. (2001) Calcium-rich tundra, wildlife, and the "Mammoth Steppe." *Quat Sci Rev* 20(1-3):149–163.
21. Zimov SA, Zimov NS, Chapin FS, III (2012) The past and future of the mammoth steppe ecosystem. *Paleontology in Ecology and Conservation*, ed Louys J (Springer, Berlin), pp 193–225.
22. Ritchie JC, Cwynar LC (1982) The late Quaternary vegetation of the north Yukon. *Paleoecology of Beringia*, eds Hopkins DM, Matthews JV, Schweger CE, Young SB (Academic, New York), pp 113–126.
23. Elias SA, Short SK, Birks HH (1997) Late Wisconsin environments of the Bering Land Bridge. *Palaeogeogr Palaeoclimatol Palaeoecol* 136(1-4):293–308.
24. Elais SA, Berman D, Alfimov A (2000) Late Pleistocene beetle faunas of Beringia: Where east meets west. *J Biogeogr* 27(6):1349–1363.
25. Zazula GD, et al. (2006) Vegetation buried under Dawson tephra (25,300 14C years BP) and locally diverse late Pleistocene paleoenvironments of Goldbottom Creek, Yukon, Canada. *Palaeogeogr Palaeoclimatol Palaeoecol* 242(3-4):253–286.
26. Zazula GD, Froese DG, Elias SA, Kuzmina S, Mathewes RW (2007) Arctic ground squirrels of the mammoth-steppe: Paleoecology of late Pleistocene middens (~24000-29450 14 C yr BP), Yukon Territory, Canada. *Quat Sci Rev* 26(7-8):979–1003.
27. Blinnikov MS, Gaglioti BV, Walker DA, Wooller MJ, Zazula GD (2011) Pleistocene graminoid-dominated ecosystems in the Arctic. *Quat Sci Rev* 30(21-22):2906–2929.
28. Haile J, et al. (2009) Ancient DNA reveals late survival of mammoth and horse in interior Alaska. *Proc Natl Acad Sci USA* 106(52):22352–22357.
29. Mann DH, Reanier RE, Peteet DM, Kunz ML (2001) Environmental change and arctic paleoindians. *Arctic Anthropol* 38(2):119–138.
30. Bartlein PJ, et al. (2015) Early-Holocene warming in Beringia and its mediation by sea-level and vegetation changes. *Clim Past Discuss* 11(2):873–932.
31. Mann DH, Peteet DM, Reanier RE, Kunz ML (2002) Responses of an arctic landscape to late glacial and early Holocene climatic changes: The importance of moisture. *Quat Sci Rev* 21(8-9):997–1021.
32. Chapin FS, III, Matson PA, Vitousek P (2011) *Principles of Terrestrial Ecosystem Ecology* (Springer, Berlin).
33. Mack MC, Schuur EA, Bret-Harte MS, Shaver GR, Chapin FS (2004) Ecosystem carbon storage in arctic tundra reduced by long-term nutrient fertilization. *Nature* 431(7007):440–443.
34. Kade A, Walker DA (2008) Experimental alteration of vegetation on nonsorted circles: Effects on cryogenic activity and implications for climate change in the Arctic. *Arct Antarct Alp Res* 40(1):96–103.
35. Baughman CA, Mann DH, Verbyla D, Kunz ML (2015) Soil-surface organic layers in the Arctic Foothills: Distribution, development, and microclimatic feedbacks. *J Geophys Res: Biogeosci*, in press.
36. Yu Z, Beilman DW, Jones MC (2009) *Sensitivity of Northern Peatland Carbon Dynamics to Holocene Climate Change. Carbon Cycling in Northern Peatlands*, Geophysical Monographs Series (AGU, Washington, DC), Vol 184, pp 55–69.
37. Guthrie RD (2006) New carbon dates link climatic change with human colonization and Pleistocene extinctions. *Nature* 441(7090):207–209.
38. Sumina OI (1994) Plant communities on anthropogenically disturbed sites on the Chukotka Peninsula, Russia. *J Veg Sci* 5(6):885–896.
39. Kade AN, Walker DA, Raynolds MK (2005) Plant communities and soils in cryoturbated tundra along a bioclimate gradient in the Low Arctic, Alaska. *Phytocoenologia* 35(4):761–820.
40. MacPhee RDE, et al. (2002) Radiocarbon chronologies and extinction dynamics of the late Quaternary mammalian megafauna of the Taimyr Peninsula, Russian Federation. *J Archaeol Sci* 29(9):1017–1042.
41. Mann DH, Meltzer DJ (2007) Millennial-scale dynamics of valley fills over the past 12,000 $^{14}$C yr in northeastern New Mexico, USA. *Geol Soc Am Bull* 119:1433–1448.
42. Williams AN (2012) The use of summed radiocarbon probability distributions in archaeology: A review of methods. *J Archaeol Sci* 39(3):578–589.
43. Guilderson TP, Reimer PJ, Brown TA (2005) Geoscience. The boon and bane of radiocarbon dating. *Science* 307(5708):362–364.
44. Contreras DA, Meadows J (2014) Summed radiocarbon calibrations as a population proxy: A critical evaluation using a realistic simulation approach. *J Archaeol Sci* 52:591–608.
45. Schirrmeister L, et al. (2002) Paleoenvironmental and paleoclimatic records from permafrost deposits in the Arctic region of Northern Siberia. *Quat Int* 89(1):97–118.
46. Svensson A, et al. (2008) A 60,000 year Greenland stratigraphic ice core chronology. *Clim Past Discuss* 4(1):47–57.
47. Rasmussen SO, et al. (2014) A stratigraphic framework for abrupt climatic changes during the Last Glacial period based on three synchronized Greenland ice-core records: Refining and extending the INTIMATE event stratigraphy. *Quat Sci Rev* 106:14–28.
48. Lozhkin AV, Anderson PM (2011) Forest or no forest: Implications of the vegetation record for climatic stability in Western Beringia during Oxygen Isotope Stage 3. *Quat Sci Rev* 30(17-18):2160–2181.
49. Wetterich S, et al. (2012) Late quaternary environmental and landscape dynamics revealed by a pingo sequence on the northern Seward Peninsula, Alaska. *Quat Sci Rev* 39:26–44.
50. Zanina OG, Gubin SV, Kuzmina SA, Maximovich SV, Lopatina DA (2011) Late-Pleistocene (MIS 3-2) palaeoenvironments as recorded by sediments, palaeosols, and ground-squirrel nests at Duvanny Yar, Kolyma lowland, northeast Siberia. *Quat Sci Rev* 30(17-18):2107–2123.
51. Andreev AA, et al. (2009) Weichselian and Holocene palaeoenvironmental history of the Bol'shoy Lyakhovsky Island, New Siberian Archipelago, Arctic Siberia. *Boreas* 38(1):72–110.
52. Stevens RE, Hedges REM (2004) Carbon and nitrogen stable isotope analysis of northwest European horse bone and tooth collagen, 40,000 BP-present: Palaeoclimatic interpretations. *Quat Sci Rev* 23(7-8):977–991.
53. Guthrie RD (2003) Rapid body size decline in Alaskan Pleistocene horses before extinction. *Nature* 426(6963):169–171.
54. Barnes I, Matheus P, Shapiro B, Jensen D, Cooper A (2002) Dynamics of Pleistocene population extinctions in Beringian brown bears. *Science* 295(5563):2267–2270.
55. Shapiro B, et al. (2004) Rise and fall of the Beringian steppe bison. *Science* 306(5701):1561–1565.
56. Debruyne R, et al. (2008) Out of America: Ancient DNA evidence for a new world origin of late quaternary woolly mammoths. *Curr Biol* 18(17):1320–1326.
57. Barnett R, et al. (2009) Phylogeography of lions (*Panthera leo* ssp.) reveals three distinct taxa and a late Pleistocene reduction in genetic diversity. *Mol Ecol* 18(8):1668–1677.
58. Campos PF, et al. (2010) Ancient DNA analyses exclude humans as the driving force behind late Pleistocene musk ox (*Ovibos moschatus*) population dynamics. *Proc Natl Acad Sci USA* 107(12):5675–5680.
59. van Aarde RJ, Jackson TP (2007) Megaparks for metapopulations: Addressing the causes of locally high elephant numbers in southern Africa. *Biol Conserv* 134(3):289–297.
60. Brigham-Grette J, Gualtieri L (2004) Response to Grosswald and Hughes (2004), Brigham-Grette et al. (2003), "Chlorine-36 and 14C chronology support a limited last glacial maximum across central Chukotka, northeastern Siberia, and no Beringian ice sheet," and Gualtieri et al. (2003), "Pleistocene raised marine deposits on Wrangel Island, northeastern Siberia: Implications for Arctic ice sheet history." *Quat Sci Res* 62(2):227–232.
61. Keigwin LD, Donnelly JP, Cook MS, Driscoll NW, Brigham-Grette J (2006) Rapid sea-level rise and Holocene climate in the Chukchi Sea. *Geology* 34(10):861–864.
62. Waelbroeck C, et al. (2002) Sea-level and deep water temperature changes derived from benthic foraminifera isotopic records. *Quat Sci Rev* 21(1-3):295–305.
63. Hu A, et al. (2010) Influence of Bering Strait flow and North Atlantic circulation on glacial sea-level changes. *Nat Geosci* 3:118–121.
64. Dyke AS (2004) An outline of North American deglaciation wiwth emphasis on central and northern Canada. *Quaternary Glaciations—Extent and Chronology, Part II: North America*, eds Ehlers J, Gibbard PL (Elsevier, Amsterdam), pp 373–424.
65. Burns JA (1996) Vertebrate paleontology and the alleged ice-free corridor: The meat of the matter. *Quat Int* 32:107–112.
66. Burns JA (2010) Mammalian faunal dynamics in late Pleistocene Alberta, Canada. *Quat Int* 217(1-2):37–42.
67. Bronk Ramsey C (2009) Bayesian analysis of radiocarbon dates. *Radiocarbon* 51(1):337–360.
68. Reimer PJ, et al. (2013) IntCal13 and Marine13 radiocarbon age calibration curves 0-50,000 years cal BP. *Radiocarbon* 55(4):1869–1887.
69. Davison AC, Hinkley DV (1997) *Bootstrap Methods and Their Applications* (Cambridge Univ Press, Cambridge, United Kingdom).
70. North BV, Curtis D, Sham PC (2002) A note on the calculation of empirical P values from Monte Carlo procedures. *Am J Hum Genet* 71(2):439–441.
71. Brigham-Grette J, Lozhkin AV, Anderson PM, Glushkova O (2004) Paloenvironmental conditions in Western Beringia before and during the Last Glacial Maximum. *Entering America: Northeast Asia and Beringia Before the Last Glacial Maximum*, ed Madsen DB (University of Utah Press, Salt Lake City), pp 29–61.
72. Jones MC, Yu Z (2010) Rapid deglacial and early Holocene expansion of peatlands in Alaska. *Proc Natl Acad Sci USA* 107(16):7347–7352.
73. Wang YJ, et al. (2001) A high-resolution absolute-dated late Pleistocene monsoon record from Hulu Cave, China. *Science* 294(5550):2345–2348.

*Supporting information for*

# LIFE AND EXTINCTION OF MEGAFAUNA IN THE ICE-AGE ARCTIC

***Authors***: Daniel H. Mann[1], Pamela Groves[2], Richard E. Reanier[3], Benjamin V. Gaglioti[4,] Michael L. Kunz[5], Beth Shapiro[6]

***Authors affiliations***:

[1]*Geosciences Department, University of Alaska, Fairbanks, AK 99775*

[2]*Institute of Arctic Biology, University of Alaska, Fairbanks, AK 99775*

[3]*Reanier & Associates, Inc., 1215 SW 170th Street, Seattle, WA 98166*

[4]*Water and Environmental Research Center, University of Alaska, Fairbanks, AK 99775*

[5]*Cooperative Extension and Resources, University of Alaska, Fairbanks, AK 99775*

[6]*Department of Ecology and Evolutionary Biology and UCSC Genomics Institute, University of California Santa Cruz, Santa Cruz, CA 9506*

# 1: $^{14}$C AGES OF ALASKAN NORTH SLOPE MEGAFAUNA USED IN THIS STUDY

| *Genus* | *species* | field ID | depository[a] | catalog number | skeletal element | $^{14}$CLab[#] and number | $^{14}$C date reported (yrs BP) | | $\delta^{13}$C ‰ (VPDB) | $\delta^{15}$N ‰ (AIR) | $\delta^{13}$C-normalized date used for calibration | | 95.4% calibrated range | | used in Monte Carlo (x) | source |
|---|---|---|---|---|---|---|---|---|---|---|---|---|---|---|---|---|
| | | | | | | | $^{14}$C date | std dev[e] | | | $^{14}$C date | std dev[e] | (cal yr BP)[f] | | | |
| *Alces* | *alces* | KIG05-4.1 | UAMES | 30186 | antler | Beta-339266 | modern | - | -23.40 | 0.50 | - | - | - | - | | (1) |
| *Alces* | *alces* | MAY12-64 | UAMES | 30187 | antler | Beta-339275 | modern | - | -21.30 | 0.60 | - | - | - | - | | (1) |
| *Alces* | *alces* | IK08-129 | UAMES | 30181 | antler | Beta-339280 | 210 | 30 | -20.80 | 0.70 | 210 | 30 | ... | 305 | | (1) |
| *Alces* | *alces* | TIT10-58 | UAMES | 30188 | antler | Beta-339271 | 290 | 30 | -20.70 | 0.90 | 290 | 30 | 288 | 458 | | (1) |
| *Alces* | *alces* | IK12-094 | UAMES | 30184 | antler | Beta-339281 | 310 | 30 | -21.10 | -0.40 | 310 | 30 | 301 | 465 | | (1) |
| *Alces* | *alces* | IK02-210 | UAMES | 10355 | mandible | CAMS-91966 | 320 | 35 | -20.30 | 0.26 | 320 | 35 | 304 | 474 | | (1) |
| *Alces* | *alces* | IK01-404 | UAMES | 11844 | mandible | CAMS-92094 | 665 | 35 | -20.87 | -0.59 | 665 | 35 | 556 | 678 | | (1) |
| *Alces* | *alces* | IK12-077 | UAMES | 30183 | cranium | Beta-339274 | 950 | 30 | -20.70 | 1.00 | 950 | 30 | 795 | 926 | | (1) |
| *Alces* | *alces* | IK99-229 | UAMES | 10691 | mandible | CAMS-64459 | 980 | 40 | -20.00 | 8.56 | 980 | 40 | 795 | 959 | | (1) |
| *Alces* | *alces* | IK08-016 | UAMES | 30180 | mandible | Beta-339268 | 1,180 | 30 | -21.30 | 1.80 | 1,180 | 30 | 999 | 1,221 | | (1) |
| *Alces* | *alces* | IK99-393 | n/a | n/a | metatarsal | Beta-134225 | 1,280 | 40 | -19.50 | n/a | 1,280 | 40 | 1,086 | 1,294 | | (1) |
| *Alces* | *alces* | IK99-776 | UAMES | 11066 | mandible | CAMS-64474 | 1,370 | 40 | -20.40 | 1.33 | 1,370 | 40 | 1,186 | 1,351 | | (1) |
| *Alces* | *alces* | IK99-556 | UAMES | 10996 | mandible | CAMS-64467 | 1,760 | 40 | -19.85 | 0.68 | 1,760 | 40 | 1,566 | 1,810 | | (1) |
| *Alces* | *alces* | IK01-023 | UAMES | 12022 | mandible | CAMS-92076 | 2,450 | 35 | -20.77 | 0.99 | 2,450 | 35 | 2,360 | 2,705 | | (1) |
| *Alces* | *alces* | GAAR-7846 | n/a | n/a | n.r.[b] | CAMS-58096 | 2,460 | 40 | -21.00 | n/a | 2,460 | 40 | 2,364 | 2,710 | | (1) |
| *Alces* | *alces* | IK98-0888 | UAMES | 3288 | mandible | CAMS-64418 | 2,540 | 50 | -20.26 | n/a | 2,540 | 50 | 2,464 | 2,756 | | (1) |
| *Alces* | *alces* | IK12-096 | UAMES | 30185 | antler | Beta-339282 | 2,790 | 30 | -21.30 | -0.60 | 2,790 | 30 | 2,795 | 2,960 | | (1) |
| *Alces* | *alces* | KIG09-2 | n/a | n/a | cranium | Beta-263035 | 2,900 | 40 | -21.10 | n/a | 2,900 | 40 | 2,925 | 3,165 | | (1) |
| *Alces* | *alces* | TIT12-35 | UAMES | 30191 | antler | Beta-339283 | 9,310 | 40 | -20.30 | -1.20 | 9,310 | 40 | 10,303 | 10,654 | x | (1) |
| *Alces* | *alces* | IK09-70 | UAMES | 30182 | antler | Beta-339270 | 9,610 | 40 | -21.00 | 0.90 | 9,610 | 40 | 10,775 | 11,161 | x | (1) |
| *Alces* | *alces* | IK99-472 | UAMES | 10922 | tooth | CAMS-91810 | 12,245 | 40 | -20.30 | -0.13 | 12,245 | 40 | 14,000 | 14,314 | x | (1) |
| *Arctodus* | *simus* | ROM:VP 43646 | n/a | n/a | n.r.[b] | TO-2539 | 27,190 | 280 | n/a | n/a | 27,190 | 280 | 30,805 | 31,530 | x | (2) |
| *Arctodus* | *simus* | T99-033 | UAMES | 8685 | metapodial | CAMS-58092[c] | 42,600 | 2,200 | -19.00 | n/a | 42,600 | 2,200 | 43,570 | ... | | (1) |
| *Arctodus* | *simus* | T99-033 | UAMES | 8685 | metapodial | CAMS-58095[c] | 46,500 | 3,600 | -18.60 | n/a | 46,500 | 3,600 | 41,365 | 64,621 | | (1) |
| *Bison* | *priscus* | IK98-0343 | UAMES | 9079 | humerus | CAMS-53767 | 10,510 | 50 | -20.61 | 2.84 | 10,510 | 50 | 12,173 | 12,644 | x | (1) |
| *Bison* | *priscus* | IK98-1114 | UAMES | 9896 | astragalus | CAMS-53891 | 10,990 | 50 | -20.10 | 2.65 | 10,990 | 50 | 12,729 | 12,996 | x | (1) |

| *Genus* | *species* | field ID | depository[a] | catalog number | skeletal element | $^{14}$CLab[#] and number | $^{14}$C date reported (yrs BP) | | $\delta^{13}$C ‰ (VPDB) | $\delta^{15}$N ‰ (AIR) | $\delta^{13}$C-normalized date used for calibration | | 95.4% calibrated range | | used in Monte Carlo (x) | source |
|---|---|---|---|---|---|---|---|---|---|---|---|---|---|---|---|---|
| | | | | | | | $^{14}$C date | std dev[e] | | | $^{14}$C date | std dev[e] | (cal yr BP)[f] | | | |
| *Bison* | *priscus* | IK98-0027 | UAMES | 8847 | astragalus | CAMS-53756 | 11,810 | 50 | -20.71 | 2.63 | 11,810 | 50 | 13,485 | 13,756 | x | (1) |
| *Bison* | *priscus* | IK98-0528 | UAMES | 9577 | humerus | CAMS-53774 | 12,270 | 50 | -20.21 | 4.10 | 12,270 | 50 | 14,011 | 14,487 | x | (1) |
| *Bison* | *priscus* | IK98-0303 | n/a | n/a | vertebra | CAMS-58091 | 12,320 | 60 | -20.24 | 3.69 | 12,320 | 60 | 14,070 | 14,686 | x | (1) |
| *Bison* | *priscus* | IK98-0142 | UAMES | 8801 | metatarsal | CAMS-53760 | 12,410 | 50 | -19.98 | 2.66 | 12,410 | 50 | 14,168 | 14,846 | x | (1) |
| *Bison* | *priscus* | IK01-428 | UAMES | 11664 | astragalus | AA-48281 | 12,560 | 130 | -20.00 | 2.66 | 12,560 | 130 | 14,218 | 15,247 | x | (1) |
| *Bison* | *priscus* | IK98-0661 | UAMES | 9464 | metapodial | CAMS-53777 | 17,160 | 80 | -20.18 | 2.82 | 17,160 | 80 | 20,476 | 20,946 | x | (1) |
| *Bison* | *priscus* | IK98-0504 | UAMES | 9238 | femur | CAMS-53772 | 19,420 | 100 | -19.97 | 3.84 | 19,420 | 100 | 23,046 | 23,682 | x | (1) |
| *Bison* | *priscus* | IK98-1090 | UAMES | 9804 | astragalus | CAMS-53890 | 21,040 | 120 | -20.04 | 6.45 | 21,040 | 120 | 25,093 | 25,679 | x | (1) |
| *Bison* | *priscus* | IK98-0401 | UAMES | 8842 | metatarsal | CAMS-53770 | 21,530 | 130 | -20.37 | 4.35 | 21,530 | 130 | 25,591 | 26,051 | x | (1) |
| *Bison* | *priscus* | IK98-1254 | UAMES | 9967 | humerus | CAMS-53901 | 23,680 | 170 | -19.85 | 5.50 | 23,680 | 170 | 27,495 | 28,111 | x | (1) |
| *Bison* | *priscus* | IK98-0302 | UAMES | 8998 | metatarsal | CAMS-53764 | 24,500 | 180 | -20.22 | 4.31 | 24,500 | 180 | 28,092 | 28,920 | x | (1) |
| *Bison* | *priscus* | IK98-1184 | UAMES | 10031 | horn core | CAMS-53899 | 25,980 | 230 | -19.70 | 4.16 | 25,980 | 230 | 29,604 | 30,779 | x | (1) |
| *Bison* | *priscus* | IK98-1043 | UAMES | 10043 | astragalus | CAMS-53888 | 26,550 | 230 | -19.46 | 5.66 | 26,550 | 230 | 30,363 | 31,129 | x | (1) |
| *Bison* | *priscus* | IK98-0095 | UAMES | 9206 | tibia | CAMS-53758 | 27,400 | 260 | -20.56 | 4.57 | 27,400 | 260 | 30,924 | 31,706 | x | (1) |
| *Bison* | *priscus* | IK98-0374 | n/a | n/a | metatarsal | CAMS-53768 | 27,590 | 280 | -20.48 | 2.65 | 27,590 | 280 | 30,998 | 32,142 | x | (1) |
| *Bison* | *priscus* | IK05-18.1 | UAMES | 29449 | cranium | Beta-308262 | 27,600 | 140 | -20.10 | n/a | 27,600 | 140 | 31,126 | 31,620 | x | (1) |
| *Bison* | *priscus* | IK98-1115 | UAMES | 9897 | astragalus | CAMS-53892 | 28,120 | 290 | -19.32 | 4.82 | 28,120 | 290 | 31,329 | 32,843 | x | (1) |
| *Bison* | *priscus* | IK98-0616 | UAMES | 9648 | metacarpal | CAMS-53775 | 29,040 | 340 | -20.20 | 5.17 | 29,040 | 340 | 32,228 | 33,926 | x | (1) |
| *Bison* | *priscus* | IK98-1164 | UAMES | 10073 | metacarpal | CAMS-53897 | 29,570 | 340 | -20.02 | 5.00 | 29,570 | 340 | 32,999 | 34,362 | x | (1) |
| *Bison* | *priscus* | IK98-0430 | UAMES | 9038 | metacarpal | CAMS-53771 | 30,000 | 540 | -20.00 | n/a | 30,000 | 540 | 33,059 | 35,128 | x | (1) |
| *Bison* | *priscus* | IK98-0256 | UAMES | 9156 | metatarsal | CAMS-53763 | 31,410 | 420 | -20.35 | 4.23 | 31,410 | 420 | 34,578 | 36,209 | x | (1) |
| *Bison* | *priscus* | IK98-0096 | UAMES | 9207 | tibia | CAMS-53759 | 31,630 | 440 | -19.85 | 4.89 | 31,630 | 440 | 34,684 | 36,430 | x | (1) |
| *Bison* | *priscus* | IK98-1035 | UAMES | 9988 | humerus | CAMS-53885 | 32,270 | 470 | -19.64 | 5.34 | 32,270 | 470 | 35,151 | 37,726 | x | (1) |
| *Bison* | *priscus* | IK01-215 | UAMES | 11742 | metatarsal | AA-48772 | 32,300 | 1,500 | -20.20 | 4.43 | 32,300 | 1,500 | 33,894 | 40,602 | x | (1) |
| *Bison* | *priscus* | IK09-15 | UAMES | 29454 | cranium | Beta-308267 | 32,870 | 200 | -19.90 | n/a | 32,870 | 200 | 36,302 | 37,701 | x | (1) |
| *Bison* | *priscus* | IK01-433 | UAMES | 11669 | radius | AA-48282 | 33,000 | 1,500 | -19.90 | 3.45 | 33,000 | 1,500 | 34,550 | 41,204 | x | (1) |
| *Bison* | *priscus* | IK98-0012 | UAMES | 9172 | femur | CAMS-53755 | 33,280 | 530 | -19.43 | 3.50 | 33,280 | 530 | 36,231 | 38,781 | x | (1) |
| *Bison* | *priscus* | IK98-1323 | UAMES | 9877 | femur | CAMS-53903 | 33,320 | 540 | -20.19 | 4.40 | 33,320 | 540 | 36,241 | 38,847 | x | (1) |
| *Bison* | *priscus* | IK01-460 | UAMES | 11934 | astragalus | AA-48775 | 33,520 | 940 | -19.90 | 5.13 | 33,520 | 940 | 35,750 | 40,210 | x | (1) |
| *Bison* | *priscus* | IK98-1121 | UAMES | 11159 | metacarpal | CAMS-53894 | 33,580 | 550 | -19.63 | 3.84 | 33,580 | 550 | 36,409 | 39,200 | x | (1) |
| *Bison* | *priscus* | IK01-234 | UAMES | 11947 | astragalus | AA-48773 | 34,100 | 1,000 | -20.00 | 5.92 | 34,100 | 1,000 | 36,273 | 40,970 | x | (1) |

| *Genus* | *species* | field ID | depository[a] | catalog number | skeletal element | $^{14}$CLab[#] and number | $^{14}$C date reported (yrs BP) | | $\delta^{13}$C ‰ (VPDB) | $\delta^{15}$N ‰ (AIR) | $\delta^{13}$C-normalized date used for calibration | | 95.4% calibrated range | | used in Monte Carlo (x) | source |
|---|---|---|---|---|---|---|---|---|---|---|---|---|---|---|---|---|
| | | | | | | | $^{14}$C date | std dev[e] | | | $^{14}$C date | std dev[e] | (cal yr BP)[f] | | | |
| *Bison* | *priscus* | TIT11-88 | UAMES | 29460 | cranium | Beta-308271 | 34,440 | 240 | -20.10 | n/a | 34,440 | 240 | 38,455 | 39,553 | x | (1) |
| *Bison* | *priscus* | IK05-18.2 | UAMES | 29450 | cranium | Beta-308263 | 35,060 | 250 | -20.50 | n/a | 35,060 | 250 | 38,952 | 40,228 | x | (1) |
| *Bison* | *priscus* | IK98-0659 | UAMES | 9462 | mandible | CAMS-53776 | 35,580 | 720 | -19.98 | 4.56 | 35,580 | 720 | 38,762 | 41,626 | x | (1) |
| *Bison* | *priscus* | IK98-0916 | UAMES | 9348 | astragalus | CAMS-53782 | 35,710 | 730 | -20.29 | 4.19 | 35,710 | 730 | 38,863 | 41,740 | x | (1) |
| *Bison* | *priscus* | IK98-1222 | UAMES | 9899 | metatarsal | CAMS-53900 | 36,320 | 780 | -20.77 | 5.70 | 36,320 | 780 | 39,422 | 42,270 | x | (1) |
| *Bison* | *priscus* | IK01-373 | UAMES | 11981 | astragalus | AA-48278 | 36,500 | 2,300 | -20.00 | 6.37 | 36,500 | 2,300 | 36,515 | 47,157 | x | (1) |
| *Bison* | *priscus* | IK98-0863 | UAMES | 9327 | astragalus | CAMS-53914 | 36,520 | 800 | -20.60 | 4.51 | 36,520 | 800 | 39,603 | 42,435 | x | (1) |
| *Bison* | *priscus* | IK98-1120 | UAMES | 9906 | metatarsal | CAMS-53893 | 37,460 | 890 | -20.70 | 6.66 | 37,460 | 890 | 40,314 | 43,280 | x | (1) |
| *Bison* | *priscus* | IK11-37 | UAMES | 29457 | cranium | Beta-306117 | 38,010 | 370 | -19.40 | n/a | 38,010 | 370 | 41,739 | 42,765 | x | (1) |
| *Bison* | *priscus* | IK08-31 | UAMES | 29452 | cranium | Beta-308265 | 38,150 | 330 | -20.20 | n/a | 38,150 | 330 | 41,877 | 42,800 | x | (1) |
| *Bison* | *priscus* | IK98-0377 | UAMES | 8811 | radius | CAMS-53769 | 38,700 | 1,000 | -19.89 | 4.46 | 38,700 | 1,000 | 41,431 | 44,679 | x | (1) |
| *Bison* | *priscus* | IK98-0889 | UAMES | 9343 | astragalus | CAMS-53779 | 38,800 | 1,100 | -20.31 | 3.66 | 38,800 | 1,100 | 41,382 | 45,006 | x | (1) |
| *Bison* | *priscus* | IK98-0890 | UAMES | 9532 | astragalus | CAMS-53780 | 38,800 | 1,100 | -20.42 | 5.26 | 38,800 | 1,100 | 41,382 | 45,006 | x | (1) |
| *Bison* | *priscus* | IK98-0915 | UAMES | 9347 | astragalus | CAMS-53781 | 39,800 | 1,200 | -20.34 | 4.51 | 39,800 | 1,200 | 41,976 | 46,005 | x | (1) |
| *Bison* | *priscus* | IK98-0174 | UAMES | 8931 | astragalus | CAMS-53761 | 39,850 | 1,200 | -20.42 | 4.50 | 39,850 | 1,200 | 42,006 | 46,046 | x | (1) |
| *Bison* | *priscus* | IK98-1122 | UAMES | 9919 | metacarpal | CAMS-53895 | 40,700 | 1,300 | -20.03 | 4.30 | 40,700 | 1,300 | 42,415 | 47,266 | x | (1) |
| *Bison* | *priscus* | IK09-16 | UAMES | 29455 | cranium | Beta-308268 | 42,000 | 490 | -19.60 | n/a | 42,000 | 490 | 44,505 | 46,280 | x | (1) |
| *Bison* | *priscus* | TIT10-09 | UAMES | 29459 | cranium | Beta-308270 | 42,400 | 520 | -20.10 | n/a | 42,400 | 520 | 44,781 | 46,761 | x | (1) |
| *Bison* | *priscus* | IK98-1045 | UAMES | 10045 | mandible | CAMS-53889 | 43,000 | 1,800 | -20.21 | 4.15 | 43,000 | 1,800 | 44,215 | 49,997 | x | (1) |
| *Bison* | *priscus* | IK10-12 | UAMES | 29456 | cranium | Beta-308269 | 44,520 | 650 | -20.00 | n/a | 44,520 | 650 | 46,411 | 49,481 | | (1) |
| *Bison* | *priscus* | IK98-1042 | n/a | n/a | radius | CAMS-53887 | 44,800 | 2,200 | -19.59 | 3.48 | 44,800 | 2,200 | 45,320 | ... | | (1) |
| *Bison* | *priscus* | IK98-1125 | UAMES | 9923 | astragalus | CAMS-53896 | 45,300 | 2,400 | -20.01 | 4.53 | 45,300 | 2,400 | 45,489 | ... | | (1) |
| *Bison* | *priscus* | IK06-22 | UAMES | 29451 | cranium | Beta-308264 | 45,610 | 740 | -20.10 | n/a | 45,610 | 740 | 47,591 | ... | | (1) |
| *Bison* | *priscus* | IK98-0032 | UAMES | 9090 | metacarpal | CAMS-53757 | 46,100 | 2,200 | -20.61 | 3.26 | 46,100 | 2,200 | 46,180 | ... | | (1) |
| *Bison* | *priscus* | IK98-0305 | UAMES | 8917 | radius | CAMS-53766 | 46,100 | 2,600 | -20.10 | 5.65 | 46,100 | 2,600 | 45,831 | ... | | (1) |
| *Bison* | *priscus* | IK09-14 | UAMES | 29453 | cranium | Beta-308266 | 46,280 | 810 | -19.00 | n/a | 46,280 | 810 | 48,108 | ... | | (1) |
| *Bison* | *priscus* | IK98-0671 | UAMES | 9303 | metatarsal | CAMS-53778 | 47,000 | 2,900 | -20.46 | 6.15 | 47,000 | 2,900 | 42,341 | 59,391 | | (1) |
| *Bison* | *priscus* | IK98-0928 | UAMES | 9506 | astragalus | CAMS-53783 | 49,600 | 4,000 | -20.25 | -3.27 | 49,600 | 4,000 | 44,325 | 70,774 | | (1) |
| *Bison* | *priscus* | IK01-216 | UAMES | 11743 | metatarsal | OxA-11136 | 49,700 | 1,400 | -19.80 | n/a | 49,700 | 1,400 | 47,230 | 53,285 | | (3) |
| *Bison* | *priscus* | IK98-0527 | UAMES | 9567 | vertebra | CAMS-53773 | 50,000 | 4,200 | -20.70 | 2.66 | 50,000 | 4,200 | 44,676 | 72,630 | | (1) |
| *Bison* | *priscus* | IK01-074 | UAMES | 11863 | metatarsal | AA-48770 | >38,000 | | -20.00 | 5.78 | >38,000 | | n/a | n/a | | (1) |

| *Genus* | *species* | field ID | depository[a] | catalog number | skeletal element | $^{14}$CLab[#] and number | $^{14}$C date reported (yrs BP) | | $\delta^{13}$C ‰ (VPDB) | $\delta^{15}$N ‰ (AIR) | $\delta^{13}$C-normalized date used for calibration | | 95.4% calibrated range | | used in Monte Carlo (x) | source |
|---|---|---|---|---|---|---|---|---|---|---|---|---|---|---|---|---|
| | | | | | | | $^{14}$C date | std dev[e] | | | $^{14}$C date | std dev[e] | (cal yr BP)[f] | | | |
| *Bison* | *priscus* | IK99-501 | UAMES | 10881 | metatarsal | AA-48766 | >39,000 | | -20.40 | 3.98 | >39,000 | | n/a | n/a | | (1) |
| *Bison* | *priscus* | IK99-145 | UAMES | 10738 | cranium | AA-48262 | >39,400 | | -19.10 | 3.95 | >39,400 | | n/a | n/a | | (1) |
| *Bison* | *priscus* | IK01-315 | UAMES | 11687 | metacarpal | AA-48774 | >40,000 | | -19.50 | 7.64 | >40,000 | | n/a | n/a | | (1) |
| *Bison* | *priscus* | IK99-717 | UAMES | 11226 | astragalus | AA-48247 | >40,300 | | -19.70 | n/a | >40,300 | | n/a | n/a | | (1) |
| *Bison* | *priscus* | IK01-098 | UAMES | 11770 | metatarsal | AA-48270 | >40,700 | | -19.70 | 5.87 | >40,700 | | n/a | n/a | | (1) |
| *Bison* | *priscus* | IK01-143 | UAMES | 11943 | metatarsal | AA-48248 | >40,900 | | -19.99 | 6.56 | >40,900 | | n/a | n/a | | (1) |
| *Bison* | *priscus* | IK01-095 | UAMES | 11701 | metacarpal | AA-48269 | >41,000 | | -19.20 | 4.91 | >41,000 | | n/a | n/a | | (1) |
| *Bison* | *priscus* | IK01-260 | UAMES | 12012 | radius | AA-48274 | >41,000 | | -19.80 | 6.50 | >41,000 | | n/a | n/a | | (1) |
| *Bison* | *priscus* | IK99-141 | UAMES | 11142 | astragalus | AA-48243 | >41,100 | | -19.16 | 2.80 | >41,100 | | n/a | n/a | | (1) |
| *Bison* | *priscus* | IK01-065 | UAMES | 11855 | astragalus | AA-48266 | >41,100 | | -20.40 | 4.26 | >41,100 | | n/a | n/a | | (1) |
| *Bison* | *priscus* | IK01-088 | UAMES | 11676 | metatarsal | AA-48268 | >41,100 | | -20.20 | 6.47 | >41,100 | | n/a | n/a | | (1) |
| *Bison* | *priscus* | IK99-530 | UAMES | 10858 | metacarpal | AA-48767 | >41,100 | | -19.80 | 6.89 | >41,100 | | n/a | n/a | | (1) |
| *Bison* | *priscus* | IK99-567 | UAMES | 11233 | astragalus | AA-48246 | >41,500 | | -20.30 | 6.23 | >41,500 | | n/a | n/a | | (1) |
| *Bison* | *priscus* | TIT11-92 | UAMES | 29461 | cranium | Beta-306118 | >43,500 | | -18.10 | n/a | >43,500 | | n/a | n/a | | (1) |
| *Bison* | *priscus* | IK12-001 | UAMES | 29458 | skeleton | Beta-324600 | >43,500 | | -20.00 | 4.20 | >43,500 | | n/a | n/a | | (1) |
| *Bison* | *priscus* | IK98-0218 | UAMES | 8851 | astragalus | CAMS-53762 | >46,600 | | -20.40 | 2.69 | >46,600 | | n/a | n/a | | (1) |
| *Bison* | *priscus* | IK98-1041 | UAMES | 10041 | radius | CAMS-53886 | >48,500 | | -19.52 | 4.04 | >48,500 | | n/a | n/a | | (1) |
| *Bison* | *priscus* | IK98-1299 | UAMES | 9819 | ulna | CAMS-53902 | >49,500 | | -20.05 | 3.30 | >49,500 | | n/a | n/a | | (1) |
| *Bison* | *priscus* | IK98-1015 | UAMES | 9912 | horn core | CAMS-53784 | >49,900 | | -20.36 | 2.03 | >49,900 | | n/a | n/a | | (1) |
| *Bison* | *priscus* | IK98-1167 | UAMES | 10090 | astragalus | CAMS-53898 | >49,900 | | -20.20 | 4.86 | >49,900 | | n/a | n/a | | (1) |
| *Canis* | *lupus* | TIT10-60 | UAMES | 30193 | mandible | Beta-339272 | 13,000 | 50 | -18.10 | 7.10 | 13,000 | 50 | 15,316 | 15,766 | x | (1) |
| *Canis* | *lupus* | IK99-702 | UAMES | 11055 | mandible | CAMS-58094 | 37,200 | 1,100 | -21.20 | n/a | 37,200 | 1,100 | 39,661 | 43,604 | x | (1) |
| *Canis* | *lupus* | IK08-096 | UAMES | 30192 | femur | Beta-339269 | >43,500 | | -20.00 | 8.90 | >43,500 | | n/a | n/a | | (1) |
| *Equus* | *ferus* | Tes57-02 | UAMES | 30196 | phalange | Beta-339279 | 10,570 | 40 | -21.20 | 2.50 | 10,570 | 40 | 12,422 | 12,660 | x | (1) |
| *Equus* | *ferus* | JDL12-1 | UAMES | 29462 | cranium | Beta-331878[c] | 11,710 | 50 | -20.70 | 4.50 | 11,710 | 50 | 13,715 | 14,016 | x | (1) |
| *Equus* | *ferus* | JDL12-1 | UAMES | 29462 | cranium | Beta-339258[c] | 12,240 | 50 | -20.50 | n/a | 12,240 | 50 | 13,973 | 14,368 | x | this study |
| *Equus* | *ferus* | IK01-353 | UAMES | 11953 | mandible | CAMS-92091 | 12,465 | 40 | -20.59 | 2.89 | 12,465 | 40 | 14,273 | 14,970 | x | (1) |
| *Equus* | *ferus* | IK02-109 | UAMES | 3294 | metacarpal | CAMS-120651[c] | 12,480 | 35 | -20.41 | 5.50 | 12,480 | 35 | 14,309 | 14,997 | x | (1) |
| *Equus* | *ferus* | IK02-109 | UAMES | 3294 | metacarpal | CAMS-121738[c] | 12,490 | 45 | -20.40 | 5.50 | 12,490 | 45 | 14,314 | 15,036 | x | (1) |
| *Equus* | *ferus* | IK99-033 | UAMES | 3300 | tooth | CAMS-120673 | 12,780 | 35 | -20.67 | 5.40 | 12,780 | 35 | 15,089 | 15,364 | x | (1) |
| *Equus* | *ferus* | IK07-08 | UAMES | 29463 | metacarpal | Beta-331866[c] | 12,980 | 50 | -20.80 | 6.40 | 12,980 | 50 | 15,298 | 15,740 | x | (1) |

| *Genus* | *species* | field ID | depository[a] | catalog number | skeletal element | $^{14}$CLab[#] and number | $^{14}$C date reported (yrs BP) | | $\delta^{13}$C ‰ (VPDB) | $\delta^{15}$N ‰ (AIR) | $\delta^{13}$C-normalized date used for calibration | | 95.4% calibrated range | | used in Monte Carlo (x) | source |
|---|---|---|---|---|---|---|---|---|---|---|---|---|---|---|---|---|
| | | | | | | | $^{14}$C date | std dev[e] | | | $^{14}$C date | std dev[e] | (cal yr BP)[f] | | | |
| *Equus* | *ferus* | IK07-08 | UAMES | 29463 | metacarpal | Beta-345282[c] | 13,010 | 50 | -20.50 | n/a | 13,010 | 50 | 15,324 | 15,779 | x | this study |
| *Equus* | *ferus* | TIT05-07.1 | UAMES | 29464 | metacarpal | Beta-331882 | 13,010 | 60 | -20.70 | 7.10 | 13,010 | 60 | 15,308 | 15,796 | x | (1) |
| *Equus* | *ferus* | TIT10-35 | UAMES | 29465 | metacarpal | Beta-331883 | 13,400 | 50 | -20.90 | 8.40 | 13,400 | 50 | 15,924 | 16,299 | x | (1) |
| *Equus* | *ferus* | IK98-0537 | UAMES | 3283 | metatarsal | CAMS-91792 | 13,685 | 40 | -20.77 | 6.60 | 13,685 | 40 | 16,300 | 16,747 | x | (1) |
| *Equus* | *ferus* | IK98-0111 | UAMES | 3284 | metatarsal | CAMS-120655 | 13,925 | 40 | -20.59 | 7.00 | 13,925 | 40 | 16,631 | 17,071 | x | (1) |
| *Equus* | *ferus* | TIT09-02 | UAMES | 29466 | cranium | Beta-263037 | 14,290 | 70 | -20.90 | n/a | 14,290 | 70 | 17,158 | 17,620 | x | (1) |
| *Equus* | *ferus* | TIT11-069 | UAMES | 29467 | mandible | Beta-331887 | 14,360 | 60 | -20.40 | 6.30 | 14,360 | 60 | 17,263 | 17,703 | x | (1) |
| *Equus* | *ferus* | T04-001 | UAMES | 3289 | tibia | CAMS-120711 | 14,540 | 45 | -20.98 | 5.00 | 14,540 | 45 | 17,550 | 17,910 | x | (1) |
| *Equus* | *ferus* | IK99-335 | UAMES | 3295 | metatarsal | CAMS-120676 | 15,095 | 40 | -21.48 | 7.00 | 15,095 | 40 | 18,162 | 18,505 | x | (1) |
| *Equus* | *ferus* | MAY08-02 | UAMES | 29468 | cranium | Beta-258461 | 15,630 | 70 | -20.20 | n/a | 15,630 | 70 | 18,723 | 19,036 | x | (1) |
| *Equus* | *ferus* | IK99-065 | UAMES | 10693 | metacarpal | Beta 369776[c] | 15,790 | 60 | -20.80 | n/a | 15,790 | 60 | 18,882 | 19,217 | x | (1) |
| *Equus* | *ferus* | IK99-065 | UAMES | 10693 | metacarpal | Beta 369785[c] | 15,890 | 60 | -20.60 | 6.30 | 15,890 | 60 | 18,960 | 19,380 | x | (1) |
| *Equus* | *ferus* | WC11-09 | UAMES | 29469 | phalange | Beta-331891 | 16,170 | 60 | -20.40 | 6.40 | 16,170 | 60 | 19,290 | 19,716 | x | (1) |
| *Equus* | *ferus* | IK99-461 | UAMES | 3299 | metatarsal | CAMS-120683 | 16,885 | 45 | -20.83 | 6.40 | 16,885 | 45 | 20,166 | 20,545 | x | (1) |
| *Equus* | *ferus* | IK99-514 | UAMES | 3290 | metacarpal | CAMS-120685 | 16,925 | 45 | -20.97 | 7.60 | 16,925 | 45 | 20,221 | 20,586 | x | (1) |
| *Equus* | *ferus* | IK99-774 | UAMES | 3297 | metacarpal | CAMS-92073 | 17,290 | 60 | -20.74 | 5.38 | 17,290 | 60 | 20,640 | 21,065 | x | (1) |
| *Equus* | *ferus* | IK99-562 | UAMES | 3286 | metatarsal | CAMS-120700 | 17,300 | 60 | -21.29 | 6.20 | 17,300 | 60 | 20,650 | 21,080 | x | (1) |
| *Equus* | *ferus* | TIT10-03 | UAMES | 29470 | cranium | Beta-283250 | 17,670 | 70 | -20.80 | n/a | 17,670 | 70 | 21,080 | 21,651 | x | (1) |
| *Equus* | *ferus* | BR12-01 | UAMES | 29471 | astragulus | Beta-331862[c] | 17,720 | 70 | -20.80 | 5.40 | 17,720 | 70 | 21,171 | 21,736 | x | (1) |
| *Equus* | *ferus* | BR12-01 | UAMES | 29471 | astragulus | Beta-339251[c] | 17,760 | 70 | -20.60 | n/a | 17,760 | 70 | 21,244 | 21,785 | x | this study |
| *Equus* | *ferus* | n/a | n/a | n/a | n.r.[b] | I-9371 | 19,250[d] | 360 | -21.10* | n/a | 19,314 | 360 | 22,477 | 24,096 | x | (4) |
| *Equus* | *ferus* | n/a | n/a | n/a | n.r.[b] | CAMS-145093 | 19,830 | 100 | n/a | n/a | 19,830 | 100 | 23,575 | 24,148 | x | (5) |
| *Equus* | *ferus* | IK98-0246 | UAMES | 3280 | metatarsal | CAMS-120656[c] | 19,880 | 70 | -20.71 | 6.20 | 19,880 | 70 | 23,679 | 24,158 | x | (1) |
| *Equus* | *ferus* | IK98-0246 | UAMES | 3280 | metatarsal | CAMS-121741[c] | 19,900 | 60 | -20.70 | 6.20 | 19,900 | 60 | 23,720 | 24,170 | x | (1) |
| *Equus* | *ferus* | IK02-191 | UAMES | 3298 | metacarpal | CAMS-91964 | 20,050 | 70 | -20.51 | 6.29 | 20,050 | 70 | 23,890 | 24,340 | x | (1) |
| *Equus* | *ferus* | IK13-23 | UAMES | 32964 | radius | Beta-362038 | 20,070 | 80 | -20.70 | 6.10 | 20,070 | 80 | 23,896 | 24,374 | x | this study |
| *Equus* | *ferus* | T02-016 | UAMES | 3292 | metatarsal | CAMS-120703 | 20,190 | 70 | -20.51 | 6.90 | 20,190 | 70 | 24,030 | 24,483 | x | (1) |
| *Equus* | *ferus* | IK01-342 | UAMES | 3285 | metacarpal | CAMS-120647[c] | 20,640 | 80 | -20.37 | 6.60 | 20,640 | 80 | 24,518 | 25,189 | x | (1) |
| *Equus* | *ferus* | IK01-342 | UAMES | 3285 | metacarpal | CAMS-121734[c] | 20,720 | 90 | -20.40 | 6.60 | 20,720 | 90 | 24,575 | 25,286 | x | (1) |
| *Equus* | *ferus* | n/a | UAMES | n/a | n.r.[b] | CAMS-145113 | 20,720 | 110 | n/a | n/a | 20,720 | 110 | 24,545 | 25,311 | x | (5) |

| *Genus* | *species* | field ID | depository[a] | catalog number | skeletal element | $^{14}$CLab[#] and number | $^{14}$C date reported (yrs BP) | | $\delta^{13}$C ‰ (VPDB) | $\delta^{15}$N ‰ (AIR) | $\delta^{13}$C-normalized date used for calibration | | 95.4% calibrated range | | used in Monte Carlo (x) | source |
|---|---|---|---|---|---|---|---|---|---|---|---|---|---|---|---|---|
| | | | | | | | $^{14}$C date | std dev[e] | | | $^{14}$C date | std dev[e] | (cal yr BP)[f] | | | |
| *Equus* | *ferus* | IK99-207 | UAMES | 3293 | metacarpal | CAMS-91802 | 20,850 | 80 | -20.48 | 5.85 | 20,850 | 80 | 24,872 | 25,481 | x | (1) |
| *Equus* | *ferus* | n/a | n/a | n/a | n.r.[b] | I-9274 | 20,810[d] | 410 | -21.10* | n/a | 20,874 | 410 | 24,179 | 25,950 | x | (4) |
| *Equus* | *ferus* | IK10-01 | UAMES | 29472 | cranium | Beta-283242 | 21,210 | 90 | -20.80 | n/a | 21,210 | 90 | 25,291 | 25,779 | x | (1) |
| *Equus* | *ferus* | AK-109-V-1 | UAMES | 23920 | mandible | GX-13939 | 21,220 | 800 | n/a | n/a | 21,220 | 800 | 23,850 | 27,316 | x | (4) |
| *Equus* | *ferus* | AK-109-V-2 | UAMES | 23919 | radius | GX-13941 | 21,420 | 440 | n/a | n/a | 21,420 | 440 | 24,583 | 26,687 | x | (4) |
| *Equus* | *ferus* | IK99-442 | UAMES | 3282 | metacarpal | CAMS-91809 | 21,560 | 80 | -20.85 | 5.91 | 21,560 | 80 | 25,685 | 26,016 | x | (1) |
| *Equus* | *ferus* | IK99-789 | UAMES | 3291 | cranium | CAMS-120702 | 21,750 | 80 | -20.95 | 5.60 | 21,750 | 80 | 25,825 | 26,144 | x | (1) |
| *Equus* | *ferus* | IK99-577 | UAMES | 10890 | metacarpal | CAMS-91983 | 22,110 | 90 | -20.76 | 5.44 | 22,110 | 90 | 26,059 | 26,595 | x | (1) |
| *Equus* | *ferus* | IK10-073 | UAMES | 29473 | metacarpal | Beta-331872[c] | 22,170 | 90 | -20.90 | 4.70 | 22,170 | 90 | 26,100 | 26,672 | x | (1) |
| *Equus* | *ferus* | IK10-073 | UAMES | 29473 | metacarpal | Beta-339244[c] | 22,300 | 100 | -20.30 | n/a | 22,300 | 100 | 26,204 | 26,968 | x | this study |
| *Equus* | *ferus* | IK02-200 | UAMES | 10354 | mandible | CAMS-91965 | 22,330 | 90 | -19.97 | 4.81 | 22,330 | 90 | 26,256 | 26,997 | x | (1) |
| *Equus* | *ferus* | IK99-430 | UAMES | 10715 | metatarsal | CAMS-120682[c] | 22,410 | 80 | -20.84 | n/a | 22,410 | 80 | 26,406 | 27,072 | x | (1) |
| *Equus* | *ferus* | IK99-711 | UAMES | 10885 | metatarsal | CAMS-120701 | 22,450 | 90 | -20.72 | 6.20 | 22,450 | 90 | 26,445 | 27,110 | x | (1) |
| *Equus* | *ferus* | IK99-430 | UAMES | 10715 | metatarsal | CAMS-121755[c] | 22,600 | 90 | -20.80 | n/a | 22,600 | 90 | 26,581 | 27,235 | x | (1) |
| *Equus* | *ferus* | IK07-02 | UAMES | 29474 | metacarpal | Beta-331864 | 22,860 | 90 | -20.30 | 5.10 | 22,860 | 90 | 26,998 | 27,450 | x | (1) |
| *Equus* | *ferus* | IK06-23 | UAMES | 30194 | cranium | Beta-339267 | 23,230 | 90 | -19.70 | 5.50 | 23,230 | 90 | 27,310 | 27,685 | x | (1) |
| *Equus* | *ferus* | IK01-320 | UAMES | 11735 | metatarsal | CAMS-120646[c] | 23,790 | 110 | -20.88 | 5.60 | 23,790 | 110 | 27,639 | 28,090 | x | (1) |
| *Equus* | *ferus* | n/a | n/a | n/a | n.r.[b] | I-9318 | 23,910[d] | 470 | -21.10* | n/a | 23,974 | 470 | 27,360 | 29,039 | x | (4) |
| *Equus* | *ferus* | IK01-320 | UAMES | 11735 | metatarsal | CAMS-121733[c] | 24,070 | 100 | -20.90 | 5.60 | 24,070 | 100 | 27,820 | 28,414 | x | (1) |
| *Equus* | *ferus* | IK08-080 | UAMES | 29484 | metacarpal | Beta-331870 | 24,690 | 110 | -21.10 | 4.80 | 24,690 | 110 | 28,446 | 28,987 | x | (1) |
| *Equus* | *ferus* | IK08-082 | UAMES | 29483 | metacarpal | Beta-346834[c] | 24,880 | 120 | -20.80 | n/a | 24,880 | 120 | 28,613 | 29,267 | | this study |
| *Equus* | *ferus* | IK99-129 | UAMES | 10814 | mandible | CAMS-91801 | 24,900 | 100 | -20.28 | 4.90 | 24,900 | 100 | 28,650 | 29,245 | x | (1) |
| *Equus* | *ferus* | n/a | n/a | n/a | n.r.[b] | AAR-11185 | 25,460 | 230 | n/a | n/a | 25,460 | 230 | 28,980 | 30,299 | x | (5) |
| *Equus* | *ferus* | T02-001 | UAMES | 8607 | mandible | CAMS-91958 | 25,680 | 140 | -20.83 | 3.70 | 25,680 | 140 | 29,425 | 30,350 | x | (1) |
| *Equus* | *ferus* | IK99-367 | UAMES | 10548 | metatarsal | CAMS-120679[c] | 26,020 | 120 | -20.58 | 5.30 | 26,020 | 120 | 29,832 | 30,713 | x | (1) |
| *Equus* | *ferus* | IK01-218 | UAMES | 11745 | metatarsal | CAMS-121731[c] | 26,130 | 120 | -20.90 | 6.00 | 26,130 | 120 | 29,986 | 30,808 | x | (1) |
| *Equus* | *ferus* | IK12-063 | UAMES | 30195 | mandible | Beta-339273 | 26,190 | 120 | -20.50 | 7.70 | 26,190 | 120 | 30,145 | 30,875 | x | (1) |
| *Equus* | *ferus* | IK01-218 | UAMES | 11745 | metatarsal | CAMS-120717[c] | 26,210 | 130 | -20.91 | 6.00 | 26,210 | 130 | 30,151 | 30,896 | x | (1) |
| *Equus* | *ferus* | IK13-36 | UAMES | 32959 | metacarpal | Beta-362040 | 26,380 | 120 | -20.00 | 4.10 | 26,380 | 120 | 30,409 | 30,960 | x | this study |
| *Equus* | *ferus* | IK99-367 | UAMES | 10548 | metatarsal | CAMS-121752[c] | 26,460 | 130 | -20.60 | 5.30 | 26,460 | 130 | 30,485 | 31,007 | x | (1) |

| *Genus* | *species* | field ID | depository[a] | catalog number | skeletal element | $^{14}$CLab[#] and number | $^{14}$C date reported (yrs BP) | | $\delta^{13}$C ‰ (VPDB) | $\delta^{15}$N ‰ (AIR) | $\delta^{13}$C-normalized date used for calibration | | 95.4% calibrated range | | used in Monte Carlo (x) | source |
|---|---|---|---|---|---|---|---|---|---|---|---|---|---|---|---|---|
| | | | | | | | $^{14}$C date | std dev[e] | | | $^{14}$C date | std dev[e] | (cal yr BP)[f] | | | |
| *Equus* | *ferus* | KIK08-01 | UAMES | 29475 | metacarpal | Beta-331879 | 26,770 | 140 | -21.60 | 4.60 | 26,770 | 140 | 30,720 | 31,146 | x | (1) |
| *Equus* | *ferus* | IK11-001 | UAMES | 29476 | metacarpal | Beta-331874 | 26,890 | 150 | -20.80 | 4.50 | 26,890 | 150 | 30,777 | 31,209 | x | (1) |
| *Equus* | *ferus* | TIT11-070 | UAMES | 29477 | mandible | Beta-331888 | 27,060 | 140 | -20.60 | 7.40 | 27,060 | 140 | 30,870 | 31,283 | x | (1) |
| *Equus* | *ferus* | IK01-080 | UAMES | 11647 | mandible | CAMS-92078[c] | 27,810 | 210 | -21.06 | 5.37 | 27,810 | 210 | 31,165 | 32,232 | x | (1) |
| *Equus* | *ferus* | IK12-015 | UAMES | 29478 | metacarpal | Beta-331877 | 27,930 | 150 | -20.70 | 6.40 | 27,930 | 150 | 31,284 | 32,209 | x | (1) |
| *Equus* | *ferus* | IK97-102 | UAMES | 8622 | metacarpal | Beta-117138 | 28,120 | 250 | -24.50 | n/a | 28,120 | 250 | 31,368 | 32,754 | x | (1) |
| *Equus* | *ferus* | IK01-459 | UAMES | 11933 | metapodial | CAMS-91957 | 28,260 | 210 | -20.92 | 7.56 | 28,260 | 210 | 31,511 | 32,818 | x | (1) |
| *Equus* | *ferus* | IK10-074 | UAMES | 29479 | metacarpal | Beta-331873 | 28,330 | 150 | -20.60 | 5.00 | 28,330 | 150 | 31,648 | 32,788 | x | (1) |
| *Equus* | *ferus* | IK13-35 | UAMES | 32961 | metatarsal | Beta-362039 | 28,500 | 150 | -20.80 | 10.30 | 28,500 | 150 | 31,818 | 33,018 | x | this study |
| *Equus* | *ferus* | IK99-244 | UAMES | 10834 | metacarpal | CAMS-120675 | 28,500 | 160 | -20.58 | 8.20 | 28,500 | 160 | 31,796 | 33,041 | x | (1) |
| *Equus* | *ferus* | IK98-1176 | UAMES | 10009 | metacarpal | CAMS-91797 | 28,500 | 200 | -20.87 | 5.14 | 28,500 | 200 | 31,722 | 33,143 | x | (1) |
| *Equus* | *ferus* | T04-004 | UAMES | 11353 | radius | CAMS-120712 | 28,540 | 170 | -21.29 | 6.10 | 28,540 | 170 | 31,826 | 33,142 | x | (1) |
| *Equus* | *ferus* | IK01-080 | UAMES | 11647 | mandible | CAMS-91781[c] | 28,600 | 200 | -21.06 | 5.37 | 28,600 | 200 | 31,860 | 33,315 | x | (1) |
| *Equus* | *ferus* | IK01-368 | UAMES | 12011 | metatarsal | CAMS-121736 | 28,690 | 160 | -21.20 | 7.60 | 28,690 | 160 | 32,146 | 33,389 | x | (1) |
| *Equus* | *ferus* | n/a | n/a | n/a | n.r.[b] | USGS-804 | 28,700 | 460 | n/a | n/a | 28,700 | 460 | 31,572 | 33,745 | x | (2) |
| *Equus* | *ferus* | IK06-17 | UAMES | 29480 | metacarpal | Beta-331863 | 29,560 | 150 | -20.90 | 6.50 | 29,560 | 150 | 33,474 | 34,030 | x | (1) |
| *Equus* | *ferus* | IK99-254 | UAMES | 10644 | metacarpal | CAMS-91806 | 29,700 | 200 | -21.23 | 9.81 | 29,700 | 200 | 33,515 | 34,201 | x | (1) |
| *Equus* | *ferus* | IK99-383 | UAMES | 11205 | metatarsal | CAMS-120680[c] | 29,830 | 190 | -21.26 | 6.40 | 29,830 | 190 | 33,620 | 34,294 | x | (1) |
| *Equus* | *ferus* | TIT11-071 | UAMES | 29481 | mandible | Beta-343824[c] | 29,880 | 180 | -20.90 | n/a | 29,880 | 180 | 33,664 | 34,324 | x | this study |
| *Equus* | *ferus* | IK07-06 | UAMES | 29495 | metacarpal | Beta-339236[c] | 30,030 | 180 | -21.40 | n/a | 30,030 | 180 | 33,769 | 34,471 | x | this study |
| *Equus* | *ferus* | TIT11-071 | UAMES | 29481 | mandible | Beta-331889[c] | 30,260 | 190 | -20.90 | 6.80 | 30,260 | 190 | 33,921 | 34,660 | x | (1) |
| *Equus* | *ferus* | IK07-06 | UAMES | 29495 | metacarpal | Beta-331865[c] | 30,560 | 160 | -21.10 | 5.80 | 30,560 | 160 | 34,159 | 34,843 | x | (1) |
| *Equus* | *ferus* | IK99-383 | UAMES | 11205 | metatarsal | CAMS-121753[c] | 30,560 | 200 | -21.30 | 6.40 | 30,560 | 200 | 34,110 | 34,892 | x | (1) |
| *Equus* | *ferus* | TIT11-072 | UAMES | 29482 | mandible | Beta-331890[c] | 30,610 | 200 | -21.70 | 8.10 | 30,610 | 200 | 34,144 | 34,936 | x | (1) |
| *Equus* | *ferus* | TIT11-072 | UAMES | 29482 | mandible | Beta-339257[c] | 30,790 | 190 | -21.10 | n/a | 30,790 | 190 | 34,300 | 35,101 | x | this study |
| *Equus* | *ferus* | IK98-0539 | UAMES | 9548 | mandible | CAMS-91793 | 30,900 | 300 | -21.16 | 7.87 | 30,900 | 300 | 34,238 | 35,479 | x | (1) |
| *Equus* | *ferus* | IK01-183 | UAMES | 11878 | metatarsal | CAMS-92083 | 31,230 | 270 | -21.70 | 5.32 | 31,230 | 270 | 34,613 | 35,732 | x | (1) |
| *Equus* | *ferus* | IK08-082 | UAMES | 29483 | metacarpal | Beta-331869[c] | 31,680 | 190 | -21.00 | 7.40 | 31,680 | 190 | 35,094 | 36,055 | x | (1) |
| *Equus* | *ferus* | TIT10-38 | UAMES | 29485 | metacarpal | Beta-331886[c] | 32,250 | 220 | -21.30 | 5.10 | 32,250 | 220 | 35,628 | 36,641 | x | (1) |
| *Equus* | *ferus* | IK08-081 | UAMES | 33201 | metacarpal | Beta 369779[c] | 32,270 | 280 | -20.90 | n/a | 32,270 | 280 | 35,518 | 36,877 | x | this study |

| *Genus* | *species* | field ID | depository[a] | catalog number | skeletal element | $^{14}$CLab[#] and number | $^{14}$C date reported (yrs BP) | | $\delta^{13}$C ‰ (VPDB) | $\delta^{15}$N ‰ (AIR) | $\delta^{13}$C-normalized date used for calibration | | 95.4% calibrated range | | used in Monte Carlo (x) | source |
|---|---|---|---|---|---|---|---|---|---|---|---|---|---|---|---|---|
| | | | | | | | $^{14}$C date | std dev[e] | | | $^{14}$C date | std dev[e] | (cal yr BP)[f] | | | |
| *Equus* | *ferus* | n/a | n/a | n/a | n.r.[b] | I-9275 | 32,270[d] | 1,500 | -21.10* | n/a | 32,334 | 1,500 | 33,921 | 40,629 | x | (4) |
| *Equus* | *ferus* | IK98-1142 | UAMES | 9972 | mandible | CAMS-91796 | 32,600 | 300 | -21.13 | 5.13 | 32,600 | 300 | 35,853 | 37,654 | x | (1) |
| *Equus* | *ferus* | IK01-282 | UAMES | 11794 | metacarpal | CAMS-92089 | 32,700 | 300 | -20.87 | 4.47 | 32,700 | 300 | 35,994 | 37,816 | x | (1) |
| *Equus* | *ferus* | TIT10-38 | UAMES | 29485 | metacarpal | Beta-339248c | 32,980 | 260 | -21.30 | n/a | 32,980 | 260 | 36,340 | 38,056 | x | this study |
| *Equus* | *ferus* | IK09-51 | UAMES | 29486 | metacarpal | Beta-339242[c] | 33,090 | 240 | -23.00 | n/a | 33,090 | 240 | 36,477 | 38,154 | | this study |
| *Equus* | *ferus* | IK09-51 | UAMES | 29486 | metacarpal | Beta-331871[c] | 33,150 | 200 | -21.60 | 5.50 | 33,150 | 200 | 36,602 | 38,157 | x | (1) |
| *Equus* | *ferus* | TIT10-36 | UAMES | 29487 | metacarpal | Beta-331884[c] | 33,200 | 240 | -21.40 | 6.20 | 33,200 | 240 | 36,615 | 38,277 | x | (1) |
| *Equus* | *ferus* | TIT10-36 | UAMES | 29487 | metacarpal | Beta-339255[c] | 33,250 | 240 | -21.40 | n/a | 33,250 | 240 | 36,678 | 38,325 | x | (1) |
| *Equus* | *ferus* | IK98-0288 | UAMES | 8859 | metatarsal | CAMS-120721[c] | 33,420 | 340 | -21.45 | 6.80 | 33,420 | 340 | 36,670 | 38,575 | x | (1) |
| *Equus* | *ferus* | IK08-081 | UAMES | 33201 | metacarpal | Beta 369782[c] | 33,700 | 300 | -22.00 | 7.40 | 33,700 | 300 | 37,049 | 38,800 | | this study |
| *Equus* | *ferus* | IK98-0112 | UAMES | 9021 | metacarpal | CAMS-91790 | 33,800 | 400 | -21.09 | 7.91 | 33,800 | 400 | 36,900 | 39,162 | x | (1) |
| *Equus* | *ferus* | IK98-0288 | UAMES | 8859 | metatarsal | CAMS-121742[c] | 33,820 | 290 | -21.50 | 6.80 | 33,820 | 290 | 37,272 | 38,959 | x | (1) |
| *Equus* | *ferus* | IK99-790 | UAMES | 10910 | mandible | CAMS-92074 | 33,870 | 350 | -20.72 | 5.86 | 33,870 | 350 | 37,126 | 39,162 | x | (1) |
| *Equus* | *ferus* | IK01-369 | UAMES | 11973 | metacarpal | CAMS-92093[c] | 33,900 | 400 | -21.16 | 5.87 | 33,900 | 400 | 37,037 | 39,336 | x | (1) |
| *Equus* | *ferus* | KIG05-2.2 | UAMES | 32769 | metacarpal | Beta 369781[c] | 34,000 | 270 | -21.10 | 8.50 | 34,000 | 270 | 37,729 | 39,161 | x | (1) |
| *Equus* | *ferus* | IK01-369 | UAMES | 11973 | metacarpal | CAMS-91782[c] | 34,200 | 400 | -21.16 | 5.87 | 34,200 | 400 | 37,694 | 39,760 | x | (1) |
| *Equus* | *ferus* | IK01-150 | UAMES | 12014 | mandible | CAMS-92081 | 34,210 | 370 | -21.20 | 7.21 | 34,210 | 370 | 37,825 | 39,690 | x | (1) |
| *Equus* | *ferus* | TIT10-37 | UAMES | 29488 | metacarpal | Beta-331885[c] | 34,320 | 270 | -20.90 | 9.10 | 34,320 | 270 | 38,321 | 39,522 | x | (1) |
| *Equus* | *ferus* | KIG05-2.2 | UAMES | 32769 | metacarpal | Beta 369780[c] | 34,360 | 290 | -20.90 | n/a | 34,360 | 290 | 38,330 | 39,605 | x | (1) |
| *Equus* | *ferus* | IK99-404 | UAMES | 11122 | metacarpal | CAMS-120681[c] | 34,690 | 340 | -22.11 | 8.30 | 34,690 | 340 | 38,524 | 39,999 | x | (1) |
| *Equus* | *ferus* | TIT10-37 | UAMES | 29488 | metacarpal | Beta-339247[c] | 34,780 | 290 | -22.30 | n/a | 34,780 | 290 | 38,652 | 39,990 | x | this study |
| *Equus* | *ferus* | IK13-57 | UAMES | 32952 | cranium | Beta-362042 | 35,200 | 290 | -20.40 | 6.40 | 35,200 | 290 | 39,021 | 40,481 | x | this study |
| *Equus* | *ferus* | IK99-404 | UAMES | 11122 | metacarpal | CAMS-121754[c] | 35,380 | 360 | -22.10 | 8.30 | 35,380 | 360 | 39,105 | 40,866 | x | (1) |
| *Equus* | *ferus* | IK13-56 | UAMES | 32958 | metacarpal | Beta-362041 | 35,460 | 300 | -21.00 | 8.50 | 35,460 | 300 | 39,339 | 40,836 | x | this study |
| *Equus* | *ferus* | n/a | n/a | n/a | n.r.[b] | CAMS-91789 | 35,500 | 400 | n/a | n/a | 35,500 | 400 | 39,183 | 41,077 | x | (5) |
| *Equus* | *ferus* | IK98-0009 | UAMES | 9169 | mandible | CAMS-91889 | 35,600 | 400 | -21.00 | 5.93 | 35,600 | 400 | 39,320 | 41,177 | x | (1) |
| *Equus* | *ferus* | T99-025 | UAMES | 8728 | metacarpal | Beta 369777[c] | 35,850 | 390 | -20.40 | n/a | 35,850 | 390 | 39,650 | 41,356 | x | (1) |
| *Equus* | *ferus* | IK98-0394 | UAMES | 8814 | metacarpal | CAMS-91791 | 36,500 | 500 | -21.40 | 6.02 | 36,500 | 500 | 40,137 | 41,980 | x | (1) |
| *Equus* | *ferus* | IK01-121 | UAMES | 11782 | metacarpal | CAMS-92079 | 37,400 | 540 | -21.15 | 6.75 | 37,400 | 540 | 40,995 | 42,645 | x | (1) |
| *Equus* | *ferus* | T99-025 | UAMES | 8728 | metacarpal | Beta 369784[c] | 37,490 | 390 | -21.00 | 4.40 | 37,490 | 390 | 41,330 | 42,478 | x | (1) |

| *Genus* | *species* | field ID | depository[a] | catalog number | skeletal element | $^{14}$CLab[#] and number | $^{14}$C date reported (yrs BP) | | $\delta^{13}$C ‰ (VPDB) | $\delta^{15}$N ‰ (AIR) | $\delta^{13}$C-normalized date used for calibration | | 95.4% calibrated range | | used in Monte Carlo (x) | source |
|---|---|---|---|---|---|---|---|---|---|---|---|---|---|---|---|---|
| | | | | | | | $^{14}$C date | std dev[e] | | | $^{14}$C date | std dev[e] | (cal yr BP)[f] | | | |
| *Equus* | *ferus* | IK99-806 | UAMES | 11068 | metacarpal | CAMS-92075 | 38,090 | 590 | -20.84 | 5.76 | 38,090 | 590 | 41,503 | 43,151 | x | (1) |
| *Equus* | *ferus* | IK12-010 | UAMES | 29492 | metacarpal | Beta-343825[c] | 38,790 | 440 | -20.90 | n/a | 38,790 | 440 | 42,129 | 43,405 | x | this study |
| *Equus* | *ferus* | IK01-165 | UAMES | 11622 | metacarpal | Beta 369783[c] | 38,850 | 450 | -20.90 | 3.70 | 38,850 | 450 | 42,150 | 43,484 | x | (1) |
| *Equus* | *ferus* | IK08-078 | UAMES | 29490 | metacarpal | Beta-339239[c] | 40,480 | 580 | -20.80 | n/a | 40,480 | 580 | 43,085 | 45,135 | x | (1) |
| *Equus* | *ferus* | IK08-079 | UAMES | 29489 | metacarpal | Beta-331868[c] | 40,880 | 400 | -21.20 | 5.70 | 40,880 | 400 | 43,602 | 45,195 | x | (1) |
| *Equus* | *ferus* | IK01-165 | UAMES | 11622 | metacarpal | Beta 369778[c] | 40,930 | 560 | -20.90 | n/a | 40,930 | 560 | 43,415 | 45,480 | x | (1) |
| *Equus* | *ferus* | IK08-078 | UAMES | 29490 | metacarpal | Beta-331867[c] | 40,960 | 370 | -20.60 | 7.00 | 40,960 | 370 | 43,731 | 45,222 | x | (1) |
| *Equus* | *ferus* | IK99-111 | UAMES | 10544 | metacarpal | CAMS-91799 | 41,000 | 800 | -20.79 | 3.07 | 41,000 | 800 | 43,160 | 45,991 | x | (1) |
| *Equus* | *ferus* | IK12-011 | UAMES | 29491 | metacarpal | Beta-339253[c] | 41,090 | 560 | -20.90 | n/a | 41,090 | 560 | 43,546 | 45,622 | x | this study |
| *Equus* | *ferus* | IK12-011 | UAMES | 29491 | metacarpal | Beta-331876[c] | 41,410 | 570 | -20.90 | 4.20 | 41,410 | 570 | 43,835 | 45,930 | x | (1) |
| *Equus* | *ferus* | IK13-58 | UAMES | 32951 | cranium | Beta-362043 | 41,830 | 630 | -21.40 | 6.70 | 41,830 | 630 | 44,140 | 46,459 | x | this study |
| *Equus* | *ferus* | IK12-010 | UAMES | 29492 | metacarpal | Beta-331875[c] | 41,840 | 410 | -20.40 | 4.30 | 41,840 | 410 | 44,495 | 45,985 | x | (1) |
| *Equus* | *ferus* | IK02-072 | UAMES | 10534 | metatarsal | CAMS-120650[c] | 42,500 | 1,000 | -21.27 | 7.70 | 42,500 | 1,000 | 44,189 | 48,357 | x | (1) |
| *Equus* | *ferus* | IK08-079 | UAMES | 29489 | metacarpal | Beta-339240[c] | 42,540 | 660 | -21.10 | n/a | 42,540 | 660 | 44,690 | 47,311 | x | this study |
| *Equus* | *ferus* | IK02-072 | UAMES | 10534 | metatarsal | CAMS-121737[c] | 43,700 | 1,000 | -21.30 | 7.70 | 43,700 | 1,000 | 45,330 | 49,411 | x | (1) |
| *Equus* | *ferus* | IK02-026 | UAMES | 10434 | mandible | CAMS-91959 | 46,770 | 1,710 | -20.70 | 1.65 | 46,770 | 1,710 | 43,796 | 51,544 | | (1) |
| *Equus* | *ferus* | n/a | n/a | n/a | n.r.[b] | I-9319 | >40,000[d] | | -21.10* | n/a | >40,064 | | n/a | n/a | | (4) |
| *Equus* | *ferus* | n/a | n/a | n/a | n.r.[b] | I-9320 | >40,000[d] | | -21.10* | n/a | >40,064 | | n/a | n/a | | (4) |
| *Equus* | *ferus* | IK10-02 | UAMES | 29493 | cranium | Beta-283243 | >42,800 | | -20.90 | n/a | >42,800 | | n/a | n/a | | (1) |
| *Equus* | *ferus* | KIK12-02 | UAMES | 29494 | phalange | Beta-331880 | >43,500 | | -21.00 | 5.70 | >43,500 | | n/a | n/a | | (1) |
| *Mammut*[g] | *americanum* | MAY12-45 | UAMES | 30200 | molar | UCIAMS-117241 | 47,000 | 2,300 | -20.94 | 3.46 | 47,000 | 2,300 | 43,099 | 54,886 | | (6) |
| *Mammut* | *americanum* | IK01-277 | UAMES | 12060 | molar | UCIAMS-117236 | 49,800 | 3,300 | -20.88 | 3.05 | 49,800 | 3,300 | 44,822 | 65,508 | | (6) |
| *Mammut* | *americanum* | MAY12-70 | n/a | n/a | molar | UCIAMS-117237 | >46,100 | | -21.13 | 3.50 | >46,100 | | n/a | n/a | | (6) |
| *Mammut* | *americanum* | KIG12-15 | UAMES | 30199 | molar | UCIAMS-117235 | >46,400 | | -20.88 | 3.16 | >46,400 | | n/a | n/a | | (6) |
| *Mammut* | *americanum* | IK10-106 | UAMES | 30201 | molar | UCIAMS-117232 | >47,500 | | -20.81 | 3.01 | >47,500 | | n/a | n/a | | (6) |
| *Mammut* | *americanum* | IK99-237 | UAMES | 2414 | molar | UCIAMS-117234 | >48,100 | | -20.76 | 4.08 | >48,100 | | n/a | n/a | | (6) |
| *Mammut* | *americanum* | IK01-321 | UAMES | 12047 | molar | UCIAMS-117240 | >48,800 | | -20.67 | 3.54 | >48,800 | | n/a | n/a | | (6) |
| *Mammut* | *americanum* | IK08-127 | UAMES | 30198 | molar | UCIAMS-117243 | >51,200 | | -20.73 | 2.98 | >51,200 | | n/a | n/a | | (6) |
| *Mammut* | *americanum* | IK99-328 | UAMES | 11095 | molar | UCIAMS-117233 | >51,200 | | -21.19 | 3.08 | >51,200 | | n/a | n/a | | (6) |
| *Mammut* | *americanum* | IK05-3.5 | UAMES | 30197 | molar | UCIAMS-117242 | >51,700 | | -21.19 | 2.80 | >51,700 | | n/a | n/a | | (6) |

| *Genus* | *species* | field ID | depository[a] | catalog number | skeletal element | $^{14}$CLab[#] and number | $^{14}$C date reported (yrs BP) | | $\delta^{13}$C ‰ (VPDB) | $\delta^{15}$N ‰ (AIR) | $\delta^{13}$C-normalized date used for calibration | | 95.4% calibrated range | | used in Monte Carlo (x) | source |
|---|---|---|---|---|---|---|---|---|---|---|---|---|---|---|---|---|
| | | | | | | | $^{14}$C date | std dev[e] | | | $^{14}$C date | std dev[e] | (cal yr BP)[f] | | | |
| *Mammut* | *americanum* | IK98-963 | UAMES | 9705 | molar | UCIAMS-117239 | >51,700 | | -20.96 | 2.77 | >51,700 | | n/a | n/a | | (6) |
| *Mammut* | *americanum* | IK98-967 | n/a | n/a | molar | CAMS-91794 | >54,000 | | -20.99 | n/a | >54,000 | | n/a | n/a | | (1) |
| *Mammuthus*[g] | *primigenius* | UNM6648 | UAMES | 30202 | n.r.[b] | AA-26006 | 11,910 | 130 | -21.20 | n/a | 11,910 | 130 | 13,470 | 14,062 | x | (7) |
| *Mammuthus* | *primigenius* | IK24 | n/a | n/a | n.r.[b] | AA-17614 | 12,190 | 130 | -21.84 | n/a | 12,190 | 130 | 13,750 | 14,707 | x | (7) |
| *Mammuthus* | *primigenius* | AK204-V-1 | UAMES | 28809 | n.r.[b] | AA-14954 | 12,490 | 170 | -21.10 | n/a | 12,490 | 170 | 14,080 | 15,250 | x | (7) |
| *Mammuthus* | *primigenius* | UNM11997 | n/a | n/a | n.r.[b] | AA-26028 | 13,290 | 140 | -21.30 | n/a | 13,290 | 140 | 15,534 | 16,400 | x | (7) |
| *Mammuthus* | *primigenius* | KIK10- SK | UAMES | 29496 | cranium | Beta-283246 | 14,070 | 60 | -19.60 | n/a | 14,070 | 60 | 16,864 | 17,380 | x | (1) |
| *Mammuthus* | *primigenius* | UMN6068c | n/a | n/a | n.r.[b] | AA-26015 | 15,740 | 230 | -22.80 | n/a | 15,740 | 230 | 18,560 | 19,584 | x | (7) |
| *Mammuthus* | *primigenius* | 49MIS117 | n/a | n/a | n.r.[b] | Shell-6713A | 17,300[d] | 800 | -21.50* | n/a | 17,357 | 800 | 19,161 | 23,040 | x | (8) |
| *Mammuthus* | *primigenius* | IK02-181 | UAMES | 10522 | fibula | CAMS-120653[c] | 17,870 | 60 | -20.90 | 7.60 | 17,870 | 60 | 21,435 | 21,865 | x | (1) |
| *Mammuthus* | *primigenius* | IK02-181 | UAMES | 10522 | fibula | CAMS-121739[c] | 17,965 | 50 | -20.90 | 7.60 | 17,965 | 50 | 21,563 | 21,945 | x | (1) |
| *Mammuthus* | *primigenius* | IK01-257 | UAMES | 12016 | molar | CAMS-92087 | 19,530 | 80 | -21.34 | 10.11 | 19,530 | 80 | 23,210 | 23,818 | x | (1) |
| *Mammuthus* | *primigenius* | IK13 | n/a | n/a | n.r.[b] | AA-17620 | 19,560 | 330 | -21.17 | n/a | 19,560 | 330 | 22,774 | 24,352 | x | (7) |
| *Mammuthus* | *primigenius* | IK3 | n/a | n/a | n.r.[b] | AA-17623 | 19,970 | 350 | -21.25 | n/a | 19,970 | 350 | 23,191 | 25,040 | x | (7) |
| *Mammuthus* | *primigenius* | HAR-057-1 | n/a | n/a | femur | Beta-192036 | 20,150 | 110 | -21.50 | n/a | 20,150 | 110 | 23,934 | 24,500 | x | (1) |
| *Mammuthus* | *primigenius* | UNM6068a | n/a | n/a | n.r.[b] | AA-26013 | 24,193 | 510 | -21.40 | n/a | 24,193 | 510 | 27,476 | 29,389 | x | (7) |
| *Mammuthus* | *primigenius* | IK98-0339 | UAMES | 9053 | scapula | CAMS-120677[c] | 24,460 | 130 | -21.49 | 7.60 | 24,460 | 130 | 28,166 | 28,797 | x | (1) |
| *Mammuthus* | *primigenius* | IK98-0339 | UAMES | 9053 | scapula | CAMS-121751[c] | 24,850 | 110 | -21.50 | 7.60 | 24,850 | 110 | 28,594 | 29,202 | x | (1) |
| *Mammuthus* | *primigenius* | T02-110 | n/a | n/a | n.r.[b] | CAMS-91967 | 26,410 | 150 | -20.49 | 8.03 | 26,410 | 150 | 30,382 | 30,995 | x | (1) |
| *Mammuthus* | *primigenius* | IK8 | n/a | n/a | n.r.[b] | AA-17616[x] | 28,020 | 810 | -21.61 | n/a | 28,020 | 810 | 30,858 | 33,854 | x | (7) |
| *Mammuthus* | *primigenius* | IK99-120b | UAMES | 10688 | mandible | CAMS-91800 | 28,200 | 200 | -21.20 | 7.86 | 28,200 | 200 | 31,475 | 32,730 | x | (1) |
| *Mammuthus* | *primigenius* | IK01-040 | UAMES | 11998 | radius | CAMS-92077[c] | 28,220 | 210 | -21.20 | 7.56 | 28,220 | 210 | 31,481 | 32,775 | x | (1) |
| *Mammuthus* | *primigenius* | IK01-040 | UAMES | 11998 | radius | CAMS-91783[c] | 29,100 | 200 | -21.20 | 7.56 | 29,100 | 200 | 32,810 | 33,762 | x | (1) |
| *Mammuthus* | *primigenius* | IK98-0063 | UAMES | 9096 | tibia | CAMS-120654[c] | 29,250 | 200 | -21.08 | 8.30 | 29,250 | 200 | 32,966 | 33,866 | x | (1) |
| *Mammuthus* | *primigenius* | IK99-495 | UAMES | 10851 | mandible | CAMS-120684 | 29,740 | 190 | -21.20 | 7.97 | 29,740 | 190 | 33,559 | 34,214 | x | (1) |
| *Mammuthus* | *primigenius* | IK98-0063 | UAMES | 9096 | tibia | CAMS-121740[c] | 30,730 | 200 | -21.10 | 8.30 | 30,730 | 200 | 34,232 | 35,055 | x | (1) |
| *Mammuthus* | *primigenius* | IK99-745 | UAMES | 10905 | molar | CAMS-92072 | 30,990 | 250 | -20.58 | 9.03 | 30,990 | 250 | 34,422 | 35,482 | x | (1) |
| *Mammuthus* | *primigenius* | AK323-V-1 | UAMES | 29130 | n.r.[b] | AA-22574 | 31,100 | 1,200 | -21.80 | n/a | 31,100 | 1,200 | 33,069 | 38,628 | x | (7) |
| *Mammuthus* | *primigenius* | IK35 | n/a | n/a | n.r.[b] | AA-17602 | 31,300 | 1,200 | -21.04 | n/a | 31,300 | 1,200 | 33,365 | 38,815 | x | (7) |
| *Mammuthus* | *primigenius* | UMN6068b | n/a | n/a | n.r.[b] | AA-26014 | 31,600 | 1,200 | -21.40 | n/a | 31,600 | 1,200 | 33,663 | 39,014 | x | (7) |

| *Genus* | *species* | field ID | depository[a] | catalog number | skeletal element | $^{14}$CLab[#] and number | $^{14}$C date reported (yrs BP) | | $\delta^{13}$C ‰ (VPDB) | $\delta^{15}$N ‰ (AIR) | $\delta^{13}$C-normalized date used for calibration | | 95.4% calibrated range | | used in Monte Carlo (x) | source |
|---|---|---|---|---|---|---|---|---|---|---|---|---|---|---|---|---|
| | | | | | | | $^{14}$C date | std dev[e] | | | $^{14}$C date | std dev[e] | (cal yr BP)[f] | | | |
| *Mammuthus* | *primigenius* | IK99-5001 | UAMES | 8632 | tusk | CAMS-91779[c] | 33,000 | 300 | -20.77 | 7.16 | 33,000 | 300 | 36,329 | 38,172 | x | (1) |
| *Mammuthus* | *primigenius* | AK268-V-1 | UAMES | 28766 | n.r.[b] | AA-22575 | 33,300 | 1,600 | n/a | n/a | 33,300 | 1,600 | 34,672 | 41,645 | x | (7) |
| *Mammuthus* | *primigenius* | T02-032 | UAMES | 8635 | femur | CAMS-121756[c] | 33,340 | 280 | -20.90 | n/a | 33,340 | 280 | 36,709 | 38,439 | x | (1) |
| *Mammuthus* | *primigenius* | T02-032 | UAMES | 8635 | femur | CAMS-120705[c] | 33,370 | 290 | -20.90 | n/a | 33,370 | 290 | 36,722 | 38,473 | x | (1) |
| *Mammuthus* | *primigenius* | IK99-575 | UAMES | 11028 | molar | CAMS-91812[c] | 33,400 | 300 | -20.75 | 9.12 | 33,400 | 300 | 36,732 | 38,509 | x | (1) |
| *Mammuthus* | *primigenius* | IK14 | n/a | n/a | n.r.[b] | AA-17619 | 33,400 | 1,600 | -26.60 | n/a | 33,400 | 1,600 | 34,745 | 41,705 | x | (7) |
| *Mammuthus* | *primigenius* | IK99-5001 | UAMES | 8632 | tusk | CAMS-91968[c] | 33,530 | 340 | -20.77 | 7.16 | 33,530 | 340 | 36,777 | 38,680 | x | (1) |
| *Mammuthus* | *primigenius* | IK99-575 | UAMES | 11028 | molar | CAMS-91780[c] | 33,600 | 400 | -20.75 | 9.12 | 33,600 | 400 | 36,701 | 38,866 | x | (1) |
| *Mammuthus* | *primigenius* | T02-033 | n/a | n/a | n.r.[b] | CAMS-120706[c] | 33,880 | 300 | -21.40 | 7.00 | 33,880 | 300 | 37,344 | 39,070 | x | (1) |
| *Mammuthus* | *primigenius* | T02-033 | n/a | n/a | n.r.[b] | CAMS-121757[c] | 33,920 | 310 | -21.40 | 7.00 | 33,920 | 310 | 37,384 | 39,162 | x | (1) |
| *Mammuthus* | *primigenius* | 49IKR-VP | n/a | n/a | n.r.[b] | USGS-807 | 36,400 | 560 | -21.80 | n/a | 36,400 | 560 | 39,928 | 41,994 | x | (2) |
| *Mammuthus* | *primigenius* | IK4 | n/a | n/a | n.r.[b] | AA-17627 | 36,700 | 2,300 | -21.98 | n/a | 36,700 | 2,300 | 36,771 | 47,391 | x | (7) |
| *Mammuthus* | *primigenius* | IK17 | n/a | n/a | n.r.[b] | AA-17616[x] | 36,800 | 2,500 | -22.98 | n/a | 36,800 | 2,500 | 36,759 | 48,085 | x | (7) |
| *Mammuthus* | *primigenius* | AK1014 | n/a | n/a | n.r.[b] | AA-22615 | 37,400 | 2,600 | -18.80 | n/a | 37,400 | 2,600 | 37,905 | 49,029 | x | (7) |
| *Mammuthus* | *primigenius* | IK10 | n/a | n/a | n.r.[b] | AA-17622 | 37,800 | 2,700 | -22.51 | n/a | 37,800 | 2,700 | 38,434 | 49,274 | x | (7) |
| *Mammuthus* | *primigenius* | IK33 | n/a | n/a | n.r.[b] | AA-17605 | 38,000 | 2,700 | -21.72 | n/a | 38,000 | 2,700 | 38,609 | 49,237 | x | (7) |
| *Mammuthus* | *primigenius* | IK6 | n/a | n/a | n.r.[b] | AA-17628 | 39,700 | 3,400 | -23.05 | n/a | 39,700 | 3,400 | 40,291 | ... | x | (7) |
| *Mammuthus* | *primigenius* | IK25 | n/a | n/a | n.r.[b] | AA-17615 | 39,800 | 3,400 | -21.05 | n/a | 39,800 | 3,400 | 40,397 | ... | x | (7) |
| *Mammuthus* | *primigenius* | IK98-1275 | UAMES | 10080 | humerus | CAMS-120670 | 40,760 | 830 | -21.80 | 7.09 | 40,760 | 830 | 42,980 | 45,840 | x | (1) |
| *Mammuthus* | *primigenius* | IK99-235 | UAMES | 10752 | molar | CAMS-91803 | 40,870 | 820 | -21.53 | 8.44 | 40,870 | 820 | 43,057 | 45,917 | x | (1) |
| *Mammuthus* | *primigenius* | IK98-1102 | UAMES | 9823 | vertebra | CAMS-120666[c] | 45,100 | 1,400 | -21.42 | 7.80 | 45,100 | 1,400 | 46,299 | ... | x | (1) |
| *Mammuthus* | *primigenius* | IK98-1102 | UAMES | 9823 | vertebra | CAMS-121748[c] | 46,900 | 1,400 | -21.40 | 7.80 | 46,900 | 1,400 | 44,430 | 50,485 | | (1) |
| *Mammuthus* | *primigenius* | IK01-250 | UAMES | 11964 | tibia | CAMS-120643[c] | 47,300 | 1,500 | -21.49 | 6.68 | 47,300 | 1,500 | 44,667 | 51,243 | | (1) |
| *Mammuthus* | *primigenius* | IK98-1013 | UAMES | 9934 | scapula | CAMS-120722[c] | 47,300 | 1,800 | -21.82 | 7.35 | 47,300 | 1,800 | 44,181 | 52,468 | | (1) |
| *Mammuthus* | *primigenius* | IK01-201 | UAMES | 11715 | molar | CAMS-92085 | 48,040 | 2,000 | -21.39 | 8.17 | 48,040 | 2,000 | 44,601 | 54,181 | | (1) |
| *Mammuthus* | *primigenius* | IK01-250 | UAMES | 11964 | tibia | CAMS-120718[c] | 48,760 | 2,200 | -21.49 | 6.68 | 48,760 | 2,200 | 45,010 | 56,022 | | (1) |
| *Mammuthus* | *primigenius* | IK01-291 | n/a | n/a | tusk | CAMS-120645[c] | 48,900 | 1,900 | -21.22 | 8.24 | 48,900 | 1,900 | 45,621 | 54,536 | | (1) |
| *Mammuthus* | *primigenius* | IK01-166 | UAMES | 11821 | ulna | CAMS-120716 | 49,310 | 1,950 | -20.85 | 6.55 | 49,310 | 1,950 | 45,950 | 55,195 | | (1) |
| *Mammuthus* | *primigenius* | IK01-355 | UAMES | 12004 | vertebra | CAMS-120648[c] | 49,400 | 2,400 | -21.66 | n/a | 49,400 | 2,400 | 45,353 | 57,952 | | (1) |
| *Mammuthus* | *primigenius* | IK01-147 | UAMES | 12001 | femur | CAMS-92080 | 49,490 | 2,400 | -21.32 | n/a | 49,490 | 2,400 | 45,443 | 58,042 | | (1) |

| *Genus* | *species* | field ID | depository[a] | catalog number | skeletal element | $^{14}$CLab[#] and number | $^{14}$C date reported (yrs BP) | | $\delta^{13}$C ‰ (VPDB) | $\delta^{15}$N ‰ (AIR) | $\delta^{13}$C-normalized date used for calibration | | 95.4% calibrated range | | used in Monte Carlo (x) | source |
|---|---|---|---|---|---|---|---|---|---|---|---|---|---|---|---|---|
| | | | | | | | $^{14}$C date | std dev[e] | | | $^{14}$C date | std dev[e] | (cal yr BP)[f] | | | |
| *Mammuthus* | *primigenius* | IK98-1033 | UAMES | 9970 | scapula | CAMS-120665 | 49,700 | 2,500 | -21.43 | 7.42 | 49,700 | 2,500 | 45,513 | 58,957 | | (1) |
| *Mammuthus* | *primigenius* | IK98-1195 | UAMES | 9811 | radius | CAMS-120667c | 50,400 | 2,700 | -21.09 | 6.08 | 50,400 | 2,700 | 45,958 | 61,173 | | (1) |
| *Mammuthus* | *primigenius* | IK98-1012 | UAMES | 9933 | cranium | CAMS-120664 | 50,800 | 2,400 | -21.39 | 7.07 | 50,800 | 2,400 | 46,753 | 59,352 | | (1) |
| *Mammuthus* | *primigenius* | IK01-291 | n/a | n/a | tusk | CAMS-121732[c] | 51,000 | 2,400 | -21.20 | 8.24 | 51,000 | 2,400 | 46,953 | 59,552 | | (1) |
| *Mammuthus* | *primigenius* | IK99-524 | UAMES | 11007 | molar | CAMS-91811 | 51,000 | 2,900 | -21.78 | 9.68 | 51,000 | 2,900 | 46,341 | 63,391 | | (1) |
| *Mammuthus* | *primigenius* | IK98-1243 | UAMES | 9945 | radius | CAMS-121750[c] | 51,800 | 2,700 | -21.70 | 6.81 | 51,800 | 2,700 | 47,358 | 62,573 | | (1) |
| *Mammuthus* | *primigenius* | IK02-173 | UAMES | 10458 | fibula | CAMS-91963 | 51,900 | 3,200 | -21.33 | 6.38 | 51,900 | 3,200 | 46,988 | 66,781 | | (1) |
| *Mammuthus* | *primigenius* | IK99-070 | UAMES | 10694 | mandible | CAMS-91778[c] | 51,900 | 3,200 | -22.32 | 9.48 | 51,900 | 3,200 | 46,988 | 66,781 | | (1) |
| *Mammuthus* | *primigenius* | IK01-355 | UAMES | 12004 | vertebra | CAMS-121735[c] | 52,800 | 3,000 | -21.70 | n/a | 52,800 | 3,000 | 48,047 | 66,018 | | (1) |
| *Mammuthus* | *primigenius* | IK01-274 | n/a | n/a | femur | CAMS-92088 | 53,000 | 3,700 | -21.42 | 9.84 | 53,000 | 3,700 | 47,823 | 71,903 | | (1) |
| *Mammuthus* | *primigenius* | IK98-1243 | UAMES | 9945 | radius | CAMS-120668[c] | 53,400 | 3,900 | -21.72 | 6.81 | 53,400 | 3,900 | 48,154 | 73,826 | | (1) |
| *Mammuthus* | *primigenius* | IK01-170 | UAMES | 11824 | molar | CAMS-92082 | 53,600 | 3,900 | -21.82 | n/a | 53,600 | 3,900 | 48,354 | 74,026 | | (1) |
| *Mammuthus* | *primigenius* | IK98-1013 | UAMES | 9934 | scapula | CAMS-121747[c] | 55,700 | 4,300 | -21.80 | 7.35 | 55,700 | 4,300 | 50,355 | 79,040 | | (1) |
| *Mammuthus* | *primigenius* | IK27 | n/a | n/a | n.r.[b] | AA-17610 | >31,000 | | -21.00 | n/a | >31,000 | | n/a | n/a | | (7) |
| *Mammuthus* | *primigenius* | n/a | n/a | n/a | n.r.[b] | I-9342 | >35,000[d] | | -21.50* | n/a | >35,057 | | n/a | n/a | | (9) |
| *Mammuthus* | *primigenius* | IK16 | n/a | n/a | n.r.[b] | AA-17612 | >35,700 | | -20.50 | n/a | >35,700 | | n/a | n/a | | (7) |
| *Mammuthus* | *primigenius* | IK23 | n/a | n/a | n.r.[b] | AA-17626 | >36,800 | | -21.21 | n/a | >36,800 | | n/a | n/a | | (7) |
| *Mammuthus* | *primigenius* | IK31 | n/a | n/a | n.r.[b] | AA-17603 | >37,000 | | -22.71 | n/a | >37,000 | | n/a | n/a | | (7) |
| *Mammuthus* | *primigenius* | IK22 | n/a | n/a | n.r.[b] | AA-17613 | >37,200 | | -21.60 | n/a | >37,200 | | n/a | n/a | | (7) |
| *Mammuthus* | *primigenius* | IK29 | n/a | n/a | n.r.[b] | AA-17611 | >37,500 | | -22.69 | n/a | >37,500 | | n/a | n/a | | (7) |
| *Mammuthus* | *primigenius* | IK15 | n/a | n/a | n.r.[b] | AA-17617 | >37,600 | | -22.07 | n/a | >37,600 | | n/a | n/a | | (7) |
| *Mammuthus* | *primigenius* | IK36 | n/a | n/a | n.r.[b] | AA-17604 | >37,600 | | -21.89 | n/a | >37,600 | | n/a | n/a | | (7) |
| *Mammuthus* | *primigenius* | IK32 | n/a | n/a | n.r.[b] | AA-17609 | >38,100 | | -20.76 | n/a | >38,100 | | n/a | n/a | | (7) |
| *Mammuthus* | *primigenius* | IK26 | n/a | n/a | n.r.[b] | AA-17608 | >39,000 | | -21.78 | n/a | >39,000 | | n/a | n/a | | (7) |
| *Mammuthus* | *primigenius* | AK72-4 | UAMES | 28848 | n.r.[b] | AA-14959[x] | >39,400 | | -21.70 | n/a | >39,400 | | n/a | n/a | | (7) |
| *Mammuthus* | *primigenius* | IK34 | n/a | n/a | n.r.[b] | AA-17607 | >39,500 | | -22.02 | n/a | >39,500 | | n/a | n/a | | (7) |
| *Mammuthus* | *primigenius* | IK30 | n/a | n/a | n.r.[b] | AA-17606 | >40,000 | | -21.85 | n/a | >40,000 | | n/a | n/a | | (7) |
| *Mammuthus* | *primigenius* | AKV-72-5 | UAMES | 29356 | n.r.[b] | AA-14961 | >40,700 | | -22.00 | n/a | >40,700 | | n/a | n/a | | (7) |
| *Mammuthus* | *primigenius* | Tusk | n/a | n/a | tusk | AA-22617 | >40,800 | | -21.90 | n/a | >40,800 | | n/a | n/a | | (7) |
| *Mammuthus* | *primigenius* | IK5 | n/a | n/a | n.r.[b] | AA-17625 | >41,000 | | -21.98 | n/a | >41,000 | | n/a | n/a | | (7) |

| *Genus* | *species* | field ID | depository[a] | catalog number | skeletal element | $^{14}$CLab[#] and number | $^{14}$C date reported (yrs BP) | | $\delta^{13}$C ‰ (VPDB) | $\delta^{15}$N ‰ (AIR) | $\delta^{13}$C-normalized date used for calibration | | 95.4% calibrated range | | used in Monte Carlo (x) | source |
|---|---|---|---|---|---|---|---|---|---|---|---|---|---|---|---|---|
| | | | | | | | $^{14}$C date | std dev[e] | | | $^{14}$C date | std dev[e] | (cal yr BP)[f] | | | |
| *Mammuthus* | *primigenius* | V-30-76 | UAMES | 23334 | molar | AA-22620 | >41,000 | | -21.80 | n/a | >41,000 | | n/a | n/a | | (7) |
| *Mammuthus* | *primigenius* | A-5 | n/a | n/a | n.r.[b] | AA-14953 | >41,100 | | -22.30 | n/a | >41,100 | | n/a | n/a | | (7) |
| *Mammuthus* | *primigenius* | AK119-V-1 | UAMES | 28789 | n.r.[b] | AA-14959[x] | >41,100 | | -21.80 | n/a | >41,100 | | n/a | n/a | | (7) |
| *Mammuthus* | *primigenius* | IK1 | n/a | n/a | n.r.[b] | AA-17621 | >41,100 | | -22.33 | n/a | >41,100 | | n/a | n/a | | (7) |
| *Mammuthus* | *primigenius* | IK2 | n/a | n/a | n.r.[b] | AA-17624 | >41,100 | | -22.62 | n/a | >41,100 | | n/a | n/a | | (7) |
| *Mammuthus* | *primigenius* | IK7 | n/a | n/a | n.r.[b] | AA-17618 | >41,100 | | -22.41 | n/a | >41,100 | | n/a | n/a | | (7) |
| *Mammuthus* | *primigenius* | My Ikpikpu, | n/a | n/a | n.r.[b] | AA-14946 | >41,100 | | -20.90 | n/a | >41,100 | | n/a | n/a | | (7) |
| *Mammuthus* | *primigenius* | IK09-07 | n/a | n/a | tusk | Beta-263032 | >42,000 | | -21.20 | n/a | >42,000 | | n/a | n/a | | (1) |
| *Mammuthus* | *primigenius* | IK98-CWB | n/a | n/a | tusk | Beta-283241 | >43,500 | | -20.90 | n/a | >43,500 | | n/a | n/a | | (1) |
| *Mammuthus* | *primigenius* | KIK10-TT | n/a | n/a | tusk | Beta-283247 | >43,500 | | -20.60 | n/a | >43,500 | | n/a | n/a | | (1) |
| *Mammuthus* | *primigenius* | Pelvis | n/a | n/a | pelvis | Beta-111034 | >46,450 | | -21.60 | n/a | >46,450 | | n/a | n/a | | (1) |
| *Mammuthus* | *primigenius* | IK98-0957 | n/a | n/a | long bone | CAMS-120662 | >48,900 | | -20.74 | 8.06 | >48,900 | | n/a | n/a | | (1) |
| *Mammuthus* | *primigenius* | IK99-070 | UAMES | 10694 | mandible | CAMS-91798[c] | >49,000 | | -22.32 | 9.48 | >49,000 | | n/a | n/a | | (1) |
| *Mammuthus* | *primigenius* | IK99-236 | UAMES | 11111 | molar | CAMS-91804 | >49,000 | | -21.84 | 8.10 | >49,000 | | n/a | n/a | | (1) |
| *Mammuthus* | *primigenius* | IK01-079 | UAMES | 11646 | rib | CAMS-120638[c] | >49,100 | | -23.18 | 8.36 | >49,100 | | n/a | n/a | | (1) |
| *Mammuthus* | *primigenius* | IK01-132 | UAMES | 12035 | radius | CAMS-120640[c] | >49,100 | | -21.46 | 6.64 | >49,100 | | n/a | n/a | | (1) |
| *Mammuthus* | *primigenius* | IK01-256 | UAMES | 11972 | molar | CAMS-92086 | >49,200 | | -21.36 | 8.18 | >49,200 | | n/a | n/a | | (1) |
| *Mammuthus* | *primigenius* | T02-038 | UAMES | 8617 | scapula | CAMS-91960 | >49,200 | | -22.44 | 6.64 | >49,200 | | n/a | n/a | | (1) |
| *Mammuthus* | *primigenius* | IK02-121 | UAMES | 10523 | radius | CAMS-120652 | >49,300 | | -21.85 | n/a | >49,300 | | n/a | n/a | | (1) |
| *Mammuthus* | *primigenius* | IK01-200 | UAMES | 11684 | molar | CAMS-92084 | >50,000 | | -22.29 | n/a | >50,000 | | n/a | n/a | | (1) |
| *Mammuthus* | *primigenius* | IK01-255 | UAMES | 11971 | femur | CAMS-120644[c] | >50,000 | | -21.98 | 7.67 | >50,000 | | n/a | n/a | | (1) |
| *Mammuthus* | *primigenius* | IK98-1312 | UAMES | 9853 | femur | CAMS-120672 | >50,100 | | -22.04 | 6.86 | >50,100 | | n/a | n/a | | (1) |
| *Mammuthus* | *primigenius* | IK99-588 | UAMES | 10941 | pelvis | CAMS-120723 | >50,400 | | -22.03 | n/a | >50,400 | | n/a | n/a | | (1) |
| *Mammuthus* | *primigenius* | IK98-0298 | UAMES | 8889 | radius | CAMS-120657 | >50,600 | | -22.09 | 7.80 | >50,600 | | n/a | n/a | | (1) |
| *Mammuthus* | *primigenius* | IK01-082 | n/a | n/a | tibia | CAMS-120639[c] | >51,000 | | -20.80 | 5.07 | >51,000 | | n/a | n/a | | (1) |
| *Mammuthus* | *primigenius* | IK99-366 | UAMES | 11180 | tusk | CAMS-120678 | >51,000 | | -21.59 | 8.50 | >51,000 | | n/a | n/a | | (1) |
| *Mammuthus* | *primigenius* | IK98-1281 | UAMES | 9996 | tibia | CAMS-120671 | >51,100 | | -21.42 | 7.19 | >51,100 | | n/a | n/a | | (1) |
| *Mammuthus* | *primigenius* | IK98-1000 | UAMES | 9773 | tusk | CAMS-120663 | >51,300 | | -21.58 | 7.63 | >51,300 | | n/a | n/a | | (1) |
| *Mammuthus* | *primigenius* | IK98-1274 | UAMES | 10079 | radius | CAMS-120669 | >51,300 | | -21.72 | 7.18 | >51,300 | | n/a | n/a | | (1) |
| *Mammuthus* | *primigenius* | IK99-130 | UAMES | 11120 | femur | CAMS-120674 | >51,500 | | -21.35 | 6.77 | >51,500 | | n/a | n/a | | (1) |

| *Genus* | *species* | field ID | depository[a] | catalog number | skeletal element | $^{14}$CLab[#] and number | $^{14}$C date reported (yrs BP) | | $\delta^{13}$C ‰ (VPDB) | $\delta^{15}$N ‰ (AIR) | $\delta^{13}$C-normalized date used for calibration | | 95.4% calibrated range | | used in Monte Carlo (x) | source |
|---|---|---|---|---|---|---|---|---|---|---|---|---|---|---|---|---|
| | | | | | | | $^{14}$C date | std dev[e] | | | $^{14}$C date | std dev[e] | (cal yr BP)[f] | | | |
| *Mammuthus* | *primigenius* | IK01-079 | UAMES | 11646 | rib | CAMS-120713[c] | >52,000 | | -23.18 | 8.36 | >52,000 | | n/a | n/a | | (1) |
| *Mammuthus* | *primigenius* | IK99-322 | UAMES | 10561 | molar | CAMS-91807 | >52,000 | | -21.88 | 9.35 | >52,000 | | n/a | n/a | | (1) |
| *Mammuthus* | *primigenius* | IK01-255 | UAMES | 11971 | femur | CAMS-120719[c] | >52,100 | | -21.98 | 7.67 | >52,100 | | n/a | n/a | | (1) |
| *Mammuthus* | *primigenius* | IK98-0759 | UAMES | 9541 | scapula | CAMS-121743 | >52,200 | | -21.20 | 9.31 | >52,200 | | n/a | n/a | | (1) |
| *Mammuthus* | *primigenius* | IK99-5000b | UAMES | 7954 | tusk | CAMS-92095 | >52,500 | | -21.60 | 7.35 | >52,500 | | n/a | n/a | | (1) |
| *Mammuthus* | *primigenius* | IK98-0761 | UAMES | 9543 | ulna | CAMS-121744 | >53,400 | | -20.80 | 7.68 | >53,400 | | n/a | n/a | | (1) |
| *Mammuthus* | *primigenius* | IK01-359 | UAMES | 12008 | molar | CAMS-92092 | >54,000 | | -21.69 | 8.41 | >54,000 | | n/a | n/a | | (1) |
| *Mammuthus* | *primigenius* | IK02-042 | n/a | n/a | pelvis | CAMS-91961 | >54,000 | | -21.40 | 6.37 | >54,000 | | n/a | n/a | | (1) |
| *Mammuthus* | *primigenius* | IK98-1087 | UAMES | 9813 | molar | CAMS-91795 | >54,000 | | -21.76 | 8.65 | >54,000 | | n/a | n/a | | (1) |
| *Mammuthus* | *primigenius* | IK01-132 | UAMES | 12035 | radius | CAMS-120715[c] | >54,500 | | -21.46 | 6.64 | >54,500 | | n/a | n/a | | (1) |
| *Mammuthus* | *primigenius* | IK01-082 | n/a | n/a | tibia | CAMS-120714[c] | >55,100 | | -20.80 | 5.07 | >55,100 | | n/a | n/a | | (1) |
| *Mammuthus* | *primigenius* | IK98-0801 | UAMES | 9424 | metapodial | CAMS-121746 | >55,500 | | -20.80 | 7.88 | >55,500 | | n/a | n/a | | (1) |
| *Mammuthus* | *primigenius* | IK98-1195 | UAMES | 9811 | radius | CAMS-121749[c] | >55,500 | | -21.10 | 6.08 | >55,500 | | n/a | n/a | | (1) |
| *Ovibos*[g] | *moschatus* | ING-99-1001 | UAMES | 8638 | cranium | AA-48776 | 226 | 59 | -19.80 | 3.76 | 226 | 59 | ... | 456 | | (1) |
| *Ovibos* | *moschatus* | Sing12-2 | UAMES | 30202 | cranium | Beta-339445 | 250 | 30 | -20.00 | 3.60 | 250 | 30 | ... | 429 | | (1) |
| *Ovibos* | *moschatus* | TUN12-1 | UAMES | 30203 | cranium | Beta-339278 | 340 | 30 | -18.50 | 4.80 | 340 | 30 | 311 | 481 | | (1) |
| *Ovibos* | *moschatus* | NIG09-1 | n/a | n/a | cranium | Beta-283248 | 350 | 40 | -19.20 | n/a | 350 | 40 | 312 | 495 | | (1) |
| *Ovibos* | *moschatus* | KEA1 | UAMES | 29498 | cranium | Beta-244761 | 900 | 40 | -19.00 | n/a | 900 | 40 | 735 | 916 | | (1) |
| *Ovibos* | *moschatus* | KEA2 | UAMES | 29499 | cranium | Beta-223266 | 1,140 | 40 | -21.00 | n/a | 1,070 | 40 | 926 | 1,061 | | (1) |
| *Ovibos* | *moschatus* | KEA3 | UAMES | 29500 | cranium | Beta-244762 | 1,080 | 40 | -20.30 | n/a | 1,080 | 40 | 926 | 1,066 | | (1) |
| *Ovibos* | *moschatus* | ING-99-1002 | UAMES | 8639 | cranium | AA-48283 | 1,148 | 42 | -20.00 | 5.56 | 1,148 | 42 | 969 | 1,177 | | (1) |
| *Ovibos* | *moschatus* | IK99-353 | UAMES | 29501 | cranium | AA-48263 | 7,127 | 59 | -19.60 | 6.81 | 7,127 | 59 | 7,799 | 8,148 | | (1) |
| *Ovibos* | *moschatus* | IK98-1032 | UAMES | 10098 | cranium | AA-48757 | 10,180 | 110 | -19.80 | 3.71 | 10,180 | 110 | 11,356 | 12,379 | x | (1) |
| *Ovibos* | *moschatus* | TIT05-08 | UAMES | 29502 | tibia | Beta-223267 | 21,050 | 90 | -20.80 | n/a | 21,050 | 90 | 25,155 | 25,640 | x | (1) |
| *Ovibos* | *moschatus* | IK98-0819 | UAMES | 9673 | metatarsal | AA-48753 | 21,670 | 370 | -19.40 | 9.26 | 21,670 | 370 | 25,228 | 26,882 | x | (1) |
| *Ovibos* | *moschatus* | IK98-0871 | UAMES | 9753 | metatarsal | AA-48239 | 27,580 | 750 | -19.60 | 9.31 | 27,580 | 750 | 30,545 | 33,582 | x | (1) |
| *Ovibos* | *moschatus* | IK11-28 | UAMES | 29503 | scapula | Beta-306116 | 27,640 | 150 | -21.00 | n/a | 27,640 | 150 | 31,135 | 31,685 | x | (1) |
| *Ovibos* | *moschatus* | TIT09-01 | UAMES | 29504 | cranium | Beta-263036 | 30,950 | 240 | -19.70 | n/a | 30,950 | 240 | 34,386 | 35,414 | x | (1) |
| *Ovibos* | *moschatus* | TIT08-17 | UAMES | 29505 | metatarsal | Beta-258464 | 31,430 | 240 | -20.60 | n/a | 31,430 | 240 | 34,796 | 35,881 | x | (1) |
| *Ovibos* | *moschatus* | TIT10-04 | n/a | n/a | cranium | Beta-283251 | 33,960 | 240 | -18.80 | n/a | 33,960 | 240 | 37,774 | 39,021 | x | (1) |

| *Genus* | *species* | field ID | depository[a] | catalog number | skeletal element | $^{14}$CLab[#] and number | $^{14}$C date reported (yrs BP) | | $\delta^{13}$C ‰ (VPDB) | $\delta^{15}$N ‰ (AIR) | $\delta^{13}$C-normalized date used for calibration | | 95.4% calibrated range | | used in Monte Carlo (x) | source |
|---|---|---|---|---|---|---|---|---|---|---|---|---|---|---|---|---|
| | | | | | | | $^{14}$C date | std dev[e] | | | $^{14}$C date | std dev[e] | (cal yr BP)[f] | | | |
| *Ovibos* | *moschatus* | IK01-159 | UAMES | 11886 | metatarsal | Beta-286418 | 34,570 | 250 | -20.20 | 8.58 | 34,570 | 250 | 38,542 | 39,699 | x | (1) |
| *Ovibos* | *moschatus* | IK01-313 | UAMES | 11685 | metatarsal | AA-48277 | 35,920 | 930 | -19.60 | 7.43 | 35,920 | 930 | 38,755 | 42,174 | x | (1) |
| *Ovibos* | *moschatus* | IK01-294 | UAMES | 11628 | metatarsal | AA-48276 | 36,400 | 770 | -20.00 | 7.27 | 36,400 | 770 | 39,531 | 42,308 | x | (1) |
| *Ovibos* | *moschatus* | IK99-179 | UAMES | 10709 | mandible | Beta-286425 | 40,080 | 340 | -20.00 | n/a | 40,080 | 340 | 43,075 | 44,400 | x | (1) |
| *Ovibos* | *moschatus* | TIT08-13 | UAMES | 29506 | cranium | Beta-258463 | 40,410 | 780 | -21.20 | n/a | 40,410 | 780 | 42,827 | 45,445 | x | (1) |
| *Ovibos* | *moschatus* | IK99-047 | UAMES | 10573 | mandible | Beta-286423 | 40,950 | 570 | -20.10 | n/a | 40,950 | 570 | 43,418 | 45,513 | x | (1) |
| *Ovibos* | *moschatus* | IK97-501 | UAMES | 29507 | cranium | Beta-117141 | 41,470 | 1,050 | -23.80 | n/a | 41,470 | 1,050 | 43,147 | 47,254 | x | (1) |
| *Ovibos* | *moschatus* | IK98-1173 | n/a | n/a | axis | CAMS-53908 | 43,000 | 1,800 | -19.90 | 4.25 | 43,000 | 1,800 | 44,215 | 49,997 | x | (1) |
| *Ovibos* | *moschatus* | IK98-0393 | UAMES | 8813 | metacarpal | AA-48748 | >35,500 | | -19.10 | 8.20 | >35,500 | | n/a | n/a | | (1) |
| *Ovibos* | *moschatus* | IK98-0673 | UAMES | 9641 | metatarsal | Beta-286422 | >36,200 | | -20.70 | 5.25 | >36,200 | | n/a | n/a | | (1) |
| *Ovibos* | *moschatus* | IK98-0654 | UAMES | 9439 | metacarpal | AA-48750 | >37,100 | | -18.70 | 2.40 | >37,100 | | n/a | n/a | | (1) |
| *Ovibos* | *moschatus* | IK98-0469 | UAMES | 9259 | metacarpal | Beta-286421 | >37,300 | | -20.20 | 7.28 | >37,300 | | n/a | n/a | | (1) |
| *Ovibos* | *moschatus* | IK98-0387 | UAMES | 8786 | cranium | Beta-286420 | >39,500 | | -20.50 | 7.24 | >39,500 | | n/a | n/a | | (1) |
| *Ovibos* | *moschatus* | IK98-1221 | UAMES | 9875 | metacarpal | AA-48258 | >39,800 | | -20.10 | 5.32 | >39,800 | | n/a | n/a | | (1) |
| *Ovibos* | *moschatus* | IK98-1324 | UAMES | 9890 | horn core | AA-48260 | >39,900 | | -19.20 | 2.73 | >39,900 | | n/a | n/a | | (1) |
| *Ovibos* | *moschatus* | IK01-086 | UAMES | 11674 | metatarsal | AA-48771 | >40,000 | | -20.40 | 3.17 | >40,000 | | n/a | n/a | | (1) |
| *Ovibos* | *moschatus* | IK09-05 | UAMES | 29508 | femur | Beta-263030 | >40,000 | | -19.50 | n/a | >40,000 | | n/a | n/a | | (1) |
| *Ovibos* | *moschatus* | IK09-06 | UAMES | 29509 | femur | Beta-263031 | >40,000 | | -21.00 | n/a | >40,000 | | n/a | n/a | | (1) |
| *Ovibos* | *moschatus* | IK98-1028 | UAMES | 9959 | cranium | AA-48756 | >40,000 | | -19.90 | 8.84 | >40,000 | | n/a | n/a | | (1) |
| *Ovibos* | *moschatus* | IK98-1309 | UAMES | 9834 | metacarpal | AA-48761 | >40,000 | | -19.20 | 8.36 | >40,000 | | n/a | n/a | | (1) |
| *Ovibos* | *moschatus* | IK99-142 | UAMES | 10682 | cranium | AA-48764 | >40,000 | | -19.40 | 3.51 | >40,000 | | n/a | n/a | | (1) |
| *Ovibos* | *moschatus* | IK99-731 | UAMES | 10845 | metatarsal | AA-48768 | >40,000 | | -19.60 | 9.17 | >40,000 | | n/a | n/a | | (1) |
| *Ovibos* | *moschatus* | IK99-754 | UAMES | 10936 | metatarsal | AA-48769 | >40,000 | | -18.90 | 8.75 | >40,000 | | n/a | n/a | | (1) |
| *Ovibos* | *moschatus* | IK98-0028 | UAMES | 9068 | metacarpal | AA-48252 | >40,100 | | -19.30 | 4.21 | >40,100 | | n/a | n/a | | (1) |
| *Ovibos* | *moschatus* | IK98-0818 | UAMES | 9677 | metatarsal | AA-48238 | >40,100 | | -19.70 | 7.96 | >40,100 | | n/a | n/a | | (1) |
| *Ovibos* | *moschatus* | IK98-1288 | UAMES | 10017 | metacarpal | AA-48259 | >40,200 | | -19.40 | 6.89 | >40,200 | | n/a | n/a | | (1) |
| *Ovibos* | *moschatus* | IK98-0441 | UAMES | 8926 | metacarpal | AA-48254 | >40,300 | | -19.90 | 5.52 | >40,300 | | n/a | n/a | | (1) |
| *Ovibos* | *moschatus* | IK01-311 | UAMES | 11662 | metacarpal | AA-48250 | >40,700 | | -20.00 | 6.96 | >40,700 | | n/a | n/a | | (1) |
| *Ovibos* | *moschatus* | IK01-398 | UAMES | 11840 | metacarpal | AA-48279 | >40,900 | | -20.20 | 5.75 | >40,900 | | n/a | n/a | | (1) |
| *Ovibos* | *moschatus* | IK01-136 | UAMES | 11888 | metatarsal | AA-48272 | >41,000 | | -19.90 | 5.54 | >41,000 | | n/a | n/a | | (1) |
| *Ovibos* | *moschatus* | IK01-160 | UAMES | 11887 | metatarsal | AA-48249 | >41,000 | | -20.00 | 7.10 | >41,000 | | n/a | n/a | | (1) |

| *Genus* | *species* | field ID | depository[a] | catalog number | skeletal element | $^{14}$CLab[#] and number | $^{14}$C date reported (yrs BP) | | $\delta^{13}$C ‰ (VPDB) | $\delta^{15}$N ‰ (AIR) | $\delta^{13}$C-normalized date used for calibration | | 95.4% calibrated range | | used in Monte Carlo (x) | source |
|---|---|---|---|---|---|---|---|---|---|---|---|---|---|---|---|---|
| | | | | | | | $^{14}$C date | std dev[e] | | | $^{14}$C date | std dev[e] | (cal yr BP)[f] | | | |
| *Ovibos* | *moschatus* | IK98-0849 | UAMES | 9336 | metacarpal | AA-48257 | >41,000 | | -19.60 | 5.53 | >41,000 | | n/a | n/a | | (1) |
| *Ovibos* | *moschatus* | IK98-0980 | UAMES | 9740 | metatarsal | AA-48755 | >41,000 | | -20.40 | n/a | >41,000 | | n/a | n/a | | (1) |
| *Ovibos* | *moschatus* | IK99-729 | UAMES | 10843 | metacarpal | AA-48265 | >41,000 | | -19.70 | 9.17 | >41,000 | | n/a | n/a | | (1) |
| *Ovibos* | *moschatus* | IK01-073 | UAMES | 11862 | cranium | AA-48267 | >41,100 | | -19.80 | 5.62 | >41,100 | | n/a | n/a | | (1) |
| *Ovibos* | *moschatus* | IK98-0029 | UAMES | 9069 | metacarpal | AA-48744 | >41,100 | | -19.30 | 3.43 | >41,100 | | n/a | n/a | | (1) |
| *Ovibos* | *moschatus* | IK98-0049 | UAMES | 8911 | metacarpal | AA-48745 | >41,100 | | -19.20 | 10.71 | >41,100 | | n/a | n/a | | (1) |
| *Ovibos* | *moschatus* | IK98-0089 | UAMES | 9095 | metacarpal | AA-48746 | .>41,100 | | -19.70 | 8.85 | >41,100 | | n/a | n/a | | (1) |
| *Ovibos* | *moschatus* | IK98-0133 | UAMES | 9122 | metacarpal | AA-48747 | >41,100 | | -20.20 | 7.69 | >41,100 | | n/a | n/a | | (1) |
| *Ovibos* | *moschatus* | IK98-0286 | UAMES | 8836 | metacarpal | AA-48236 | >41,100 | | -19.80 | 2.25 | >41,100 | | n/a | n/a | | (1) |
| *Ovibos* | *moschatus* | IK98-0461 | UAMES | 9251 | metacarpal | AA-48237 | >41,100 | | -19.90 | 6.01 | >41,100 | | n/a | n/a | | (1) |
| *Ovibos* | *moschatus* | IK98-0513 | UAMES | 9610 | metatarsal | AA-48255 | >41,100 | | -20.10 | 6.62 | >41,100 | | n/a | n/a | | (1) |
| *Ovibos* | *moschatus* | IK98-0653 | UAMES | 9438 | metacarpal | AA-48256 | >41,100 | | -19.60 | 5.97 | >41,100 | | n/a | n/a | | (1) |
| *Ovibos* | *moschatus* | IK98-0742 | UAMES | 9471 | metatarsal | AA-48752 | >41,100 | | -19.70 | 2.64 | >41,100 | | n/a | n/a | | (1) |
| *Ovibos* | *moschatus* | IK98-0930 | UAMES | 9504 | metacarpal | AA-48754 | >41,100 | | -20.10 | 6.57 | >41,100 | | n/a | n/a | | (1) |
| *Ovibos* | *moschatus* | IK98-1027 | UAMES | 9958 | cranium | AA-48240 | >41,100 | | -19.60 | 3.07 | >41,100 | | n/a | n/a | | (1) |
| *Ovibos* | *moschatus* | IK98-1044 | UAMES | 10044 | metacarpal | AA-48241 | >41,100 | | -19.00 | 7.37 | >41,100 | | n/a | n/a | | (1) |
| *Ovibos* | *moschatus* | IK98-1124 | UAMES | 9918 | metacarpal | AA-48242 | .>41,100 | | -19.40 | 6.10 | >41,100 | | n/a | n/a | | (1) |
| *Ovibos* | *moschatus* | IK99-143 | UAMES | 10683 | cranium | AA-48244 | >41,100 | | -20.40 | 4.66 | >41,100 | | n/a | n/a | | (1) |
| *Ovibos* | *moschatus* | IK99-320 | UAMES | 10559 | metacarpal | AA-48245 | >41,100 | | -20.10 | 3.80 | >41,100 | | n/a | n/a | | (1) |
| *Ovibos* | *moschatus* | IK99-504 | UAMES | 10883 | metatarsal | AA-48264 | >41,100 | | -20.00 | 8.79 | >41,100 | | n/a | n/a | | (1) |
| *Ovibos* | *moschatus* | IK98-1123 | UAMES | 9922 | metacarpal | AA-48758 | >41,100 | | -19.90 | 6.46 | >41,100 | | n/a | n/a | | (1) |
| *Ovibos* | *moschatus* | IK98-1289 | UAMES | 10018 | metacarpal | AA-48760 | >41,100 | | -20.60 | 7.30 | >41,100 | | n/a | n/a | | (1) |
| *Ovibos* | *moschatus* | IK98-1267 | UAMES | 10058 | cranium | AA-48759 | >41,100 | | -20.50 | 6.41 | >41,100 | | n/a | n/a | | (1) |
| *Ovibos* | *moschatus* | IK99-045 | UAMES | 11130 | cranium | AA-48762 | >41,100 | | -19.60 | n/a | >41,100 | | n/a | n/a | | (1) |
| *Ovibos* | *moschatus* | IK99-096 | UAMES | 10729 | metatarsal | AA-48763 | .>41,100 | | -20.60 | n/a | >41,100 | | n/a | n/a | | (1) |
| *Ovibos* | *moschatus* | IK99-255 | UAMES | 10645 | metacarpal | AA-48765 | >41,100 | | -19.50 | 9.14 | >41,100 | | n/a | n/a | | (1) |
| *Ovibos* | *moschatus* | KIK09-01 | UAMES | 29510 | cranium | Beta-263034 | >41,500 | | -20.60 | n/a | >41,500 | | n/a | n/a | | (1) |
| *Ovibos* | *moschatus* | IK09-08 | UAMES | 29511 | mandible | Beta-263033 | >42,000 | | -18.60 | n/a | >42,000 | | n/a | n/a | | (1) |
| *Ovibos* | *moschatus* | IK10-04 | UAMES | 29512 | cranium | Beta-283245 | >43,500 | | -19.70 | n/a | >43,500 | | n/a | n/a | | (1) |
| *Ovibos* | *moschatus* | IK99-133 | UAMES | 10832 | mandible | Beta-286424 | >43,500 | | -19.70 | n/a | >43,500 | | n/a | n/a | | (1) |
| *Ovibos* | *moschatus* | IK08-17 | UAMES | 29514 | mandible | Beta-258459 | >44,000 | | -20.20 | n/a | >44,000 | | n/a | n/a | | (1) |

| *Genus* | *species* | field ID | depository[a] | catalog number | skeletal element | $^{14}$CLab[#] and number | $^{14}$C date reported (yrs BP) | | $\delta^{13}$C ‰ (VPDB) | $\delta^{15}$N ‰ (AIR) | $\delta^{13}$C-normalized date used for calibration | | 95.4% calibrated range | | used in Monte Carlo (x) | source |
|---|---|---|---|---|---|---|---|---|---|---|---|---|---|---|---|---|
| | | | | | | | $^{14}$C date | std dev[e] | | | $^{14}$C date | std dev[e] | (cal yr BP)[f] | | | |
| *Ovibos* | *moschatus* | IK08-33 | UAMES | 29515 | cranium | Beta-258460 | >44,000 | | -20.20 | n/a | >44,000 | | n/a | n/a | | (1) |
| *Ovibos* | *moschatus* | IK98-1220 | UAMES | 9874 | phalange | Beta-175459 | >45,720 | | -20.50 | 6.41 | >45,720 | | n/a | n/a | | (1) |
| *Ovibos* | *moschatus* | IK99-142 | UAMES | 10682 | cranium | Beta-175460 | >48,420 | | -19.90 | 3.51 | >48,420 | | n/a | n/a | | (1) |
| *Ovibos* | *moschatus* | TIT05-06.1 | UAMES | 29516 | cranium | Beta-223269 | >49,800 | | -20.70 | n/a | >49,800 | | n/a | n/a | | (1) |
| *Panthera* | *spelaea* | IK98-278 | UAMES | 8807 | mandible | CAMS-53909 | 11,290 | 50 | -18.60 | 4.89 | 11,290 | 50 | 13,064 | 13,256 | x | (1) |
| *Panthera* | *spelaea* | IK01-409 | UAMES | 12041 | humerus | OxA-13473[c] | 12,630 | 60 | -18.50 | 8.03 | 12,630 | 60 | 14,716 | 15,231 | x | (10) |
| *Panthera* | *spelaea* | IK01-409 | UAMES | 12041 | humerus | AA-48280[c] | 12,930 | 130 | -18.40 | 8.03 | 12,930 | 130 | 15,099 | 15,878 | x | (1) |
| *Panthera* | *spelaea* | MAY12-24 | UAMES | 29517 | humerus | Beta-331881 | 15,990 | 60 | -18.50 | 8.80 | 15,990 | 60 | 19,084 | 19,516 | x | (1) |
| *Panthera* | *spelaea* | TIT12-07 | UAMES | 30204 | calcaneus | Beta-339277 | 30,520 | 180 | -18.70 | 9.20 | 30,520 | 180 | 34,107 | 34,835 | x | (1) |
| *Panthera* | *spelaea* | IK06-18 | UAMES | 29518 | humerus | Beta-286419 | 33,260 | 230 | -18.60 | n/a | 33,260 | 230 | 36,710 | 38,321 | x | (1) |
| *Panthera* | *spelaea* | IK97-1001 | UAMES | 11013 | humerus | Beta-117142 | 35,710 | 1,180 | -22.50 | 8.53 | 35,670 | 1,180 | 38,040 | 42,628 | x | (1) |
| *Panthera* | *spelaea* | IK98-436 | UAMES | 8983 | phalanx | CAMS-53910 | 40,900 | 1,140 | -18.10 | 8.78 | 40,900 | 1,140 | 42,697 | 46,891 | x | (1) |
| *Panthera* | *spelaea* | IK02-164 | UAMES | 10389 | humerus | CAMS-91784 | 48,300 | 2,100 | -19.47 | 10.97 | 48,300 | 2,100 | 44,704 | 54,980 | | (1) |
| *Panthera* | *spelaea* | IK01-112 | UAMES | 12045 | humerus | AA-48271 | >41,100 | | -18.80 | 7.79 | >41,100 | | n/a | n/a | | (1) |
| *Rangifer* | *tarandus* | IK98-0804 | UAMES | 9426 | mandible | CAMS-64413 | 160 | 40 | -19.19 | 3.80 | 150 | 40 | ... | 285 | | (1) |
| *Rangifer* | *tarandus* | IK98-0589 | UAMES | 9283 | humerus | CAMS-64409 | 200 | 50 | -18.26 | 2.14 | 190 | 50 | ... | 308 | | (1) |
| *Rangifer* | *tarandus* | IK98-0875 | UAMES | 9496 | mandible | CAMS-64416 | 220 | 40 | -18.66 | 2.91 | 210 | 40 | ... | 421 | | (1) |
| *Rangifer* | *tarandus* | IK99-421 | UAMES | 10579 | humerus | CAMS-64465 | 350 | 30 | -18.67 | 2.30 | 340 | 40 | 308 | 489 | | (1) |
| *Rangifer* | *tarandus* | IK98-0385 | UAMES | 8784 | humerus | CAMS-64403 | 390 | 40 | -18.15 | 2.74 | 370 | 40 | 315 | 505 | | (1) |
| *Rangifer* | *tarandus* | XCL-010 | n/a | n/a | n.r.[b] | GaK-2304 | 1,470[d] | 80 | -18.70* | n/a | 573 | 80 | 499 | 676 | | (8) |
| *Rangifer* | *tarandus* | IK98-0155 | n/a | n/a | metapodial | CAMS-64397 | 1,120 | 40 | -18.11 | 2.49 | 1,100 | 40 | 929 | 1,173 | | (1) |
| *Rangifer* | *tarandus* | IK99-314 | UAMES | 10766 | mandible | CAMS-64462 | 1,190 | 30 | -18.18 | 2.29 | 1,170 | 40 | 978 | 1,221 | | (1) |
| *Rangifer* | *tarandus* | XPH-003 | n/a | n/a | n.r.[b] | P-98 | 1,619[d] | 210 | -18.70* | n/a | 1,722 | 210 | 1,264 | 2,291 | | (8) |
| *Rangifer* | *tarandus* | IK98-1284 | UAMES | 10013 | humerus | CAMS-64453 | 2,140 | 40 | -18.52 | 2.65 | 2,130 | 40 | 1,995 | 2,304 | | (1) |
| *Rangifer* | *tarandus* | XBP-007 | n/a | n/a | n.r.[b] | Uga-3719 | 2,075[d] | 70 | -18.70* | n/a | 2,178 | 70 | 2,004 | 2,336 | | (8) |
| *Rangifer* | *tarandus* | IK98-1038 | UAMES | 9983 | metatarsal | CAMS-64420 | 2,600 | 40 | -17.59 | 2.36 | 2,580 | 50 | 2,490 | 2,785 | | (1) |
| *Rangifer* | *tarandus* | IK98-0898 | n/a | n/a | n.r.[b] | CAMS-64418 | 2,640 | 50 | -20.60 | -0.49 | 2,640 | 50 | 2,548 | 2,868 | | (1) |
| *Rangifer* | *tarandus* | XCL-002 | n/a | n/a | n.r.[b] | SM-917 | 3,042[d] | 188 | -18.70* | n/a | 3,145 | 188 | 2,878 | 3,828 | | (8) |
| *Rangifer* | *tarandus* | IK98-0083 | UAMES | 8988 | mandible | CAMS-64395 | 7,830 | 40 | -19.11 | 2.42 | 7,820 | 50 | 8,455 | 8,765 | | (1) |
| *Rangifer* | *tarandus* | IK99-397 | UAMES | 10740 | humerus | CAMS-64463 | 8,830 | 40 | -18.10 | 1.74 | 8,810 | 40 | 9,684 | 10,147 | | (1) |
| *Rangifer* | *tarandus* | IK99-044 | UAMES | 10571 | metatarsal | CAMS-64454 | 8,890 | 50 | -17.81 | 1.36 | 8,870 | 50 | 9,765 | 10,180 | | (1) |

| *Genus* | *species* | field ID | depository[a] | catalog number | skeletal element | $^{14}$CLab[#] and number | $^{14}$C date reported (yrs BP) | | $\delta^{13}$C ‰ (VPDB) | $\delta^{15}$N ‰ (AIR) | $\delta^{13}$C-normalized date used for calibration | | 95.4% calibrated range | | used in Monte Carlo (x) | source |
|---|---|---|---|---|---|---|---|---|---|---|---|---|---|---|---|---|
| | | | | | | | $^{14}$C date | std dev[e] | | | $^{14}$C date | std dev[e] | (cal yr BP)[f] | | | |
| *Rangifer* | *tarandus* | IK98-0627 | UAMES | 9601 | metapodial | CAMS-64410 | 12,370 | 50 | -18.79 | 2.80 | 12,360 | 50 | 14,120 | 14,720 | x | (1) |
| *Rangifer* | *tarandus* | IK97-601 | n/a | n/a | n.r.[b] | Beta-117140 | 12,710 | 100 | -23.30 | n/a | 12,680 | 100 | 14,558 | 15,435 | x | (1) |
| *Rangifer* | *tarandus* | IK99-594 | UAMES | 11000 | metacarpal | CAMS-64470 | 13,250 | 50 | -18.94 | 3.06 | 13,240 | 50 | 15,730 | 16,101 | x | (1) |
| *Rangifer* | *tarandus* | IK98-0585 | UAMES | 9704 | metacarpal | CAMS-64408 | 14,380 | 50 | -19.25 | 3.00 | 14,370 | 50 | 17,307 | 17,696 | x | (1) |
| *Rangifer* | *tarandus* | IK98-0879 | UAMES | 3296 | metacarpal | CAMS-64417 | 16,950 | 50 | -18.88 | 9.17 | 16,940 | 60 | 20,210 | 20,624 | x | (1) |
| *Rangifer* | *tarandus* | IK98-0846 | UAMES | 9325 | humerus | CAMS-64415 | 17,610 | 60 | -19.16 | 7.56 | 17,600 | 60 | 21,014 | 21,519 | x | (1) |
| *Rangifer* | *tarandus* | IK99-089 | UAMES | 10654 | metatarsal | CAMS-64456 | 18,410 | 60 | -18.88 | 5.90 | 18,400 | 60 | 22,027 | 22,453 | x | (1) |
| *Rangifer* | *tarandus* | IK98-0265 | UAMES | 9186 | humerus | CAMS-64398 | 20,480 | 80 | -18.95 | 7.15 | 20,470 | 80 | 24,329 | 24,983 | x | (1) |
| *Rangifer* | *tarandus* | IK98-0031 | UAMES | 9089 | metacarpal | CAMS-64392 | 24,750 | 110 | -19.87 | 8.70 | 24,750 | 110 | 28,498 | 29,060 | x | (1) |
| *Rangifer* | *tarandus* | M-98-064 | UAMES | 9110 | mandible | CAMS-64475 | 24,940 | 110 | -19.17 | 6.23 | 24,940 | 110 | 28,676 | 29,316 | x | (1) |
| *Rangifer* | *tarandus* | IK97-402 | n/a | n/a | n.r.[b] | Beta-117139 | 25,190 | 190 | -22.70 | n/a | 25,190 | 190 | 28,775 | 29,706 | x | (1) |
| *Rangifer* | *tarandus* | IK98-0690 | UAMES | 9598 | humerus | CAMS-64412 | 27,420 | 190 | -17.86 | 6.27 | 27,400 | 190 | 31,006 | 31,535 | x | (1) |
| *Rangifer* | *tarandus* | IK98-0311 | UAMES | 8944 | humerus | CAMS-64400 | 28,760 | 160 | -18.36 | 3.73 | 28,740 | 170 | 32,240 | 33,465 | x | (1) |
| *Rangifer* | *tarandus* | IK98-0833 | UAMES | 9300 | humerus | CAMS-64414 | 28,930 | 170 | -18.51 | 7.02 | 28,920 | 170 | 32,631 | 33,606 | x | (1) |
| *Rangifer* | *tarandus* | IK98-0079 | UAMES | 8900 | metacarpal | CAMS-64394 | 30,050 | 210 | -18.34 | 3.34 | 30,040 | 210 | 33,751 | 34,528 | x | (1) |
| *Rangifer* | *tarandus* | IK98-1207 | UAMES | 9831 | mandible | CAMS-64471 | 30,270 | 200 | -18.21 | 3.75 | 30,250 | 200 | 33,905 | 34,665 | x | (1) |
| *Rangifer* | *tarandus* | IK99-171 | UAMES | 10994 | metacarpal | CAMS-64457 | 30,820 | 200 | -19.00 | 3.92 | 30,810 | 200 | 34,300 | 35,143 | x | (1) |
| *Rangifer* | *tarandus* | IK99-570 | UAMES | 10847 | cranium | CAMS-64468 | 31,830 | 330 | -17.73 | 2.26 | 31,820 | 330 | 34,995 | 36,381 | x | (1) |
| *Rangifer* | *tarandus* | IK99-409 | UAMES | 3281 | humerus | CAMS-64464 | 31,920 | 240 | -18.16 | 3.95 | 31,900 | 240 | 35,240 | 36,310 | x | (1) |
| *Rangifer* | *tarandus* | IK98-0983 | UAMES | 9743 | humerus | CAMS-64419 | 32,570 | 250 | -18.64 | 2.59 | 32,550 | 250 | 35,877 | 37,372 | x | (1) |
| *Rangifer* | *tarandus* | IK98-0479 | UAMES | 9270 | metapodial | CAMS-64406 | 37,570 | 580 | -17.65 | 1.61 | 37,570 | 580 | 41,093 | 42,810 | x | (1) |
| *Rangifer* | *tarandus* | IK99-543 | UAMES | 10919 | metacarpal | CAMS-64466 | 38,830 | 540 | -18.12 | 3.77 | 38,810 | 540 | 42,026 | 43,667 | x | (1) |
| *Rangifer* | *tarandus* | IK99-066 | UAMES | 10547 | humerus | CAMS-64455 | 40,840 | 950 | -18.11 | 5.40 | 40,820 | 950 | 42,870 | 46,192 | x | (1) |
| *Rangifer* | *tarandus* | IK98-0350 | UAMES | 9107 | metatarsal | CAMS-64401 | 41,100 | 1,100 | -18.03 | 0.95 | 41,100 | 1,100 | 42,859 | 46,979 | x | (1) |
| *Rangifer* | *tarandus* | IK98-0450 | UAMES | 9032 | metatarsal | CAMS-64404 | 42,040 | 800 | -19.38 | 2.39 | 42,030 | 800 | 44,021 | 47,180 | x | (1) |
| *Rangifer* | *tarandus* | IK99-764 | UAMES | 11016 | humerus | CAMS-64473 | 42,500 | 1,200 | -18.50 | 1.82 | 42,500 | 1,200 | 43,930 | 48,913 | x | (1) |
| *Rangifer* | *tarandus* | IK98-0478 | UAMES | 9269 | metapodial | CAMS-64405 | 44,200 | 1,000 | -17.30 | 2.99 | 44,200 | 1,000 | 45,824 | 49,729 | | (1) |
| *Rangifer* | *tarandus* | IK98-0041 | UAMES | 9204 | metacarpal | CAMS-64393 | 44,300 | 1,100 | -17.76 | 1.16 | 44,300 | 1,100 | 45,889 | 49,875 | | (1) |
| *Rangifer* | *tarandus* | IK98-0687 | UAMES | 9596 | metapodial | CAMS-64411 | 45,500 | 1,200 | -17.22 | 1.88 | 45,460 | 1,210 | 46,777 | ... | | (1) |
| *Rangifer* | *tarandus* | IK98-1051 | UAMES | 10065 | metatarsal | CAMS-64421 | 46,300 | 1,400 | -18.72 | 3.85 | 46,300 | 1,400 | 47,169 | ... | | (1) |
| *Rangifer* | *tarandus* | IK98-1108 | UAMES | 9867 | metapodial | CAMS-64422 | 46,500 | 1,600 | -18.09 | 3.32 | 46,500 | 1,600 | 43,705 | 50,824 | | (1) |

| *Genus* | *species* | field ID | depository[a] | catalog number | skeletal element | $^{14}$CLab# and number | $^{14}$C date reported (yrs BP) | | $\delta^{13}$C ‰ (VPDB) | $\delta^{15}$N ‰ (AIR) | $\delta^{13}$C-normalized date used for calibration | | 95.4% calibrated range | | used in Monte Carlo (x) | source |
|---|---|---|---|---|---|---|---|---|---|---|---|---|---|---|---|---|
| | | | | | | | $^{14}$C date | std dev[e] | | | $^{14}$C date | std dev[e] | (cal yr BP)[f] | | | |
| *Rangifer* | *tarandus* | IK98-0351 | UAMES | 9108 | metatarsal | CAMS-64402 | 48,000 | 2,600 | -18.87 | 4.32 | 48,000 | 2,600 | 43,681 | 58,001 | | (1) |
| *Rangifer* | *tarandus* | IK98-0153 | UAMES | 9045 | humerus | CAMS-64396 | 48,300 | 1,700 | -18.11 | 1.65 | 48,300 | 1,700 | 45,343 | 53,031 | | (1) |
| *Rangifer* | *tarandus* | IK99-247 | UAMES | 10566 | humerus | CAMS-64460 | 52,000 | 2,700 | -18.51 | 4.60 | 52,000 | 2,700 | 47,558 | 62,773 | | (1) |
| *Rangifer* | *tarandus* | IK99-199 | UAMES | 12288 | metapodial | CAMS-64458 | 52,600 | 3,500 | -17.61 | 1.75 | 52,600 | 3,500 | 47,511 | 69,932 | | (1) |
| *Rangifer* | *tarandus* | IK99-740 | UAMES | 10876 | humerus | CAMS-64472 | 53,300 | 3,800 | -16.97 | 2.91 | 53,200 | 3,800 | 47,987 | 72,873 | | (1) |
| *Rangifer* | *tarandus* | IK98-0310 | UAMES | 8943 | humerus | CAMS-64399 | >46,900 | | -19.71 | 5.03 | >46,900 | | n/a | n/a | | (1) |
| *Rangifer* | *tarandus* | IK98-1227 | UAMES | 9903 | humerus | CAMS-64424 | >47,200 | | -18.50 | 1.73 | >47,200 | | n/a | n/a | | (1) |
| *Rangifer* | *tarandus* | TIT05-09 | UAMES | 29519 | tibia | Beta-223268 | >49,800 | | -18.50 | n/a | >49,800 | | n/a | n/a | | (1) |
| *Rangifer* | *tarandus* | IK98-1228 | UAMES | 9876 | humerus | CAMS-64425 | >49,900 | | -18.03 | 4.34 | >49,900 | | n/a | n/a | | (1) |
| *Rangifer* | *tarandus* | IK99-286 | UAMES | 10726 | humerus | CAMS-64461 | >49,900 | | -17.51 | 2.01 | >49,900 | | n/a | n/a | | (1) |
| *Rangifer* | *tarandus* | IK98-1158 | UAMES | 10053 | tibia | CAMS-64423 | >51,200 | | -17.45 | 0.14 | >51,200 | | n/a | n/a | | (1) |
| *Rangifer* | *tarandus* | IK99-585 | UAMES | 10938 | mandible | CAMS-64469 | >51,700 | | -17.17 | 2.28 | >51,700 | | n/a | n/a | | (1) |
| *Rangifer* | *tarandus* | IK98-0573 | UAMES | 9457 | mandible | CAMS-64407 | >52,800 | | -19.71 | 3.10 | >52,800 | | n/a | n/a | | (1) |
| *Rangifer* | *tarandus* | IK98-1230 | UAMES | 9921 | metatarsal | CAMS-64426 | >54,000 | | -17.84 | 1.52 | >54,000 | | n/a | n/a | | (1) |
| *Saiga* | *tatarica* | n/a | n/a | n/a | cranium | AA-3073 | 28,930 | 560 | n/a | n/a | 28,930 | 560 | 31,584 | 34,072 | x | (11) |
| *Saiga* | *tatarica* | USGS M1422 | n/a | n/a | cranium | GSC-3050 | 37,000 | 990 | n/a | n/a | 37,000 | 990 | 39,694 | 43,123 | x | (2) |
| *Ursus* | *arctos* | IK98-1065 | UAMES | 10003 | radius | CAMS-53913 | 36,310 | 780 | -18.40 | n/a | 36,310 | 780 | 39,411 | 42,262 | x | (1) |
| *Ursus* | *arctos* | n/a | n/a | n/a | n.r.[b] | AA-17510 | 48,164 | 3,224 | n/a | n/a | 48,164 | 3,224 | 43,235 | 63,245 | | (12) |
| *Ursus* | *maritimus* | Coast09-1 | UAMES | 29513 | cranium | Beta-283240 | >43,500 | | -11.70 | n/a | >43,500 | | n/a | n/a | | (1) |

[a] UAMES=University of Alaska Museum of the North Earth Sciences Collection

[b] Dated skeletal element not recorded by source.

[c] Duplicate dates were obtained for some samples. Both dates are reported here. The mean of both dates was used in analyses.

[d] $^{14}$C age not normalized for $\delta^{13}$C by laboratory.

[e] Standard deviations for isotope and $^{14}$C are one sigma, with the exception of "," which indicate infinite date returned from laboratory.

[f] 95.4% Calibrated probability range calculated using OxCal 4.2 and the IntCal13 calibration curve.

[g] Although it is often challenging to distinguish *Mammuthus*/*Mammut* and *Ovibos*/*Bootherium* using postcranial elements, *Mammut* and *Bootherium* were both forest-dependent animals and there were no trees growing north of the Brooks range during the interval studied here (12-45 cal ka BP) (all dated black spruce and poplar logs from the study site yield non-finite $^{14}$C ages); we therefore classify appropriate postcranial elements as either *Mammuthus* or *Ovibos*.

[*] $\delta^{13}$C values not reported from dating laboratory; this value was estimated based on mean of measured $\delta^{13}$C values for that genus from this data set and used for

normalizing dates prior to calibration.

[x] These laboratory numbers each appear twice in Guthrie (2004) and are probably transcription errors. Because the rest of each record is distinct, we include both dates here.

[#] Laboratory Codes: AA=Arizona Accelerator Mass Spectrometry Laboratory , USA; AAR=University of Aarhus, Denmark; Beta=Beta Analytic, USA; CAMS=Lawrence Livermore National Laboratory Center for Accelerator Mass Spectrometry , USA; GaK=Gakushuin University, Japan; GSC=Geological Survey, Canada; GX=Geochron Laboratories, USA; I=Teledyne Isotopes, USA; OxA=Oxford Radiocarbon Accelerator Unit, England; P=Univ. of Pennsylvania, USA; Shell=Shell Development Co., USA; SM=Mobil Oil Corp., Dallas, USA; TO=IsoTrace Laboratory, Canada; UCIAMS=University of California, Irvine Keck Carbon Cycle Accelerator Mass Spectrometry Laboratory, USA; UGa=University of Georgia, USA; USGS=USGS, Menlo Park, USA.

## 2- RANGE ECOLOGY IN ARCTIC ALASKA DURING THE ICE AGE

As Guthrie (9, 11) emphasized, the relatively high species diversity and abundance of megafaunal herbivores that were present in Alaska when it supported mammoth steppe vegetation indicate that range quality was much higher than it is today (1, 13). Moreover, these mammals invested heavily in large tusks, horns, and antlers that could only have been fueled by a productive landscape (14). We also know that the average size of horses rapidly shrank as mammoth steppe vegetation was replaced by shrub tundra at the end of the Pleistocene in Interior Alaska (15). Species diversity, biomass, investments in energy-expensive anatomy, and trends in body size all support the idea that the nutritional status of the mammoth steppe was much higher than that of the present-day vegetation cover, at least during brief episodes of maximum megafaunal abundance.

The nutritional value of vegetation is directly influenced by soil processes, and nitrogen (N) availability illustrates some of the complexities involved (16). N is important because it is a crucial component of protein. In the Arctic, N cycling is slow in moss- dominated vegetation growing on cold, wet soils because of the low nutrient content of the plant litter and the slow rates of decomposition and hence of nutrient turnover (17). Restricted N cycling is probably one of the reasons why horse bone collagen $\delta^{15}N$ values became less positive at the end of the ice age, as organic soils spread (Fig. 5). N cycling was probably significantly faster in the well-drained soils and moss-scarce vegetation cover of the mammoth steppe.

The availability of nutrients like N to herbivores is further conditioned by the highly evolved, anti-herbivore strategies of plants. The total amount of available N matters less for herbivores than does its form and palatability (9). For instance, foliar N concentrations in moist acidic tundra (a widespread vegetation type on the North Slope today) are about the same as in moist non-acidic tundra (a drier, less peaty vegetation type growing in some areas of the North Slope). Nonetheless, megafaunal herbivores like caribou prefer the latter (18). Hence, a nutrient's distribution in time and space can be less important than the palatability of the plants containing that nutrient.

Many of the plant species growing in the moist acidic tundra vegetation that covers much of the North Slope of Alaska today are well-defended from grazers by unpalatable secondary compounds (17, 19). Such defenses are necessary for these plants' persistence because paludified soils tend to be cold, wet, and nutrient poor. Consequently, resident plant species must pursue conservative growth strategies restricted by the scant supply of nutrients (13, 20). To maintain this conservative strategy, they must avoid being eaten, and so there has been ecological sorting favoring plants whose secondary compounds make them unavailable to herbivores (18, 21).

Further clues about the grazing system that operated on the mammoth steppe come from the nature of the present-day, moist non-acidic tundra (22), that non-peat- accumulating vegetation type found on some parts of the North Slope where loess deposition still occurs. Caribou prefer this vegetation type over the more peat-rich, moist acidic tundra because

it contains relatively palatable plants. Moist non-acidic tundra is relatively high in calcium, an important nutrient in animal growth. Today, caribou heavily rely on this type throughout the year, especially during the calving season (18).

The nutritional value of vegetation is indirectly influenced by the foraging efficiency of the herbivore utilizing that vegetation, and foraging efficiency depends in part on the efficacy of locomotion, especially in rangelands like the mammoth steppe where primary productivity was probably relatively low, highly seasonal, and widely dispersed in space. Firm footing would have enabled large-bodied animals like horse, mammoth, and bison that had relatively small feet to range widely and hence forage efficiently even in cold, dry rangelands. But as tundra vegetation and organic soils replaced the mammoth steppe and the ground surface became boggy and peat- covered, mobility was inhibited and required more food energy for taxa with high indices of foot-loading (9).

To summarize, the relatively high species diversity and large biomass of Pleistocene megafauna on the North Slope testifies to the relatively high productivity of this vanished biome. Our results suggest these peaks in primary productivity and megafaunal biomass occurred infrequently and episodically, but nonetheless did occur. Today's cold, wet soils restrict nutrient cycling and create nutrient limitations that favor plants investing in long-lived foliage, and hence in chemical and physical traits discouraging herbivory. Animal mobility and forage quality are closely interconnected because restrictions on movement increase nutritional demands. As Guthrie (9) emphasized, the spread of organic soils and concomitant increases in snow depths during the Pleistocene-Holocene transition would have challenged the mobility of megafauna like horse, bison, and mammoth who possessed high foot-loading indices at the same time that the spread of peat-associated plants lowered the nutritional quality of their arctic rangelands.

## 3- COLLAGEN EXTRACTION, ULTRAFILTRATION, AND CORRECTING $^{14}$C-CALIBRADION NOISE

**Collagen extraction** Without exception, every bone we attempted to dating. This high degree of preservation is attributable to the anoxic and/or frozen state in which these bones were stored in nature. For the samples we dated, the bone collagen was prepared for dating as follows. Bones were manually inspected, and outer surfaces were cleaned by abrasion. All the bones we dated were freshly collected from the field and therefore had no surface contamination requiring solvent extraction. Two to ten grams of abraded bone were placed in a beaker with 0.2N HCl at 20 degrees Celsius (< pH 1). The sample was inspected several times daily to monitor demineralization and collagen evolution. Where possible, the initially evolved collagen was removed and discarded to reduce physical contamination. The underlying collagen was then collected for further pretreatment. Once sufficient collagen was available, it was separated from the remaining mineral fraction and rinsed to neutrality with deionized water. It was then placed in 1-2 % reagent grade NaOH for two hours. The actual concentration and exposure of each sample to the alkali solution was regulated depending on the preservation state of the collagen. Any extraneous matter (roots, sand, etc.) was simultaneously removed during repetitions of this step. This was repeated until the solution was clear or until diminishing returns on the collagen remaining was reached.

**Ultrafiltration**

In permafrost and fluvial settings, where plant roots rarely penetrate more than several decimeters into the ground, the most problematic aspect of $^{14}$C-dating bone collagen is contamination by younger organic matter carried by groundwater. As a bone decomposes, its collagen can bind with younger humic substances, which are abundant in certain settings (23). Contamination of older bones by younger humic substances is generally unimportant when the bone is relatively young, say < 20,000 years, but it can significantly skew the dating result when the true age of the bone is > 40,000 years because by this time approximately seven $^{14}$C half-lives have passed, and only about 0.8% of the initial $^{14}$C remains. Humic compounds derived from older organic matter also can contaminate bone collagen, but contamination by older carbon has comparatively minor effects on the resultant $^{14}$C age (24).

The main laboratory technique used to counter the potential effects of contamination of collagen by younger organic compounds is ultrafiltration (25). Ultrafiltration separates the higher molecular weight components of the gelatinized collagen from the lower molecular weight components that include humic and fulvic acids bound to partly degraded collagen (26, 27). In some depositional settings, such as limestone caves located in the temperate zone, the use of ultrafiltration to remove the younger, organic contaminants from bone samples has resulted in ages 2,000 to 7,000 years older than non- ultrafiltered dates on the same samples (28-30).

Although first devised more than twenty years ago (25), the ultrafiltration technique continues to evolve, and has only become commercially available in the last several years. Its utility is still debated. In cases where bone preservation is excellent and

contamination by younger organics is minimal, ultrafiltration may be unnecessary (31, 32). Further subsampling of already tiny amounts of $^{14}C$ increases the risks of other types of contamination. In some instances, the filter membrane itself has been found to introduce younger carbon into samples (33, 34).

Before ultrafiltration became commercially available, large numbers of $^{14}C$ dates were obtained on bone collagen using non-ultrafiltration techniques. For instance, we (1) reported finite ages for 245 bones of Pleistocene megafauna from the North Slope of Alaska and used these ages to infer paleoenvironments and extinction causes. Given what is now known about ultrafiltration techniques, it is reasonable to ask whether these non-ultrafiltered dates are valid.

The presence of permafrost creates very different preservational environments for bone than the limestone caves of Europe studied by Highham et al. (28, 29). Apart from one, recent study (6), there have been no large-scale comparisons between ultrafiltered and non- ultrafiltered $^{14}C$ ages estimated from bones from arctic settings. That study re-dated six mastodon (*Mammut americanum*) bones from Alaska and the Yukon previously dated using non-ultrafiltration methods. Of the six mastodon teeth collected on Alaska's North Slope, non-ultrafiltration methods produced three non-finite $^{14}C$ ages and three $^{14}C$ ages ranging between 31,780 and 38,800 cal yr BP (6). Repeated dating of ultrafiltered collagen resulted in non-finite ages for these three teeth as well, suggesting that these first dates had been contaminated by young carbon.

Mastodon teeth preserved in the sediment of an arctic river provide an ideal setting for humic contamination of bone collagen. The risk of obtaining an erroneous, younger date on bone collagen because of contamination by younger humic substances is greatest when a bone whose own $^{14}C$ has long since decayed away is exposed to dissolved organic compounds with younger $^{14}C$ content over tens of thousands of years. Hence using ultra-filtration to re-date the collagen of a taxon like mastodon that has been locally extinct for at least 75,000 years has a high likelihood of revising the $^{14}C$ age upward. The likelihood is much lower that ultrafiltration will significantly revise $^{14}C$ ages obtained by non-ultrafiltration methods on the bones of animals that were alive <45,000 years ago. Preliminary results of a study we are now engaged in support this assertion.

To examine the effects of using ultrafiltration in dating of permafrost bones, we randomly selected 30 bones of *Equus*, *Bison*, and *Ovibos* collected along the Ikpikpuk River whose non- ultrafiltered $^{14}C$ ages ranged between 11 and 46 $^{14}C$ ka BP. These non-ultrafiltered dates on bone collagen were obtained using accelerator mass spectrometry at Beta Analytic Inc. in the years prior to 2013. Starting in 2013, we submitted additional bone samples from these same thirty bones to Beta Analytic for ultrafiltration and AMS dating of collagen.

Results show that differences between ultrafiltered and non-ultrafiltered dates increase at ages greater than 30,000 $^{14}C$ years BP (roughly 5 half lives), when remaining $^{14}C$ content drops below a few percent of its initial value (Fig. S1). Interestingly, the age differences between the two techniques are equally spread in both directions. In ten of the date pairs, the non-ultrafiltered date was older than the ultrafiltered one; while in eleven of the date

pairs, the ultrafiltered date was younger. This project is still in progress, but these preliminary results indicate that the use of ultrafiltration in $^{14}$C dating of bone collagen sourced from permafrost settings like Alaska's North Slope does not systematically "correct" $^{14}$C dates obtained using non-ultrafiltration methods, and so ultrafiltration is unwarranted when dating bone collagen from this particular depositional environment.

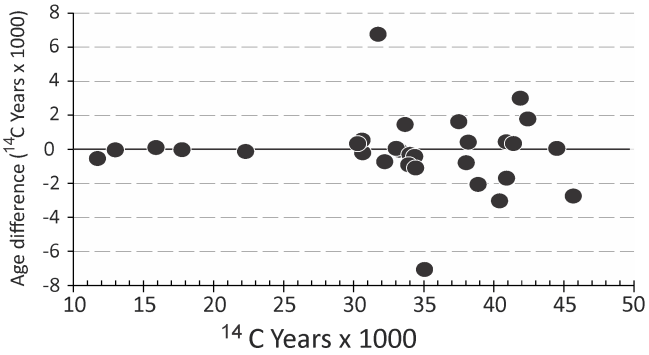


**Fig. S1.** Differences in $^{14}$C ages obtained after ultrafiltration and non-ultrafiltration pretreatment of collagen from the same megafauna bones. Thirty bones (ten each of horse, bison, and musk ox) from the North Slope were chosen to span the age range from 10 to 45 cal ka BP based on their initial, non-ultrafiltered $^{14}$C ages. Age differences are calculated by subtracting the ultrafiltered from non-ultrafiltered dates. Although previous studies in some temperate- zone settings have found that ultrafiltration can remove younger contaminants that cause systematic "younging" of $^{14}$C ages, these results indicate ultrafiltration is not necessary for dating bones < 45,000 years old that are sourced from permafrost environments.

## Coping with calibration noise in the cumulative probability distributions of $^{14}$C dates

$^{14}$C dates are frequently combined into cumulative probability distributions for time-series analyses following their calibration to calendar years (35, 36). These cumulative probability distributions (CPDs) depict changes in the abundance of dated samples through time. Some peaks and valleys in cumulative probability distributions of calibrated $^{14}$C dates are artifacts resulting from the calibration process (Fig. S2) (36, 37). At steep parts of the curve, multiple $^{14}$C dates can correspond to nearly identical calendar ages. On plateaus, $^{14}$C ages can correspond to widely spaced calendar ages, some of which may be reversed in age relative to their corresponding $^{14}$C ages.

Various methods have been proposed to remove calibration artifacts from the CPDs of $^{14}$C dates. Williams (36) used moving averages to reduce calibration effects. Johnstone et al. (38) subtracted a curve generated from a uniform distribution based on the observed CPD. Hoffman et al. (39) suggested dividing the observed CPD by a CPD derived from a uniform distribution or dividing the CPD derived from a subset of the data by the CPD of the entire dataset. Chiverrell et al. (40) and Perry et al. (41) suggested avoiding use of CPDs altogether.

These previous methods of dealing with calibration artifacts in the CPDs of $^{14}$C dates all have their limitations. For studies like ours, where our goal is to compare a CPD to

climate history, moving averages smooth out the very peaks we seek to compare, while comparisons between observed CPD and theoretical CPDs - like those derived from uniformly distributed radiocarbon dates - do not entirely remove the calibration effect.

Although structured as a Monte Carlo hypothesis test, we consider our new method to be a data- exploration technique in the sense of Tukey (42) for identifying events that are unlikely to occur by chance, rather than a test with a rigid *accept-reject* significance criterion (43). Note that this Monte Carlo approach is vulnerable to type II errors (failing to detect an effect that is actually present) because of the limited number of dated bones. If we had 1000 instead of just 263 bones, additional peaks in the CPD curve would undoubtedly prove to be significantly different from the simulated background. Minima in the CPD are particularly vulnerable to type II errors because they represent the periods where dates are rare in an already small dataset. Therefore it is the presences rather than the absences of statistically significant peaks in bone abundance that provide the most informative temporal patterns.

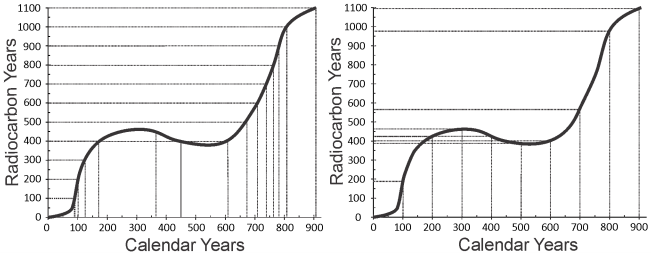


**Fig. S2.** Hypothetical radiocarbon-calibration curves being used to correct $^{14}C$ dates to calendar years. Because the amount of radiocarbon in Earth's atmosphere has fluctuated, the $^{14}C$ -calibration curve wiggles through time. As a result, evenly spaced $^{14}C$ ages (*left*) correspond to clusters of calibrated (calendar) ages at the steep portions of the calibration curve. Evenly spaced calendar ages (*right*) correspond $^{14}C$ ages clustering on plateaus in the curve. These calibration effects generate peaks in any cumulative probability distribution (CPD) composed of a large series of calibrated $^{14}C$ dates and need to be taken into account before making any inferences based on temporal patterns displayed by the CPD.

## 4- TAPHONOMY

The megafaunal bones we studied come from low-energy floodplains in an arctic, permafrost environment. Their often exceptional states of morphological and chemical preservation regardless of age, combined with the rarity of specimens displaying root etching, indicate most of them were never exposed to chemical weathering in soils. Instead, most of these bones appear to have been stored in anoxic and/or permanently frozen states for millennia.

As detailed in an earlier paper (1), there are two main pathways for bone deposition and preservation in the Ikpikpuk and Titaluk River valleys where most of these bones originate. Upstream of the loess belt (a 50-km wide area where windblown silts accumulated downwind of the now stabilized Ikpikpuk Sand Sea), most bones were deposited in the active stream channel. The rarity of scavenger gnawing suggests rapid burial by sediment. Concentrations of bones occur where the channel crosses beds of clay, suggesting these are places where animals were bogged down. A different mechanism of bone accumulation operated within the loess belt where large ice wedges provided another type of natural trap. Ongoing loess deposition buried these remains, and lateral erosion of river channels later carved into these loess deposits, reworking bones into the active channel. This process can occasionally be seen occurring today along eroding cut banks.

Once entering the river channel through either of the two pathways, bones gradually work their way downward through the sediment column through a process of elutriation until they end up concentrated below the water table under anoxic conditions. If the active channel shifts elsewhere on the floodplain, the bones become incorporated in permafrost. Given the sheer number of bones, the fact that the collections span two different drainage basins, the diversity of bone ages, and the complexity of the taphonomic pathways, we think it unlikely that multiple bones of the same individual of any taxon have been dated in this study.

Most of the bones we dated come from upstream of the loess belt, so we think that death-in-the- channel has been the dominant taphonomic pathway. Unlike the loess belt, where bone preservation probably varied according to the rate of aeolian sedimentation, bones have been incorporated, elutriated, and stored in the floodplains regardless of whether the channels were aggrading or incising. The upper reaches of both the Ikpikpuk and Titaluk Rivers have progressively incised their floodplains since ca. 7500 years ago (44), yet abundant wood and bones of moose, muskoxen and caribou continue to enter via this taphonomic pathway. We have found no support for the alternate hypothesis that the highs and lows in bone abundance through time are the result of differential weathering under different vegetation covers or from differential deposition/preservation under differing geomorphic regimes.

## REFERENCES CITED


1. Mann DH, Groves P, Kunz ML, Reanier RE, & Gaglioti BV (2013) Ice-age megafauna in Arctic Alaska: extinction, invasion, survival. *Quaternary Sci Rev* 70:91-108.
2. Harington CR (2003) *Annotated Bibliography of Quaternary Vertebrates of Northern North America* (University of Toronto Press, Toronto).
3. Shapiro B*, et al.* (2004) Rise and fall of the Beringian steppe bison. *Science* 306(5701):1561-1565.
4. Guthrie RD & Stoker S (1990) Paleoecological Significance of Mummified Remains of Pleistocene Horses from the North Slope of the Brooks Range, Alaska. *Arctic* 43(3):267-274.
5. Lorenzen ED*, et al.* (2011) Species-specific responses of Late Quaternary megafauna to climate and humans. *Nature* 479(7373):359-U195.
6. Zazula GD*, et al.* (2014) American mastodon extirpation in the Arctic and Subarctic predates human colonization and terminal Pleistocene climate change. *P Natl Acad Sci USA* 111(52):18460-18465.
7. Guthrie RD (2004) Radiocarbon evidence of mid-Holocene mammoths stranded on an Alaskan Bering Sea island. *Nature* 429(6993):746-749.
8. Gal R (1982) An annotated and indexed roster of archaeological radiocarbon dates fro Alaska, north of 68˚ latitude. *Archaeological Investigations in the National Petroleum Reserve in Alaska* 2:159-180.
9. Gurhrie RD (1990) *Frozen Fauna of the Mammoth Steppe: The Story of Blue Babe* (University of Chicago Press, Chicago, IL).
10. Barnett R*, et al.* (2009) Phylogeography of lions (Panthera leo ssp.) reveals three distinct taxa and a late Pleistocene reduction in genetic diversity. *Mol Ecol* 18(8):1668-1677.
11. Guthrie RD (2001) Origin and causes of the mammoth steppe: a story of cloud cover, woolly mammal tooth pits, buckles, and inside-out Beringia. *Quaternary Sci Rev* 20(1-3):549-574.
12. Barnes I, Matheus P, Shapiro B, Jensen D, & Cooper A (2002) Dynamics of Pleistocene population extinctions in Beringian brown bears. *Science* 295(5563):2267-2270.
13. Zimov SA*, et al.* (1995) Steppe-Tundra Transition - a Herbivore-Driven Biome Shift at the End of the Pleistocene. *Am Nat* 146(5):765-794.
14. Gurhrie RD (1984) Mosaics, allelochemics and nutrients. *Quaternary extinctions, a Prehistoric Revolution*, eds Martin PS & Klein RG (University of Arizona Press, Tuscon, AZ), pp 259-298.
15. Guthrie RD (2003) Rapid body size decline in Alaskan Pleistocene horses before extinction. *Nature* 426(6963):169-171.
16. Aerts R & Chapin FS (2000) The mineral nutrition of wild plants revisited: A re-evaluation of processes and patterns. *Adv Ecol Res* 30:1-67.
17. Chapin FS, Mckendrick JD, & Johnson DA (1986) Seasonal-Changes in Carbon Fractions in Alaskan Tundra Plants of Differing Growth Form - Implications for Herbivory. *J Ecol* 74(3):707-731.
18. Walker DA*, et al.* (2001) Calcium-rich tundra, wildlife, and the "Mammoth Steppe". *Quaternary Sci Rev* 20(1-3):149-163.
19. Chapin FS, Johnson DA, & Mckendrick JD (1980) Seasonal Movement of Nutrients in Plants of Differing Growth Form in an Alaskan Tundra Ecosystem - Implications for Herbivory. *J Ecol* 68(1):189-209.
20. Zimov SA, Zimov NA, & Chapin FS (2012) The past and future of the mammoth steppe ecosystem. *Paleontology in Ecology and Conservation*, ed Louys J (Springer-Verlag, Berlin), pp 193-225.

21. White RG & Trudell J (1980) Habitat Preference and Forage Consumption by Reindeer and Caribou near Atkasook, Alaska. *Arctic Alpine Res* 12(4):511-529.
22. Walker DA*, et al.* (1998) Energy and trace-gas fluxes across a soil pH boundary in the arctic. *Nature* 394(6692):469-472.
23. Vanklinken GJ & Hedges REM (1995) Experiments on Collagen Humic Interactions - Speed of Humic Uptake, and Effects of Diverse Chemical Treatments. *J Archaeol Sci* 22(2):263-270.
24. Bowman S (1995) *Radiocarbon Dating* (British Museum Press, London).
25. Brown TA, Nelson DE, Vogel JS, & Southon JR (1988) Improved Collagen Extraction by Modified Longin Method. *Radiocarbon* 30(2):171-177.
26. Brock F, Geoghegan V, Thomas B, Jurkschat K, & Higham TFG (2013) Analysis of Bone "Collagen" Extraction Products for Radiocarbon Dating. *Radiocarbon* 55(2-3):445-463.
27. Higham TFG, Jacobi RM, & Ramsey CB (2006) AMS radiocarbon dating of ancient bone using ultrafiltration. *Radiocarbon* 48(2):179-195.
28. Higham T (2011) European Middle and Upper Palaeolithic radiocarbon dates are often older than they look: problems with previous dates and some remedies. *Antiquity* 85(327):235-249.
29. Higham T*, et al.* (2014) The timing and spatiotemporal patterning of Neanderthal disappearance. *Nature* 512(7514):306-309.
30. Jacobi RM, Higham TFG, & Ramsey CB (2006) AMS radiocarbon dating of Middle and Upper Palaeolithic bone in the British Isles: improved reliability using ultrafiltration. *J Quaternary Sci* 21(5):557-573.
31. Hajdas I, Michczynski A, Bonani G, Wacker L, & Furrer H (2009) Dating Bones near the Limit of the Radiocarbon Dating Method: Study Case Mammoth from Niederweningen, Zh Switzerland. *Radiocarbon* 51(2):675-680.
32. Minami M, Sakata K, Takigami M, Nagaoka T, & Nakamura T (2013) Ultrafiltration Pretreatment for C-14 Dating of Fossil Bones from Archaeological Sites in Japan. *Radiocarbon* 55(2-3):481-490.
33. Brock F, Ramsey CB, & Higham T (2007) Quality assurance of ultrafiltered bone dating. *Radiocarbon* 49(2):187-192.
34. Hüls CM, Grootes PM, & Nadeau MJ (2009) Ultrafiltration: Boon or Bane? *Radiocarbon* 51(2):613-625.
35. Contreras DA & Meadows J (2014) Summed radiocarbon calibrations as a population proxy: a critical evaluation using a realistic simulation approach. *J Archaeol Sci* 52:591-608.
36. Williams AN (2012) The use of summed radiocarbon probability distributions in archaeology: a review of methods. *J Archaeol Sci* 39(3):578-589.
37. Guilderson TP, Reimer PJ, & Brown TA (2005) The boon and bane of radiocarbon dating. *Science* 307(5708):362-364.
38. Johnstone E, Macklin MG, & Lewin J (2006) The development and application of a database of radiocarbon-dated Holocene fluvial deposits in Great Britain. *Catena* 66(1-2):14-23.
39. Hoffmann T, Lang A, & Dikau R (2008) Holocene river activity: analysing (14)C-dated fluvial and colluvial sediments from Germany. *Quaternary Sci Rev* 27(21-22):2031-2040.
40. Chiverrell RC, Thorndycraft VR, & Hoffmann TO (2011) Cumulative probability functions and their role in evaluating the chronology of geomorphological events during the Holocene. *J Quaternary Sci* 26(1):76-85.
41. Perry GLW, Wheeler AB, Wood JR, & Wilmshurst JM (2014) A high-precision chronology for the rapid extinction of New Zealand moa (Aves, Dinornithiformes). *Quaternary Sci Rev* 105:126-135.

42. Tukey JW (1977) *Exploratory Data Analysis* (Addison Wesley, Reading, MS).
43. Kempthorpe O & Doerfler TE (1969) Behaviour of some significance tests under experimental randomization. *Biometrika* 56(2):231-248.
44. Mann DH, Groves P, Reanier RE, & Kunz ML (2010) Floodplains, permafrost, cottonwood trees, and peat: What happened the last time climate warmed suddenly in arctic Alaska? *Quaternary Sci Rev* 29(27-28):3812-3830.